THE EFFECT OF CARBIDES AND TOUGHNESS ON THE RESISTANCE OF THREE MARTENSITIC STEELS TO SULFIDE STRESS CRACKING

by

J. D. Gottschling

Submitted in Partial Fulfillment of the Requirements

for the Degree of

Master of Science in Engineering

in the

Materials Science Program

Richard W Jones — 16 August 1976

Adviser — Date

Lee Caird — 18, August 1976

Adviser — Date

Youngstown State University

August 1976

ABSTRACT

THE EFFECT OF CARBIDES AND TOUGHNESS ON
THE RESISTANCE OF THREE MARTENSITIC STEELS
TO SULFIDE STRESS CRACKING

J. D. Gottschling

Master of Science in Engineering

Youngstown State University, 1976

Sulfide stress cracking tests were conducted at 75°F on a plain carbon, a chromium and a vanadium steel each quenched and tempered to various strength levels. The results of the tests were correlated with carbide parameters determined from the microstructures of the steels. The resistance of the steels to sulfide stress cracking increased with increasing volume fraction of carbides and total particle surface area per unit length of line. In addition, there was a critical volume fraction of carbides and/or total particle surface area above which failure did not occur. These results are in agreement with the theory that hydrogen can be trapped in an innocuous state at the interface between precipitates and the matrix.

Instrumented Charpy impact tests were conducted at -100°F and 75°F on the three steels at the strength levels used in the sulfide stress cracking tests. The data from the two tests were correlated. The resistance of the steels to sulfide stress cracking increased as the toughness increased, with the best correlation existing for the -100°F

test temperature. These results suggest that the carbides in the microstructures not only controlled the sulfide stress cracking resistance but also governed toughness. The results also suggest that the inherent resistance of a martensitic steel to hydrogen induced failure is directly related to its inherent toughness, i.e., that at the lower shelf.

Since precipitates appear to act as sites for trapping hydrogen, it may be possible to develop high strength steels that resist sulfide stress cracking by carefully controlling the amount of precipitates. In such development studies, the Charpy impact test can be a useful tool for screening potential materials and in evaluating the effect of various heat treatments on cracking resistance.

ACKNOWLEDGEMENTS

The author is indebted to the Alliance Research Center of the Babcock and Wilcox Company for providing the material and research equipment used in this investigation.

The author also wishes to thank his adviser, Dr. R. W. Jones, Department of Chemical Engineering and Material Science at Youngstown State University for guidance in this study.

TABLE OF CONTENTS

TABLE OF CONTENTS (Cont'd)

TABLE OF CONTENTS (Cont'd)

LIST OF FIGURES (Cont'd)

LIST OF FIGURES (Cont'd)

LIST OF TABLES

CHAPTER I

INTRODUCTION

Phenomenon of Sulfide Stress Cracking

Exposure of tubing in oil and gas wells to low temperature aqueous environments containing hydrogen sulfide has frequently led to failures. Such failures are characterized by a marked reduction in ductility and cracking is often rapid and complete. In addition, the failures can occur at stresses well below the yield strength of the material.

Early researchers could not agree whether the tubing failures were caused by stress corrosion or hydrogen embrittlement and hence the general term "sulfide stress cracking" was coined to describe the phenomenon. However, a NACE* sponsored research program conducted by Schultz and Robertson in 1957 showed that the basic cause of the cracking was the absorption of hydrogen[1]. Thus sulfide stress cracking is actually a form of hydrogen embrittlement. Since this work, considerable effort has been made to develop steels that resist cracking, but the problem still exists today.

Mechanism of Embrittlement

In sulfide stress cracking, the source of hydrogen is the atomic hydrogen produced at the steel surface by the reaction

$$Fe + H_2S \text{ (aq soln.)} \longrightarrow FeS + 2H \qquad (1)$$

---

*National Association of Corrosion Engineers.

These hydrogen atoms are adsorbed on the surface and enter the steel at active high energy sites[2]. The rate of adsorption increases with increasing hydrogen ion concentration (decreasing pH).

Presumably, hydrogen diffuses to volumes of metal under triaxial stress or to crystalline imperfections such as microcracks, voids around inclusions or regions of high dislocation density[3]. The accumulation of hydrogen at these sites acts as a source of internal stress and can result in brittle failure if accompanied by other internal or external stresses. Thus sulfide stress cracking depends on both the level of applied stress and the concentration of dissolved hydrogen.

Basic Studies of Hydrogen Embrittlement

The importance of the interaction between the applied stress and the concentration of hydrogen in hydrogen induced failure was determined by Troiano and coworkers[4]. In the investigation, notched tensile specimens of quenched and tempered AISI 4340 steel were cathodically charged and cadmium plated to retain the hydrogen. The specimens were baked at 300°F to distribute the hydrogen uniformly and loaded to various stress levels. The study showed that hydrogen embrittlement occurred over a wide range of stresses, but there was a minimum critical stress below which failure would not occur. The study also showed that the minimum critical stress increased with decreasing hydrogen concentration, indicating that crack initiation was governed by the interaction between hydrogen and stress.

The study of Troiano also established the basic characteristics of crack initiation and propagation in hydrogen embrittlement[5]. Failure consisted of three stages:

1) an incubation period prior to crack initiation
2) a period of slow crack propagation
3) a period of rapid crack propagation resulting in catastrophic failure.

Thus hydrogen embrittlement exhibits a very distinct failure process.

During the incubation period, the distribution of hydrogen changes continuously. Thus the incubation time is actually the time required for the critical concentration of hydrogen to collect at a potential crack initiation site.

Once a crack initiates, the slow crack propagation period follows. During this period, crack propagation occurs by a discontinuous series of new crack initiations. Presumably the first crack propagates out of the hydrogen enriched region and eventually stops. Hydrogen then diffuses to the region just ahead of the crack tip and a new crack initiates when the critical concentration of hydrogen is reached. Finally the two cracks connect by a tearing of the intermediate material.

The discontinuous crack propagation process repeats several times until the remaining cross section of material can no longer support the applied load. Then rapid crack propagation occurs, resulting in catastrophic failure.

Theories of Classical Hydrogen Embrittlement

Several theories have been proposed to explain the mechanism for classical hydrogen embrittlement. However, the theories fall into two

main groups - one based on atomic decohesion and the other due to pressure buildup.

The atomic decohesion theory proposed by Troiano suggests that hydrogen induced failure is essentially a normal fracture on which the embrittling effect of hydrogen has been superimposed[6]. The notch in the tensile specimen of Troiano produces a local stress concentration upon loading. Flow takes place at the base of the notch, resulting in blocked arrays of dislocations. These dislocation arrays are essentially fracture embryos. Hydrogen segregates to the stress field of the dislocation arrays and localized fracture occurs when the hydrogen concentration together with the stress reach critical levels in the surrounding lattice.

Presumably the cohesive strength of the lattice is lowered by the hydrogen at the tip of the dislocation array thus making cleavage easier. Troiano suggests that this occurs in transition metals because the electrons of the hydrogen in solution will enter the d bands of the metal[7]. Since the repulsive forces which determine the interatomic spacing are governed by the overlapping of the d bands in the transition metals, one might expect an increase in the number of electrons in these bands to produce an increase in the repulsive forces between atoms. Such an increase in the repulsive forces between atoms in effect decreases the cohesive strength of the lattice.

From the Griffith criterion for brittle fracture, the fracture stress or stress required for crack propagation, σ_F, is given by[8]:

$$\sigma_F = \left(\frac{2E\gamma}{\pi C}\right)^{1/2} \qquad (2)$$

where E = elastic modulus of the material
C = half length of the existing crack
γ = surface energy of the crack

In the atomic decohesion theory, the decrease in cohesive strength results in a decrease in the surface energy of the crack and thus from the above equation, a reduction in the stress needed for crack propagation[9].

The pressure buildup theory proposed by Tetelman suggests that hydrogen induced failure is caused by gas pressure which results from the formation of molecular hydrogen[10]. The hydrogen atoms in the lattice collect at the interface between inclusions and the matrix and form hydrogen molecules. This produces a hydrogen atom concentration gradient in the lattice which causes the diffusion of more atomic hydrogen to the inclusions. Thus more molecules of hydrogen form and the resulting pressure increases. When the stresses associated with the hydrogen pressure become high enough, microcracks form.

The hydrogen pressure causes the microcracks to grow by cleavage in susceptible materials. In effect, the internal pressure, P, lowers the external stress needed for crack propagation. Thus in terms of the Griffith criterion for brittle fracture[11]

$$\sigma_F = \left(\frac{2E\gamma}{\pi C}\right)^{1/2} - P \qquad (3)$$

In this sense, the pressure buildup theory is similar to the decohesion theory since both predict a reduction in the stress required to propagate a crack.

Evidence to support the decohesive theory of Troiano lies in the fact that only the transition metals are susceptible to hydrogen embrittlement[12]. On the other hand, evidence to support the pressure theory of Tetelman lies in the fact that hydrogen cracks can be produced in the absence of an applied stress[13]. Very recent work by Tetelman indicates that both mechanisms can operate[14]. A lowering of lattice cohesion occurs whenever hydrogen is present and this is the main cause of embrittlement at low concentrations of hydrogen. However, at high hydrogen concentrations, i.e., 1-2 ppm or greater, the pressure effect dominates. Thus two types of hydrogen embrittlement are possible, both of which lower the stress required for brittle fracture.

Factors Affecting Resistance to Sulfide Stress Cracking

As indicated earlier, sulfide stress cracking is caused by the absorption of hydrogen into a material during exposure to aqueous environments containing hydrogen sulfide. Furthermore, an interaction exists between the applied stress and the concentration of hydrogen in hydrogen induced failures. Thus there are three types of factors that can affect sulfide stress cracking - environmental, stress and material[15].

In terms of environmental factors, the resistance to sulfide stress cracking decreases with increasing concentration of hydrogen sulfide and decreasing pH[16]. The cracking resistance also decreases with decreasing temperature in the range 75°F to 200°F[17]. In terms of stress factors, the resistance to sulfide stress cracking decreases with increasing cold work (residual stress)[18]. Also there is evidence that

cracking can not occur in torsion - a tensile stress state is required[19]. In addition, the material factors that can influence sulfide stress cracking resistance are composition, strength and microstructure. Since the present study is concerned with the effect of material factors on the resistance to sulfide stress cracking, these factors will be covered in detail.

Material Factors Affecting Cracking Resistance

The numerous studies concerned with the effect of composition on the resistance to sulfide stress cracking present many conflicting conclusions. A study of 104 alloys by Fraser and Eldredge indicated that cracking resistance increased with increasing carbon content[21]. On the other hand, Snape, Herzog and Vollmer concluded in independent studies that the resistance to sulfide stress cracking decreased with increasing carbon level[22-24]. Similarly, Fraser and Eldredge found that increasing the manganese and molybdenum levels of a steel decreased the cracking resistance[25]. Kowaka and Nagata, on the other hand, found that manganese had a detrimental effect on the resistance to sulfide stress cracking, but molybdenum had no effect[26]. Finally, Herzog concluded that molybdenum had a beneficial effect on the cracking resistance[27]. Inconsistencies like these exist for most of the alloying elements added to steels. The only agreement concerning compositional effects is that certain elements like sulfur, phosphorus, arsenic, selenium and tellerium lower the resistance to sulfide stress cracking because they promote hydrogen absorption in steel[20].

The main problem in the earlier studies attempting to correlate composition with resistance to sulfide stress cracking was that most investigators did not take into account the changes in microstructure and strength that occurred with changes in composition. From this standpoint, Snape probably conducted the most thorough and comprehensive studies on sulfide stress cracking. Several carbon and low alloy steels were tested in the normalized, normalized and tempered, and quenched and tempered conditions[29-30]. Snape analyzed the test results in terms of strength level, composition and microstructure. The conclusions from these studies are summarized below:

1) The strength level of a steel is quite important in determining its resistance to sulfide stress cracking. In general, the cracking resistance decreases with increasing strength level.

2) The cracking resistance of a steel is closely related to its microstructure. Composition only appears to be important from the standpoint of how it affects microstructure.

3) Small amounts of untempered martensite markedly decrease the resistance of a steel to sulfide stress cracking.

4) At comparable strength levels, quenched and tempered steels with microstructures of spheroidized carbides uniformly dispersed in ferrite, have a greater cracking resistance than normalized and tempered steels with microstructures of globular or lamellar carbides in ferrite.

Thus the studies conducted by Snape showed that the microstructure of a steel is the most important material related factor in sulfide stress cracking.

Purpose of Present Work

Because of the current energy crisis, oil and gas wells are being drilled to depths in excess of 20,000 feet. Many of these deeper wells have hydrogen sulfide associated with them and hence there is a demand for high strength steels that resist sulfide stress cracking. However, despite the extensive research conducted in the area of sulfide stress cracking over the last twenty years, the development of such steels still represents a major task. A better understanding of the role of microstructure in sulfide stress cracking is needed to develop these high strength steels.

In this regard, a study was conducted with two objectives:

(1) to determine if the cracking resistance of low alloy martensitic steels could be correlated with a measurable carbide parameter such as size, volume fraction or interparticle spacing.

(2) to determine if the Charpy impact test, which is sensitive to changes in microstructure, could be used to predict the resistance of these steels to sulfide stress cracking.

In this study, sulfide stress cracking tests were conducted on three low alloy steels quenched and tempered to various strength levels. The results of the cracking tests were correlated with the general microstructures of the steels utilizing both optical and transmission electron microscopy. In addition, the results of the cracking tests were correlated with the Charpy impact properties of the three steels using instrumented impact tests.

CHAPTER II

EXPERIMENTAL PROCEDURE

Materials

Three steels were selected for the sulfide stress cracking study; a plain carbon steel and two alloy steels - one containing chromium and one containing vanadium (see Table 1 for compositions). The chromium

TABLE 1

COMPOSITIONS OF THE STEELS

Material	C	Mn	S	P	Si	Cr	Ni	Mo	V	B
Carbon Steel	.30	1.52	.008	.005	.19	-	.54	.02	-	.0022
Cr Steel	.31	1.62	.003	.006	.25	2.66	.55	.02	-	.0030
V Steel	.31	1.54	.005	.005	.24	-	.58	.02	1.57	.0039

and vanadium levels in the alloy steels were chosen to assure the precipitation of alloy carbides during tempering. Boron was added to all three steels to increase hardenability.

The steels were induction melted in 100 lb. heats, cast and forged into 1.25 inch diameter bars. As a preliminary heat treatment the bars were normalized at 1750°F for one hour.

Heat Treating Study

Small samples were sectioned from the normalized bars for the heat treating study. Seven samples from each steel were austenitized

at 1750°F for one hour and water quenched. One sample was saved for each steel in the as quenched condition and the remaining samples were tempered at various temperatures between 800°F and 1275°F for one hour.

Each heat treated sample was rough ground on a silicon carbide water wheel and its hardness was measured. At least 0.010 inch was removed from each sample to remove the decarburized layer. Wet grinding was used to minimize tempering effects. The hardness values shown in Figure 10 represent an average of five readings for each sample.

Metallographic Examination of Heat Treated Specimens

Select specimens from the heat treating study were sectioned and prepared for metallographic examination. The select specimens corresponded to the as quenched condition and after tempering for one hour at the temperatures 900°F, 1100°F and 1275°F for each steel. The transverse plane (parallel to the working direction) of each specimen was mounted in bakelite. The metallographic specimens were ground on successively finer silicon carbide papers, followed by 6μ diamond paste in oil and polished by a slurry of 0.25μ alumina powder in water. The specimens were etched by immersion in 2% nital and the general microstructures were examined optically at 600x and 1200x.

Grain Size Measurements

Grain size measurements were made on the etched specimens using the standard Graff-Snyder intercept method[31]. This method involved counting the number of grains on the specimen surface intercepted by

a line 0.005 inch in length. Twenty random determinations were made for each steel. The total length of line divided by the total number of grains intercepted gave the average grain intercept length for each material (see Table 3). This quantity was also converted to a standard ASTM grain size number using Table 2 in ASTM Designation E 112-63, "Standard Methods for Estimating the Average Grain Size of Metals"[32].

Examination of Carbon Extraction Replicas

Carbon extraction replicas were made on the metallographic specimens to identify the carbides that precipitated during tempering. Carbon was deposited on the etched specimens to a thickness of ∿50 A° in the vacuum evaporator. A vacuum of 10^{-5} torrs was used and the carbon source was positioned 90° from the specimens. The vacuum evaporator was returned slowly to atmospheric pressure and the deposited carbon layer was cut into 3-mm squares. The replicas were released by submerging the specimens in a solution of 2% nital which etched away the metal below the deposited carbon layer and left the carbides intact. The replicas were examined on the JEM 6A transmission electron microscope using an operating voltage of 50KV and a magnification of 14000X. The carbides present were identified by their characteristic morphologies.

Tensile Testing

Tensile blanks (0.750 inch diameter x 6.00 inch long) were austenitized, water quenched and tempered at various temperatures for each steel (see Table 2 for heat treatments). Standard 0.505 inch diameter tensile specimens were machined from the specimen blanks.

Tensile tests were conducted at room temperature on a Baldwin testing machine using a strain rate of 0.05 inch per inch per minute. A dual range extensometer (Satec Systems Model PSH 8MSD) was used to measure strain during testing. Elastic modulus and yield data was recorded using a high magnification (500:1), while plastic flow data was recorded using a low magnification (20:1).

TABLE 2

HEAT TREATMENTS FOR THE TENSILE SPECIMENS

	Carbon Steel	Cr Steel	V Steel
Normalize	1750°F/1hr	1750°F/1hr	1750°F/1hr
Austenitize	1750°F/1hr	1750°F/1hr	1750°F/1hr
Quench	water	water	water
Temper	a) 1100°F/1hr	a) 1250°F/1hr	a) 1250°F/1hr
	b) 1175°F/2hrs	b) 1300°F/2hrs	b) 1275°F/2hrs
	c) 1250°F/1hr	c) 1320°F/2hrs	c) 1300°F/2hrs

Sulfide Stress Cracking Tests

Test Specimens

Sulfide stress cracking tests were conducted on the three steels using notched C-ring specimens (see Figure 1). The notch introduced a triaxial stress state into the specimen and thus increased the probability that if failure occurred, it would be the result of hydrogen embrittlement and not some other mechanism such as stress corrosion. The preparation of the specimens is outlined as follows:

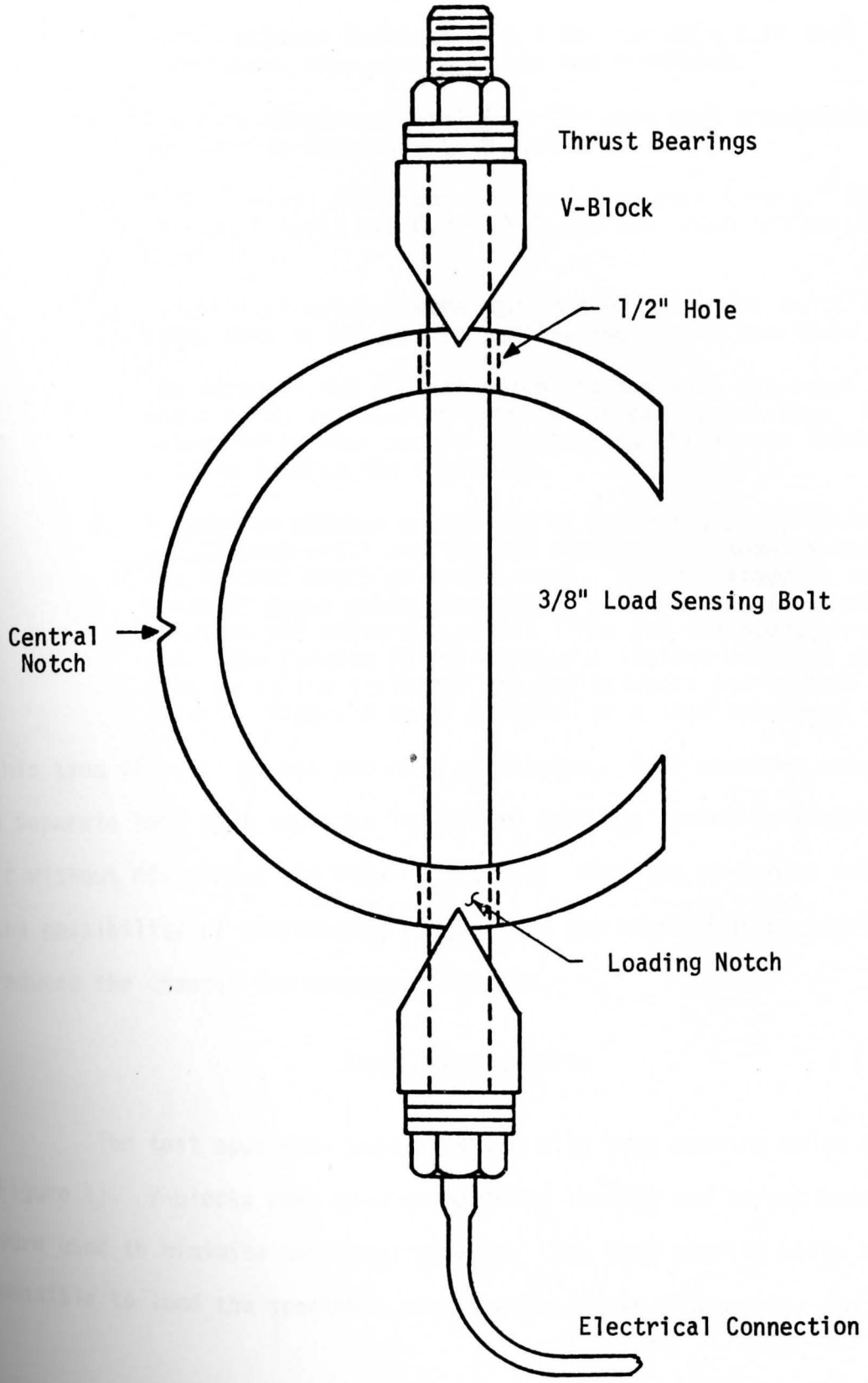

Figure 1. Geometry of C-Ring Used in Sulfide Stress Cracking Study and Manner of Loading Specimen.

1) Ring specimens (nominal size 2.20 inch OD x 0.25 inch wall) were formed from one inch wide strip samples.

2) The ring specimens were given the same heat treatments as the tensile specimens (see Table 2).

3) A 45° central notch was machined into each C-ring. Nominally, the notch depth was 0.040 inch and the notch radius was 0.010 inch.

4) Two similar notches were machined 90° from the central notch. These were to be used in loading the C-ring specimens.

5) The depth of the central notch and the wall thickness were measured on each C-ring with an optical comparator. These measurements were needed to calculate the stress levels used in loading the specimens.

6) A specimen chamber consisting of Tygon tubing (1.50 inch ID x 0.25 inch wall) and two end stoppers was made to enclose the central notch of each C-ring. The end stoppers contained lines of Tygon tubing for adding and removing the test solution and inlet and outlet lines for the hydrogen sulfide gas. Dow Corning 90-092 Aerospace Sealant was used as a coating on the inside of the end stoppers and to seal all joints. Figure 2 shows a sketch of a test specimen.

This type of specimen had two main advantages. Each specimen comprised a separate test that could be introduced into the system or removed from it without disturbing the other specimens. Also the specimens minimized the possibility of introducing oxygen into the test solution and thus reduced the chances for erroneous results.

Load Sensing Bolts

The test specimens were stressed with load sensing bolts (see Figure 1). V-blocks were used to maximize loading and thrust bearings were used to minimize torsional effects. The load sensing bolts made it possible to load the specimens with a high degree of accuracy due to the

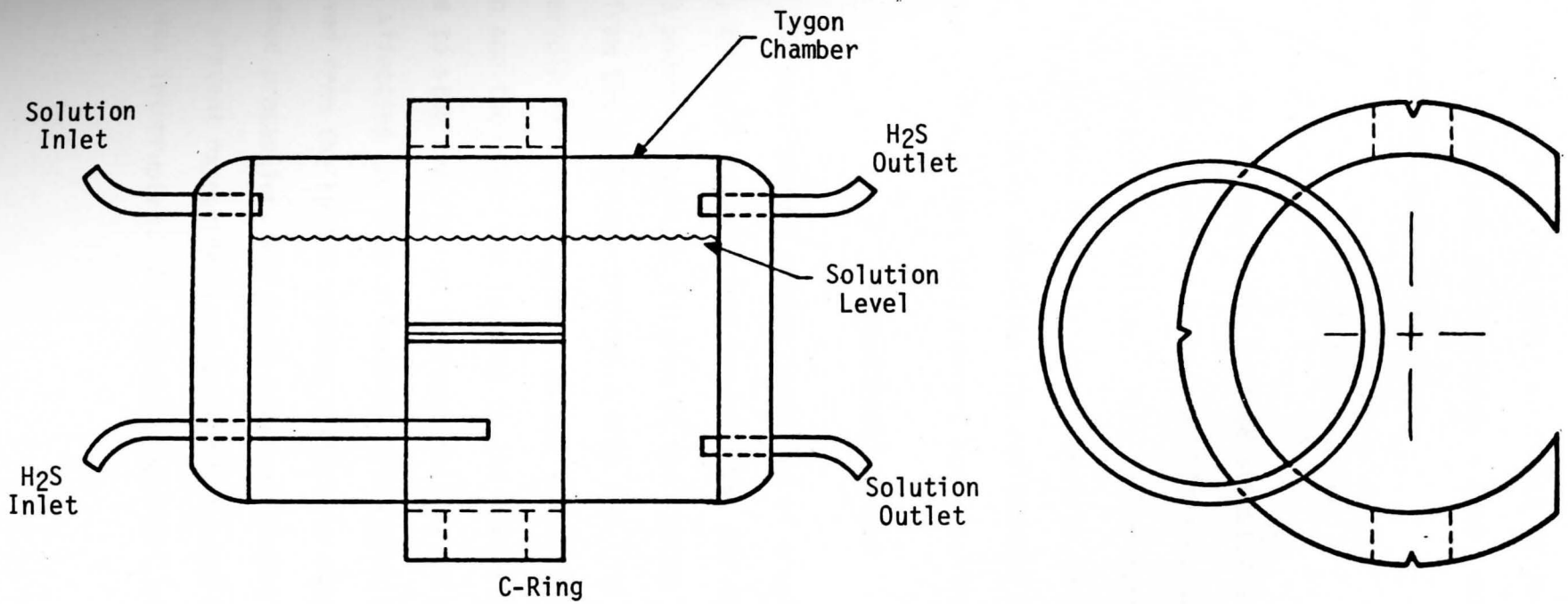

Figure 2. Test Specimen used in Sulfide Stress Cracking Study.

internal strain gages. The bolts also made it possible to monitor the loads without disturbing the specimens - a decrease in the load on the bolt indicated that failure occurred.

Test Solution

The test medium in the sulfide stress cracking tests was an aqueous solution containing 5% sodium chloride, 0.5% acetic acid and saturated with hydrogen sulfide. This is the test solution recommended by NACE for studying the resistance of metals to sulfide stress cracking[33]. The solution simulates the environment found in sour wells - salt water with a slight acid content and dissolved hydrogen sulfide gas.

Experimental System

The experimental system consisted of a cylinder of hydrogen sulfide, the test solution and ten stations for testing specimens. Figure 3 shows a schematic diagram of the system. Hydrogen sulfide flowed from the cylinder, through a trap and into the central manifold. The reservoir in turn had eleven outlet lines, one leading to the test solution and the other ten leading to the test stations. This made it possible to stop the flow of hydrogen sulfide to any part of the system without affecting the flow elsewhere. Thus specimens could be added to or removed from the system without disturbing other tests in progress. As an added precaution, air locks were positioned in all inlet and outlet lines to prevent oxygen from entering the system if the flow of hydrogen sulfide was interrupted. As suggested earlier, oxygen can cause erroneous

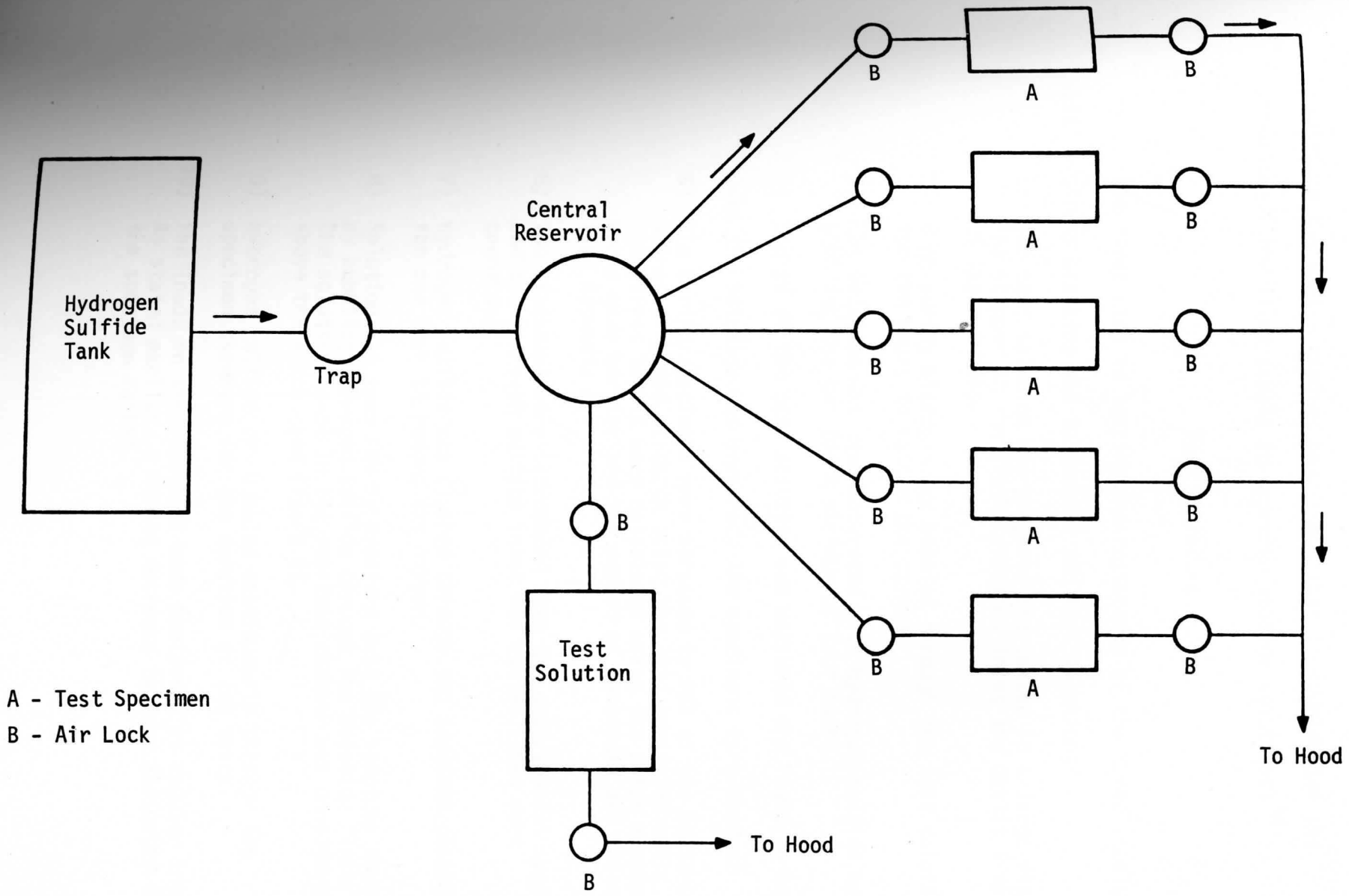

Figure 3. Experimental System used in Sulfide Stress Cracking Study.

results in the test - studies have shown that it accelerates the corrosion of low alloy steels in hydrogen sulfide solutions[34].

Test Procedure

The first step in testing the resistance of the three steels to sulfide stress cracking was to prepare the test solution:

1) The test solution was prepared and sealed in a large flask. The stopper on the flask contained inlet and outlet lines of Tygon tubing.

2) High-purity nitrogen was bubbled through the test solution for two hours to remove the oxygen.

3) The solution was then saturated with hydrogen sulfide by bubbling the gas for a minimum of four hours.

4) The pH of the test solution was measured and found to be 2.7.

Once the solution was prepared, the specimens were tested:

5) The C-ring specimens were stressed to 98% of the measured values of yield strength using the load sensitive bolts. The stress levels were calculated using the notch measurements made earlier and the method of Fernandez and Tisinai[35] (see Appendix A).

6) The specimens were introduced into the experimental system, and the hydrogen sulfide inlet and outlet lines were connected.

7) Hydrogen sulfide was flushed through the specimen chambers for one hour to remove the oxygen.

8) Solution was then fed by pressure into the specimen chambers by bubbling hydrogen sulfide through the solution flask. The solution level in the specimen chamber was considerably above the notch (see Figure 2).

9) Hydrogen sulfide was bubbled continuously through the specimen chambers for the duration of the tests.

10) The loads on the specimens were monitored at regular intervals. As stated earlier, a marked decrease in load indicated that the specimen failed.

11) In seven days, the pH of the solution in the specimen chambers changed from 2.7 to 3.7. Since hydrogen absorption can vary quite markedly with small changes in pH(36), the solution was changed in the chambers every seven days.

12) If the specimens did not fail, they were run for a minimum of 500 hours (about 21 days) before the tests were terminated.

13) After the tests were completed, each specimen was examined for cracks with a low power (20X) microscope.

Crack Propagation Measurements

The kinetics of crack initiation and propagation in the sulfide stress cracking tests were measured on select specimens of the three steels using a Brush Model 240 Recorder. The cracking tests were conducted as described earlier, however, in this case the chart recorder continuously monitored the load on the specimens versus time of exposure in the test.

Metallographic Examination of Cracking Specimens

The C-ring specimens from the sulfide stress cracking tests were sectioned and the transverse plane was mounted in bakelite. The specimens were then prepared for metallographic examination in the same manner used for the heat treated specimens. The metallographic specimens were etched in 2% nital and the general microstructures were examined at 1500X using oil immersion techniques. Finally, crack depth measurements were made on the specimens that had failed.

Examination of Two Stage Carbon Replicas

The etch was removed from the mounted C-ring specimens and the specimens were re-etched, first in 4% picric acid to reveal the carbide particles and then in 2% nital to bring out the general microstructure. Two stage carbon replicas were made of the metallographic specimens.

The preparation of the two stage carbon replicas is outlined below:

1) Pieces of 0.034 mm thick acetylcellulose plastic were cut slightly larger than the surfaces to be replicated and were immersed in acetone.

2) Once softened, the strips were placed on the etched surfaces of the metallographic specimens.

3) After drying, the replicas were stripped from the specimens by lifting one corner at a time until they separated.

4) The replicas were trimmed to size and were attached replication side up to a glass slide with double stick tape.

5) The replicas were shadowed with palladium in a vacuum evaporator. Shadowing was performed at 10^{-5} torrs using a shadow angle of 20°.

6) Carbon was deposited on the replicas to a thickness of ∿200A° in the vacuum evaporator. Again a vacuum of 10^{-5} torrs was used, but in this case the carbon source was positioned 90° from the replica.

7) The replicas were cut into 3 mm squares and placed plastic side down on a 200 mesh copper grid.

8) The two stage replicas were washed in acetone for 45 minutes to separate the plastic portions from the carbon portions.

9) The carbon replicas were washed again in acetone to insure that all of the plastic was removed.

The replicas were examined on the JEM 6A transmission electron microscope using an operating voltage of 50 KV and a magnification of 5600X. Several photomicrographs were taken of representative areas of the replicas for use in the lineal analysis of the carbide particles.

Lineal Analysis of Carbide Particles

The photomicrographs made of the replicated C-ring specimens were enlarged to a magnification of 16,800X (covering an 8-1/2 inch x 11 inch page) and the lineal analysis of the carbides was performed. On each photomicrograph, the number and length of carbide particles that intercepted any of five random lines six inches in length were measured. The measurements were made on five photomicrographs (five different specimen areas) for each material condition. The total number and total length of carbide particles were determined for each set of photomicrographs along with the total line length examined. The values along with the magnification were used to calculate the volume fraction of carbides, the average particle diameter, the number of particles per unit length of line and the mean interparticle spacing for each material condition (see Table 7).

Instrumented Charpy Impact Test

Plate specimens of the three steels were given the same heat treatments as the sulfide stress cracking specimens (see Table 2). Standard Charpy V-notch impact specimens were machined from the plates. The orientation of the specimens was parallel to the rolling direction, as was the case in the C-ring specimens.

Two Charpy impact specimens were tested at both 75°F and -100°F for each material condition. The impact machine was equipped with a Dynatup instrumented tup and an Effects Technology Model 500 System for

obtaining load-time and energy-time curves. Load-time data were also recorded on a transient recorder.

The instrumented Charpy impact test provided considerably more data than the conventional Charpy test. In addition to the standard parameters of energy absorbed, lateral expansion and percent shear fracture, the test gave the energy absorbed at maximum load, i.e., the energy needed to initiate fracture, the time to maximum load, i.e., the time lapsed until fracture initiated and the total time for the impact specimen to fracture[37] (see Table 8). These additional parameters were measured to determine if crack initiation in the impact test could be related to crack initiation in the sulfide stress cracking test.

CHAPTER III

RESULTS

Microstructures

Figures 4 thru 6 show the general microstructures of the three steels in the as quenched condition and after tempering for one hour at each of the temperatures 900°F, 1100°F and 1275°F. In addition, Figures 7 thru 9 show the morphologies of the carbides in the microstructures after the various tempering treatments.

The microstructure of the carbon steel consisted primarily of martensite in the as quenched condition (see Figure 4). Tempering at 900°F resulted in a decomposition of the martensite into ferrite and carbides. Tempering at 1100°F resulted in slightly coarser carbides and tempering at 1275°F produced very distinct particles. The carbides corresponding to each temper treatment were globular in nature (see Figure 7). This morphology[38] and the composition of the steel suggests that the carbides were M_3C. M_3C is an iron rich carbide which has the orthorhombic structure of cementite, but a considerable solubility for Mo, Cr and V[39].

The microstructure of the chromium steel also consisted primarily of martensite in the as quenched condition (see Figure 5). Tempering at 900°F resulted in a microstructure of ferrite and carbides. Little change in microstructure occurred on tempering at 1100°F, but tempering at 1275°F resulted in a more uniform dispersion of particles.

a) 1750°F/1 hr/WQ

b) 1750°F/1 hr/WQ + 900°F/1 hr

c) 1750°F/1 hr/WQ + 1100°F/1 hr

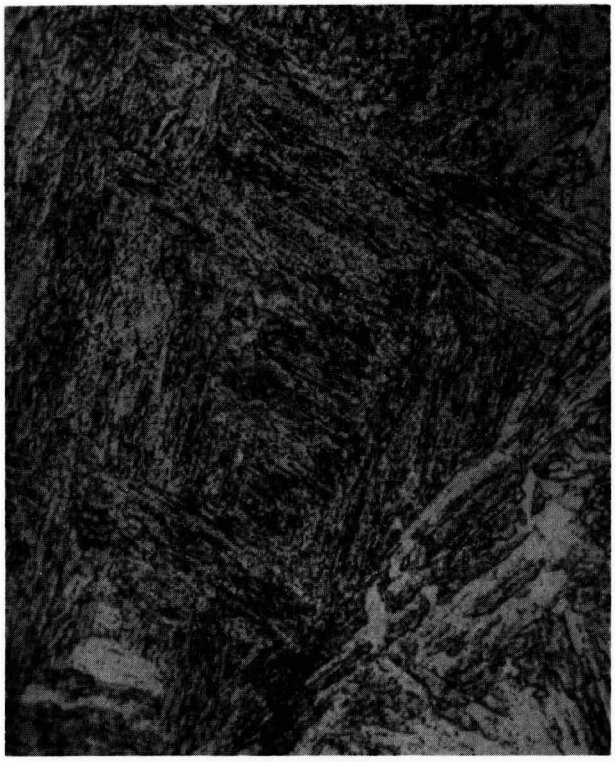

d) 1750°F/1 hr/WQ + 1275°F/1 hr

Figure 4. Microstructures of Carbon Steel Specimens from Heat Treating Study. Etchant 2% Nital. 1200X. Oil Immersion.

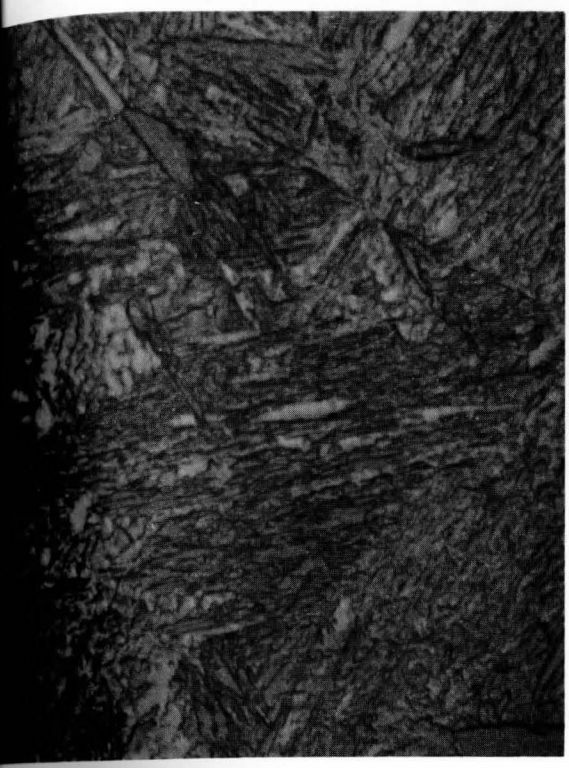

a) 1750°F/1 hr/WQ

b) 1750°F/1 hr/WQ + 900°F/1 hr

c) 1750°F/1 hr/WQ + 1100°F/1 hr

d) 1750°F/1 hr/WQ + 1275°F/1 hr

Figure 5. Microstructures of Chromium Steel Specimens from Heat treating study. Etchant 2% Nital. 1200X. Oil Immersion.

a) 1750°F/1 hr/WQ

b) 1750°F/1 hr/WQ + 900°F/1 hr

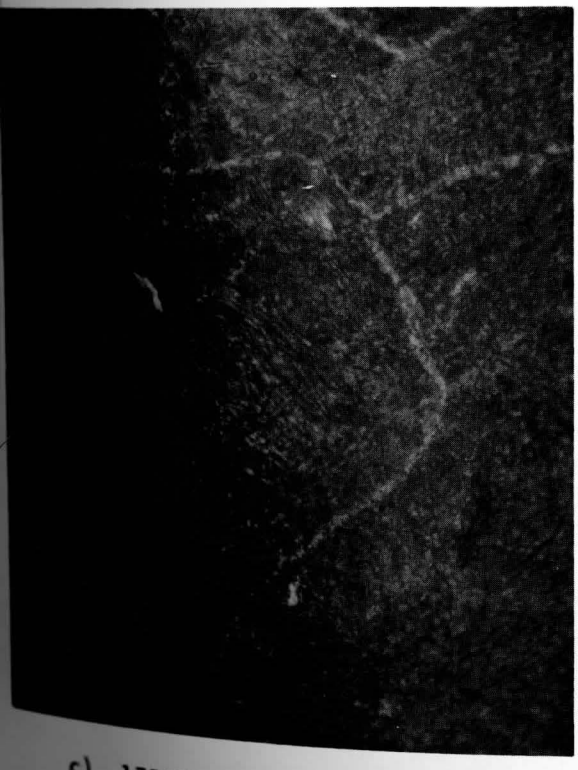

c) 1750°F/1 hr/WQ + 1100°F/1 hr

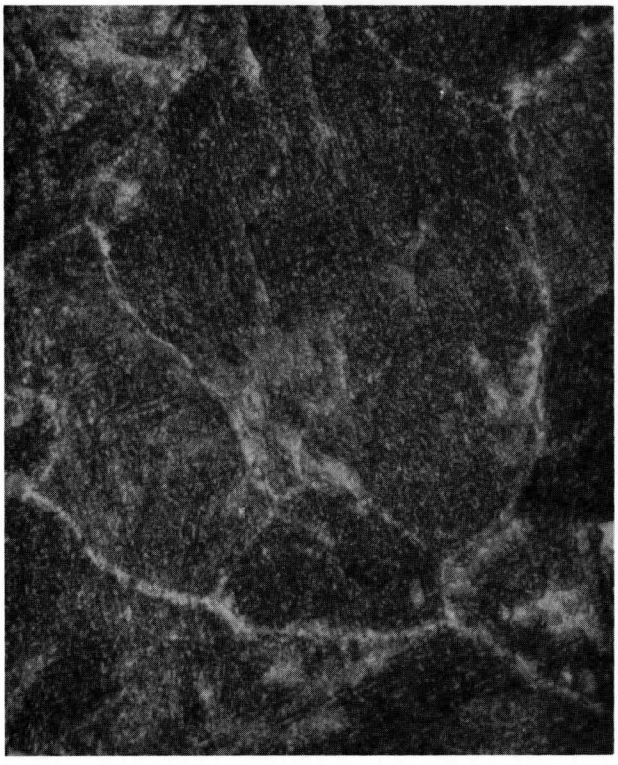

1750°F/1 hr/ WQ + 1275°F/1 hr

Figure 6. Microstructures of Vanadium Steel Specimens from Heat Treating Study. Etchant 2% Nital. 1200X. Oil Immersion.

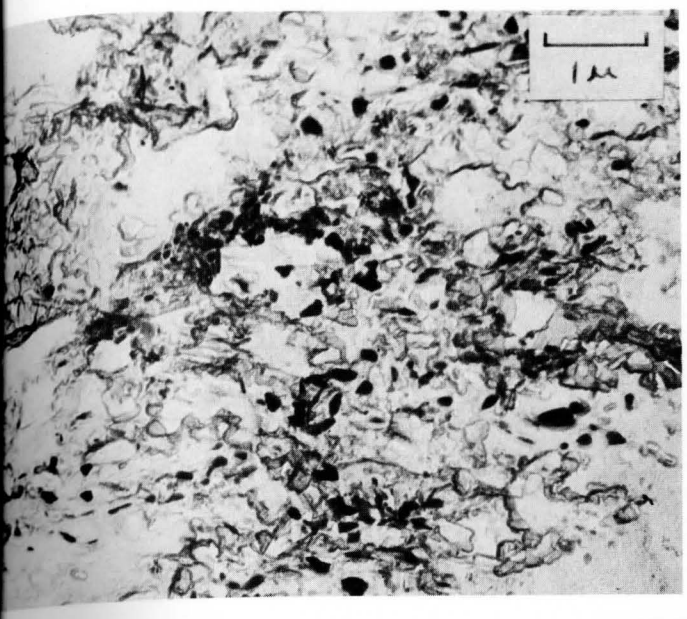

a) 1750°F/1 hr/WQ + 900°F/1 hr.
Globular M_3C Particles.

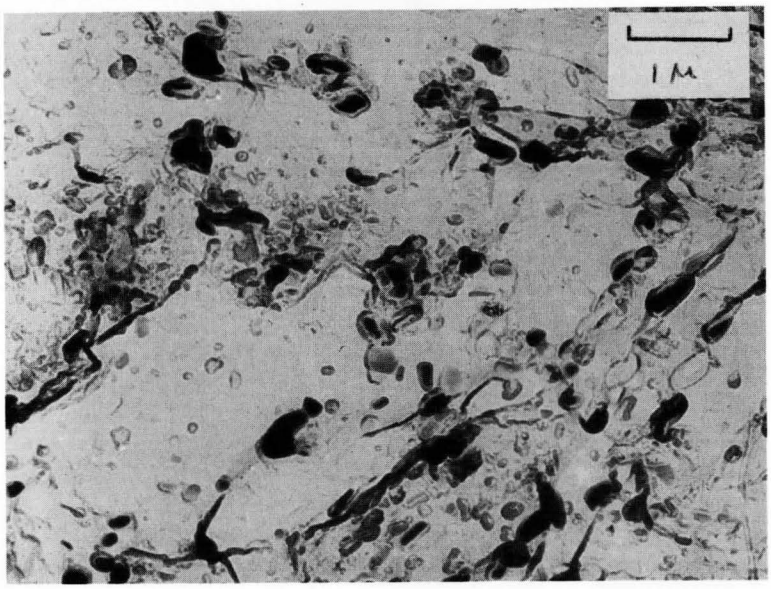

b) 1750°F/1 hr/WQ + 1100°F/1 hr.
Globular M_3C Particles.

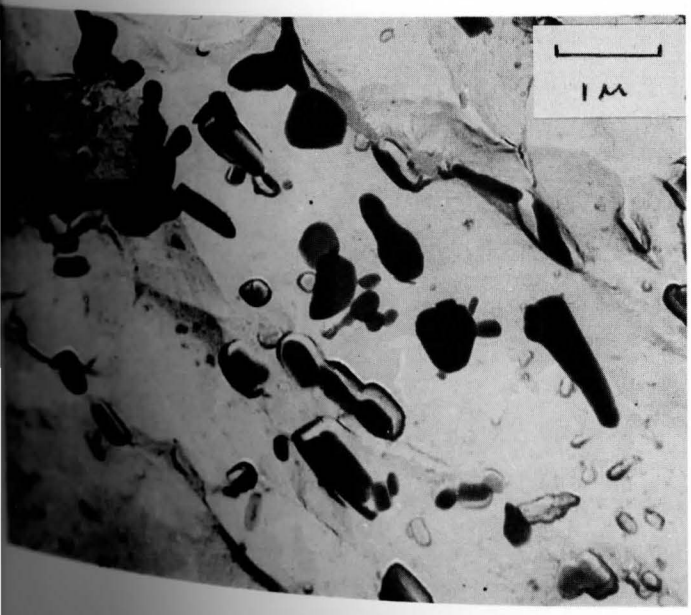

c) 1750°F/1 hr/WQ + 1275°F/1 hr.
Globular M_3C Particles.

Figure 7. Carbides in Carbon Steel Specimens from Heat Treating Study. Carbon Extraction Replicas. 14,000X.

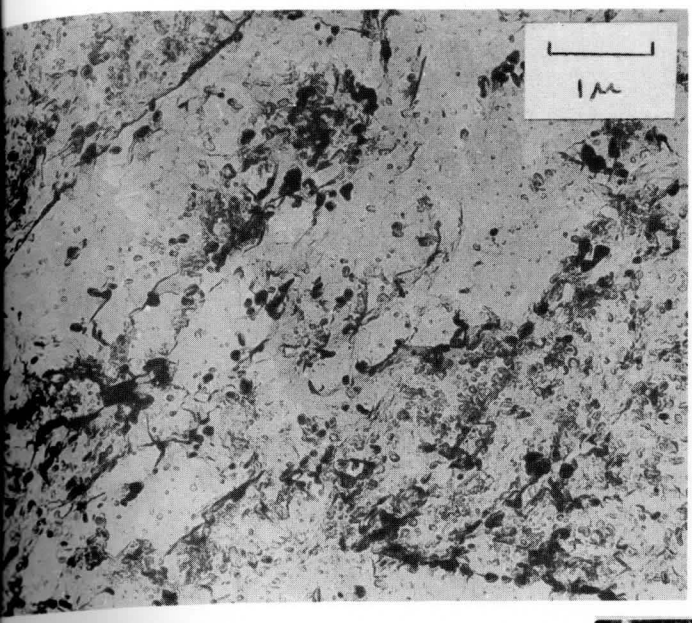

a) 1750°F/1 hr/WQ + 900°F/1 hr. Globular M_3C Particles.

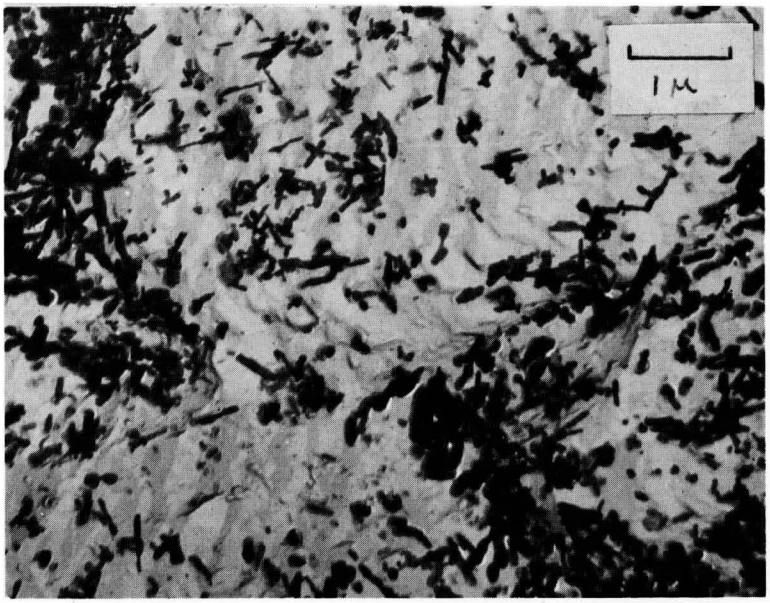

b) 1750°F/1 hr/WQ + 1100°F/1 hr. Globular M_3C and Fine Rods of M_7C_3.

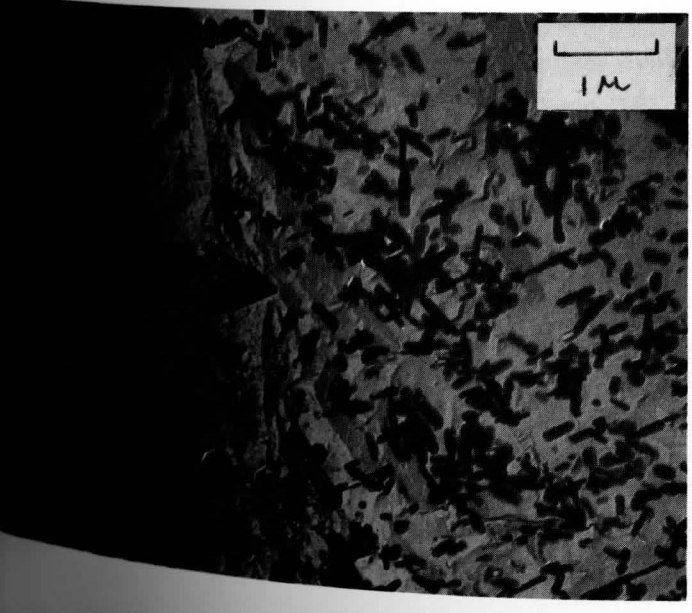

c) 1750°F/1 hr/WQ + 1275°F/1 hr. Globular M_3C and Well Developed Rods of M_7C_3.

Figure 8. Carbides in Chromium Steel Specimens from Heat Treating Study. Carbon Extraction Replicas. 14,000X.

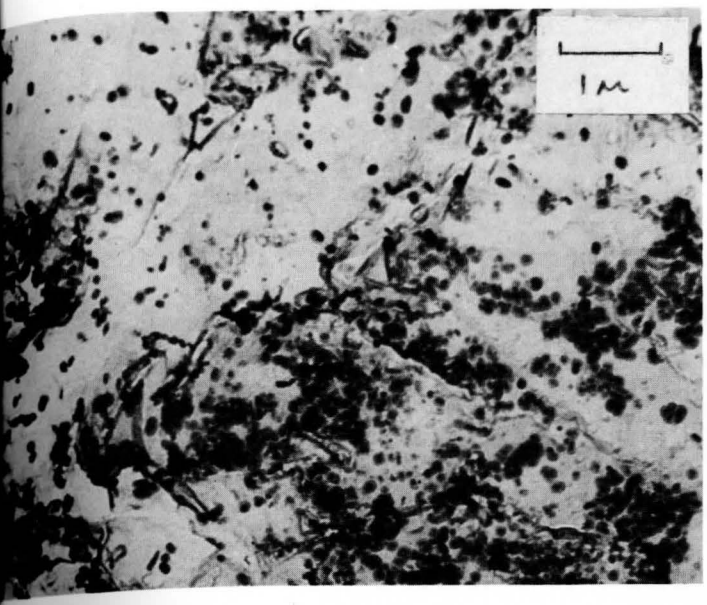

a) 1750°F/1 hr/WQ + 900°F/1 hr. Globular M_3C Particles.

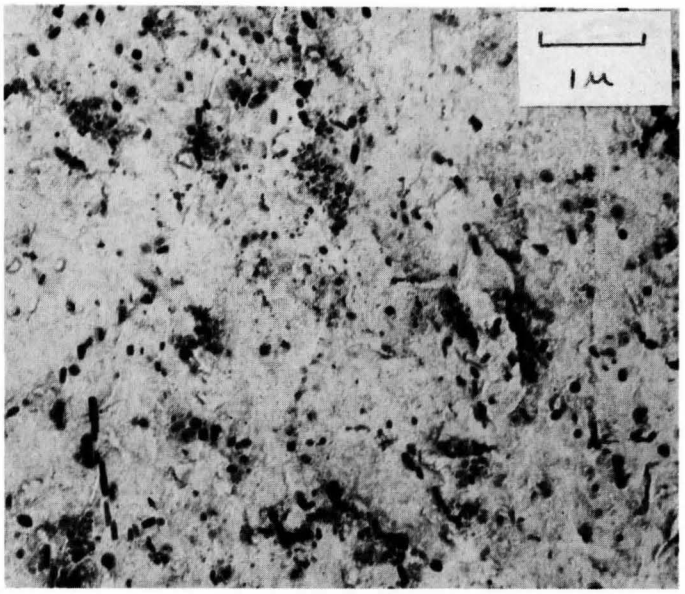

b) 1750°F/1 hr/WQ + 1100°F/1 hr. Globular M_3C and Very Fine Particles of V_4C_3.

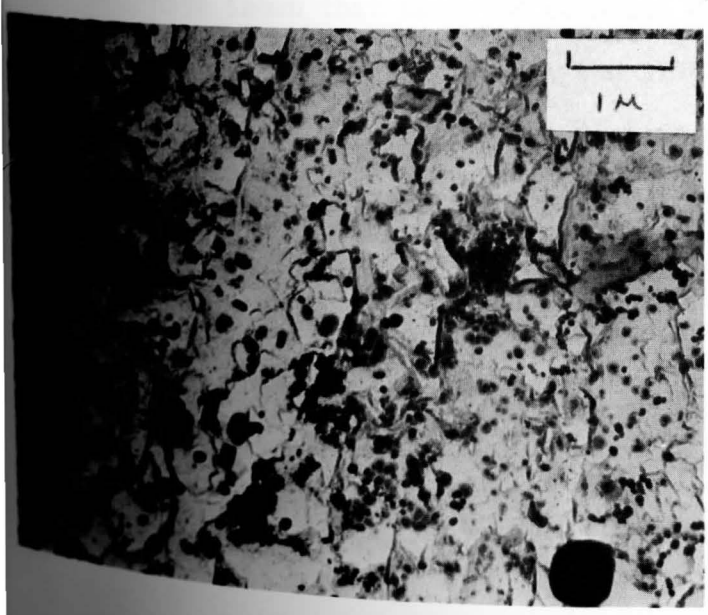

c) 1750°F/1 hr/WQ + 1275°F/1 hr. Globular M_3C and Fine Particles of V_4C_3.

Figure 9. Carbides in Vanadium Steel Specimens from Heat Treating Study. Carbon Extraction Replicas. 14,000X.

As was the case in the carbon steel, the carbides present after tempering at 900°F were globular (see Figure 8), and thus were presumably M_3C. However, at 1100°F small rod shaped particles were visible and the change in microstructure at 1275°F corresponded to the precipitation of considerable quantities of these carbides. The rod shaped morphology is characteristic of M_7C_3[40]. M_7C_3 is a chromium rich carbide which has the trigonal structure of Cr_7C_3, but a high solubility for Fe and Mn[41].

The microstructural observations for the chromium steel are in agreement with investigations made by Sato and coworkers on a similar steel. This work showed that M_3C precipitates during tempering for temperatures up to ~1100°F. At higher temperatures the M_7C_3 carbide forms at the expense of M_3C[42].

The microstructure of the vanadium steel also consisted primarily of martensite in the as quenched condition (see Figure 6). However, unlike the other two steels, large carbides were present in the martensite. These particles did not result from autotempering, but instead were vanadium carbides that did not dissolve during austenitizing. Studies[43] have shown that vanadium carbides go into solution over a range of austenitizing temperatures and 1750°F (the austenitizing temperature used in the present study) was not high enough to dissolve all of the carbides. Subsequent tempering at 900°F resulted in a fine dispersion of carbides in ferrite. However, tempering at 1100°F produced a marked change in microstructure - the particles within the grains were finer and other particles precipitated at the prior austenite grain boundaries. Little subsequent change occurred in microstructure on tempering at 1275°F. As was the case in the other two steels, the carbides present

after tempering at 900°F were globular (see Figure 9) and thus were presumably M_3C. The change in microstructure at 1100°F, however, corresponded to the precipitation of extremely fine (<.01μ), regularly shaped particles. The morphology and size of the particles suggest that the carbides were V_4C_3[44-45]. V_4C_3 has an NaCl cubic structure and is basically VC, but the composition limit extends to V_4C_3 by the formation of a defect lattice[46].

The microstructural observations for the vanadium steel are also in agreement with investigations made by Sato on a similar steel. This work showed that M_3C precipitates during tempering for temperatures up to ~900°F. At higher tempering temperatures V_4C_3 forms at the expense of M_3C[47].

Grain Size Measurements

Table 3 lists the mean linear grain intercept and the corresponding ASTM grain size of the three steels austenitized at 1750°F. A sample calculation is presented in Appendix B along with the raw data. The data

TABLE 3

GRAIN SIZE OF THE STEELS AFTER AUSTENITIZING AT 1750°F

Material	Mean Linear Intercept (in)	Approximate ASTM Grain Size Number
Carbon Steel	.00165	6.00
Cr Steel	.00175	5.75
V Steel	.00145	6.25

of Table 3 show that the three steels had nearly the same grain size after austenitizing at 1750°F. The slightly finer grain size in the vanadium steel was expected because the undissolved carbides pin migrating grain boundaries and thus retard grain growth[48].

Heat Treating Response

The results of the hardness measurements made on the heat treated specimens of the three steels are shown in Figure 10 as characteristic tempering curves. Several important points are evident from these curves:

1) In the as quenched condition, the vanadium steel had a lower hardness than the carbon and chromium steels.

2) During tempering, neither the chromium nor the vanadium steels softened as much as the carbon steel.

3) The carbon and chromium steels both exhibited a continuous decrease in hardness with increasing tempering temperature, while the vanadium steel exhibited secondary hardening.

The microstructural examination of the specimens provided explanations for the response of the steels to heat treating. The lower hardness of the vanadium steel in the as quenched condition was associated with the large undissolved vanadium carbides (see Figure 9). The fact that the chromium and vanadium steels did not soften as much as the carbon steel on tempering was related to the finer dispersions of carbides in these materials (compare Figures 7, 8 and 9). In addition, the phenomenon of secondary hardening in the vanadium steel was associated with the precipitation of fine V_4C_3 particles throughout the matrix (see Figure 9).

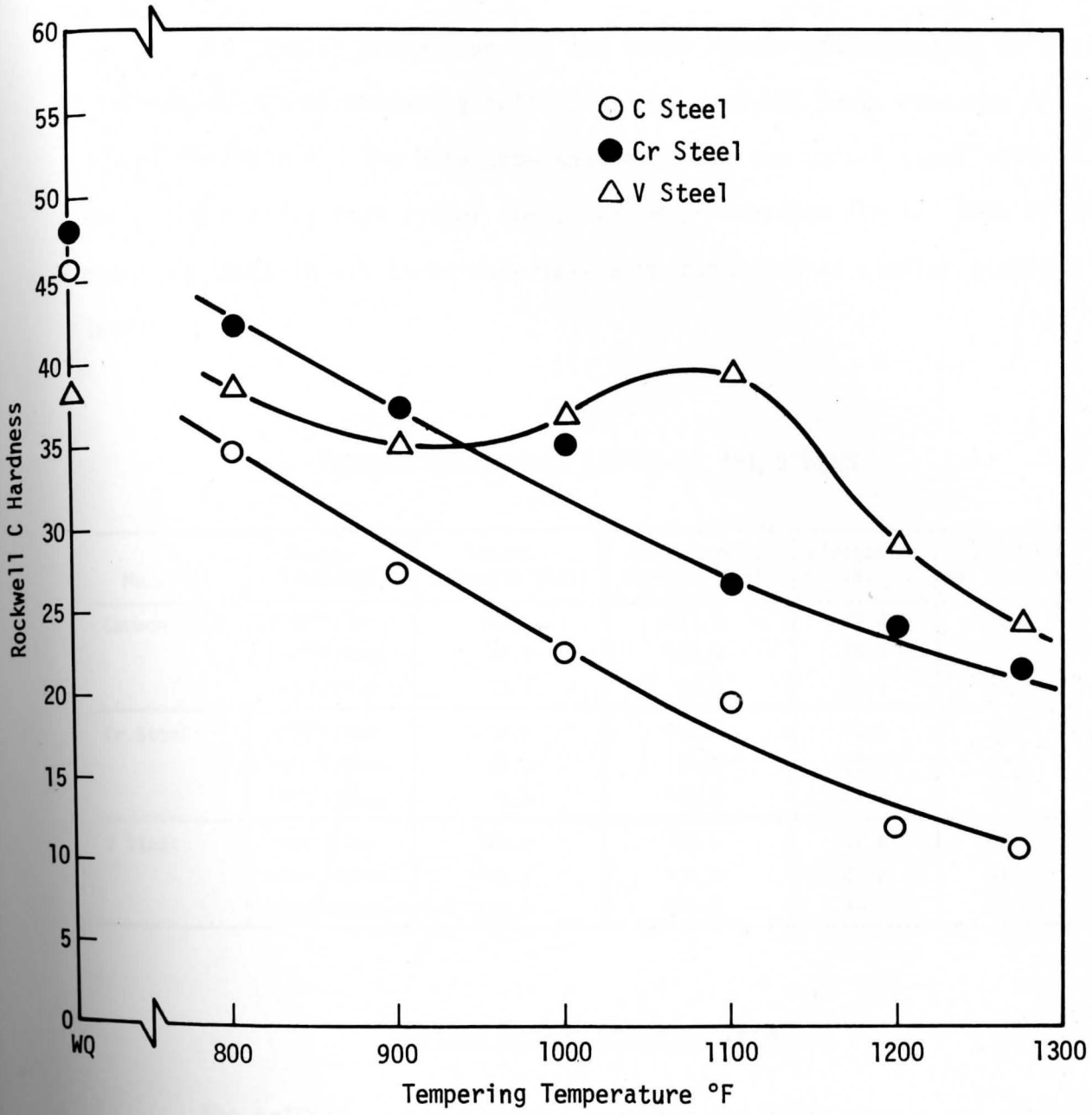

Figure 10. Tempering Curves for the Steels.

Tensile Properties

The tensile properties for the three steels corresponding to the strength levels at which the sulfide stress cracking tests were run are listed in Table 4. The data show that although the carbon steel softened more rapidly than either the chromium or vanadium steels, some of the cracking tests in all three materials were conducted at similar strength levels.

TABLE 4

TENSILE PROPERTIES (75°F) OF THE STEELS

Material	Temper Treatment	Yield Strength (ksi)	Ult. Tensile Strength (ksi)	Elongation (%)	Reduction of Area (%)
Carbon Steel	1100°F/1hr	100.6	119.9	21.0	65.0
	1175°F/2hrs	84.0	104.3	25.0	68.0
	1250°F/1hr	73.1	94.9	27.5	70.2
Cr Steel	1250°F/1hr	107.0	127.5	15.5	50.7
	1300°F/2hrs	82.8	104.6	22.5	63.6
	1320°F/2hrs	73.8	100.8	23.0	53.4
V Steel	1250°F/1hr	148.5	153.5	17.5	57.1
	1275°F/2hrs	119.6	131.4	21.0	61.5
	1300°F/2hrs	107.1	129.6	19.5	60.4

Sulfide Stress Cracking Data

The sulfide stress cracking data for the three steels are presented in Table 5. The data include:

1) The strength level at which each specimen was tested.

2) Whether or not each specimen failed.

TABLE 5

SULFIDE STRESS CRACKING DATA FOR THE STEELS

Material	Yield Strength (ksi)	Specimen	Test Results	Ratio of Crack Depth to Wall Thickness (mils)
Carbon Steel	100.6	1	F. between 1.7-17.1 hrs	160/185
		2	F. between 1.7-17.1 hrs	119/198
		3	F. between 3.4-17.3 hrs+	144/170
	84.0	1	NF in 500 hrs	---
		2	NF in 500 hrs	---
		3	NF in 500 hrs	---
	73.1	1	NF in 500 hrs	---
		2	NF in 500 hrs	---
		3	NF in 500 hrs	---
Cr Steel	100.0	1	F. between 1.9-17.6 hrs	186/205
		2	F. between 1.9-17.6 hrs	180/208
		3	F. between 0.6-18.9 hrs+	186/210
	82.8	1	F. between 5.0-21.0 hrs	120/216
		2	NF in 500 hrs	---
		3	NF in 500 hrs	---
	73.8	1	F. between 1.9-16.6 hrs	177/210
		2	NF in 500 hrs	---
		3	NF in 500 hrs	---
V Steel	148.5	1	F. between 1.7-17.0 hrs	197/212
		2	F. between 1.7-17.0 hrs	180/224
		3	F. between 0.3-16.2 hrs+	188/212
	119.6	1	F. between 1.2-22.6 hrs	175/225
		2	F. between 75.4-96.8 hrs	195/210
		3	F. between 1.2-10.5 hrs+	182/202
	107.1	1	F. between 1.9-17.6 hrs	175/212
		2	F. between 1.9-17.6 hrs	145/213
		3	F. between 1.4-14.3 hrs+	115/220

F = failure
NF = no failure
+crack propagation specimens

3) The approximate failure time, or time the cracking test was terminated if failure did not occur. It must be stressed that the failure time interval represents actual crack propagation times only for the indicated specimens. In all other cases, the failure time interval represents the last time that the load on the specimen was constant and the first time that failure was discovered.

4) The ratio of crack depth to wall thickness for each specimen that failed.

The sulfide stress cracking data of Table 5 show several important points:

1) In general, the resistance of the three steels to sulfide stress cracking increased with decreasing strength level.

2) Tempering at high temperatures increased the resistance to cracking in the carbon and chromium steels, but not in the vanadium steel.

3) In all cases the failure times were relatively short.

4) The cracks propagated beyond midwall before relaxing.

Failure occurred by large non-branched cracks in all specimens, which is typical of hydrogen embrittlement[49]. In the carbon and chromium steels, the cracks were singular in nature and ran perpendicular to the OD surface of the C-rings. However, more than one crack was often found in the vanadium steel specimens and the cracks ran at an angle to the OD surface. This occurred mostly at the highest strength level (YS∿148 ksi), where presumably the resistance to sulfide stress cracking was so low that more than one crack initiated. Figures 11 thru 15 show examples of the cracks in the C-ring specimens.

The non-branched nature of the cracks in the three steels made optical identification of the fracture path impossible. However, studies have shown that both transgranular and intergranular cracking can occur with hydrogen embrittlement[50].

Figure 11. Crack in Carbon Steel C-Ring Specimen Corresponding to Yield Strength 100.6 ksi. Failed Between 3.4-17.3 Hours. Unetched 10X.

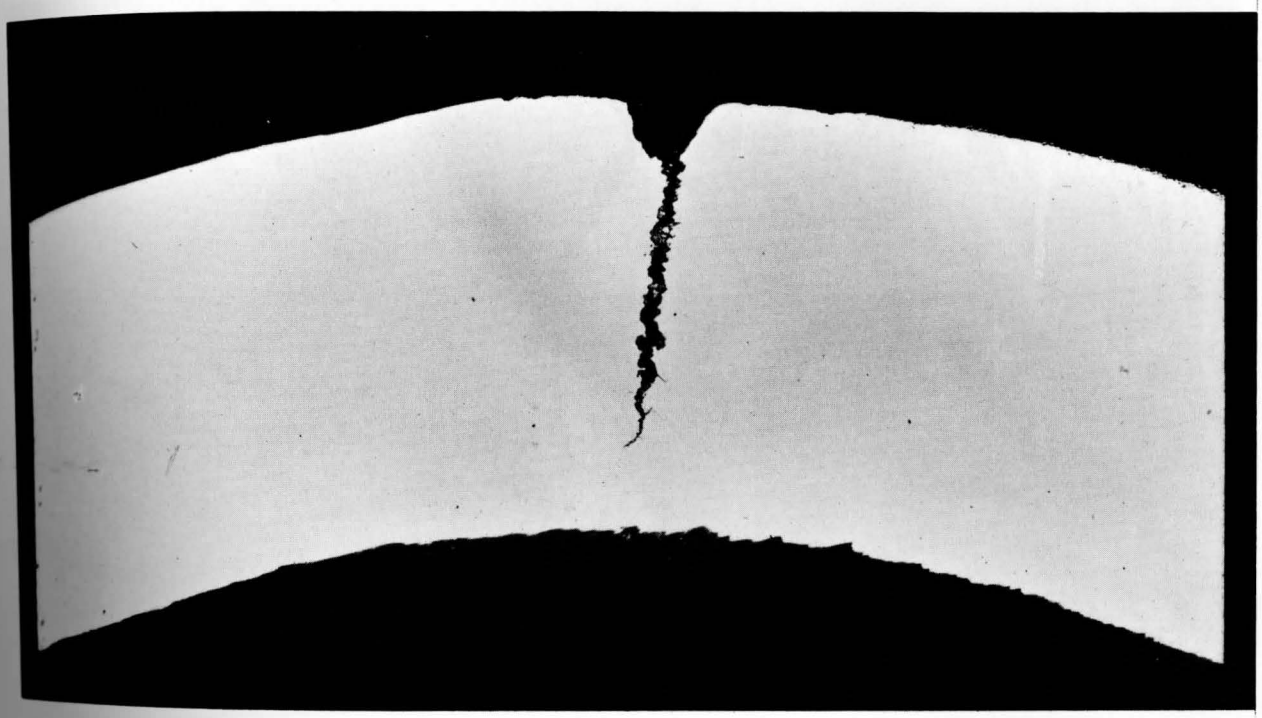

Figure 12. Crack in Chromium Steel C-Ring Specimen Corresponding to Yield Strength 100.0 ksi. Failed Between 0.6-18.9 Hours. Unetched 10X.

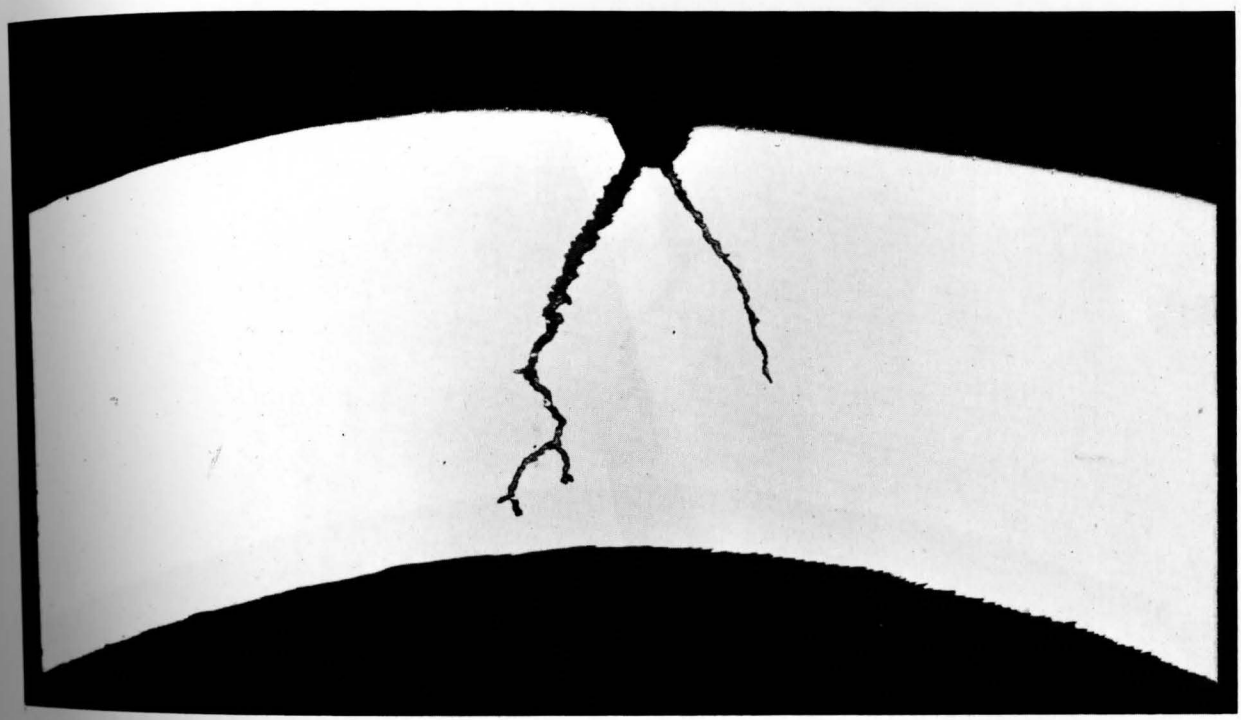

Figure 13. Cracks in Vanadium Steel C-Ring Specimen Corresponding to Yield Strength 148.5 ksi. Failed Between 0.3-16.3 Hours. Unetched 10X.

Figure 14. Crack in Vanadium Steel C-Ring Specimen Corresponding to Yield Strength 119.6 ksi. Failed Between 1.2-10.3 Hours. Unetched 10X.

Figure 15. Crack in Vanadium Steel C-Ring Specimen Corresponding to Yield Strength 107.1 ksi. Failed Between 1.4-14.3 Hours. Unetched 10X.

Cracking Susceptibility Factors

The data in Table 5 were used to calculate a cracking susceptibility factor for each material condition. The factor, S, derived by Gottschling and Ayres[51] is given by:

$$S = \frac{1}{n} \sum_{i=1}^{n} \left(\frac{r}{t}\right)_i \qquad (4)$$

where n = total number of specimens tested
t = earliest possible time of failure (hrs)
r = ratio of measured yield strength to applied stress.

The factor S has a lower limit of zero for the case where no specimens fail and increases with increasing susceptibility to cracking.

The calculated susceptibility factors for the three steels are listed in Table 6. A sample calculation is shown in Appendix C. It must be stressed that the values of S are subject to scatter due to the small

TABLE 6

CRACKING SUSCEPTIBILITY FACTORS FOR THE STEELS

Material	Yield Strength (ksi)	S
Carbon Steel	100.6	0.492
	84.0	0
	73.1	0
Cr Steel	100.0	0.537
	82.8	0.068
	73.0	0.179
V Steel	148.5	0.923
	119.6	0.442
	107.1	0.537

number of samples tested at each strength level and the inaccuracy in determining failure times. However, the values were useful in studying if correlations existed between the cracking susceptibility and either the carbide parameters or the Charpy impact properties for the three steels.

Crack Propagation Measurements

Figures 16 thru 20 show the results of the crack propagation measurements made using the continuous chart recorder on the C-ring specimens:

1) Carbon steel - yield strength 100.6 ksi
2) Cr steel - yield strength 100.0 ksi
3) V steel - yield strengths 148.5 ksi, 119.6 ksi and 107.1 ksi.

The data show several important points about crack initiation and propagation in the sulfide stress cracking test:

1) In all specimens, the failure process consisted of a finite period prior to crack initiation and a period of relatively slow crack propagation.
2) The period prior to crack initiation, i.e., the incubation time, was relatively short, ranging from 0.3-3.4 hours.
3) The period of slow crack propagation was quite long, ranging from 9.1 to 18.3 hours.
4) There was evidence of stepwise crack propagation in some specimens - the crack appeared to arrest for a finite time and then began to propagate again.

Thus the crack propagation measurements not only suggest that an incubation period preceded the onset of cracking in the C-ring specimens, but also that failure occurred by a discontinuous process.

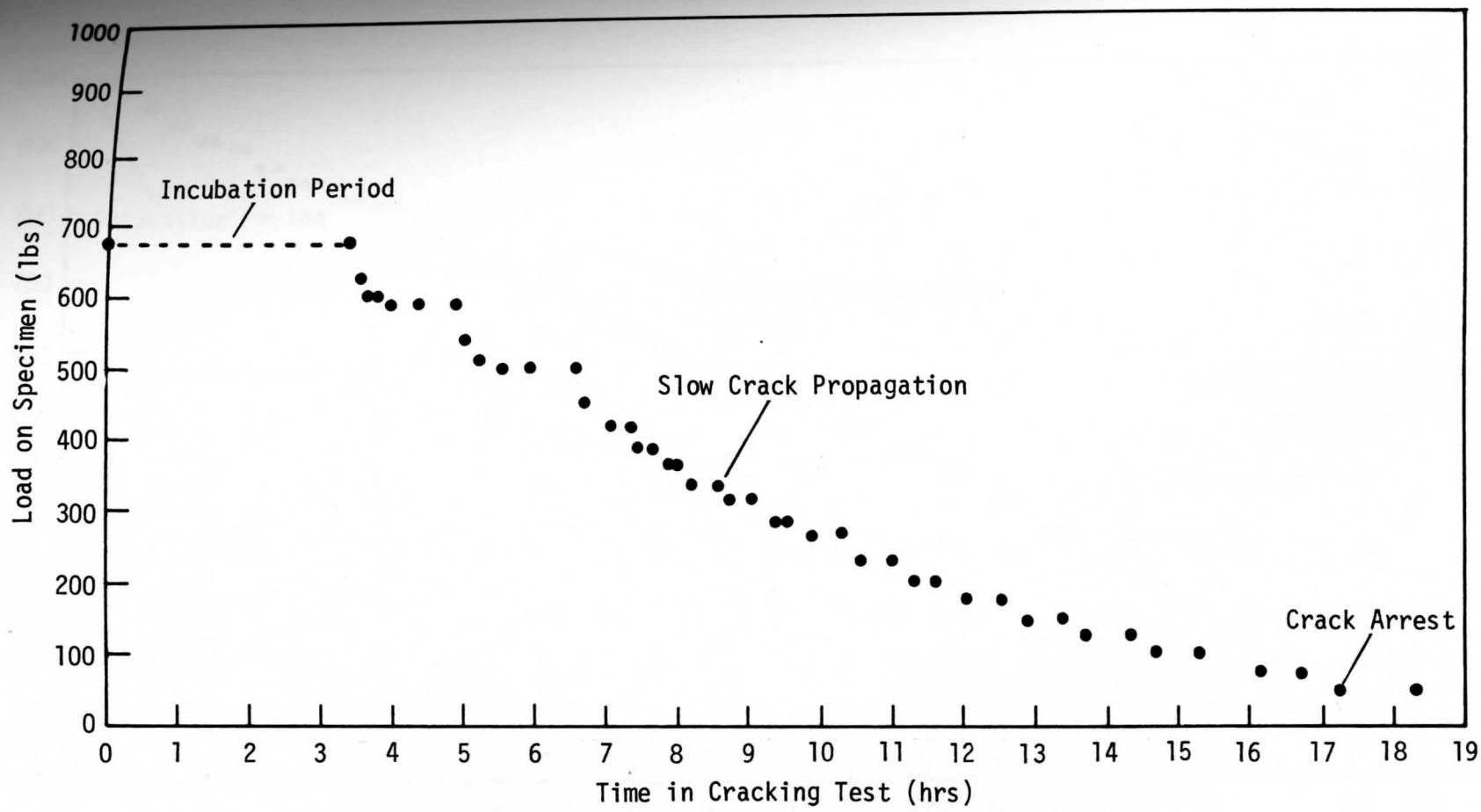

Figure 16. Load-Time Curve for Carbon Steel Specimen Corresponding to Yield Strength 100.6 ksi.

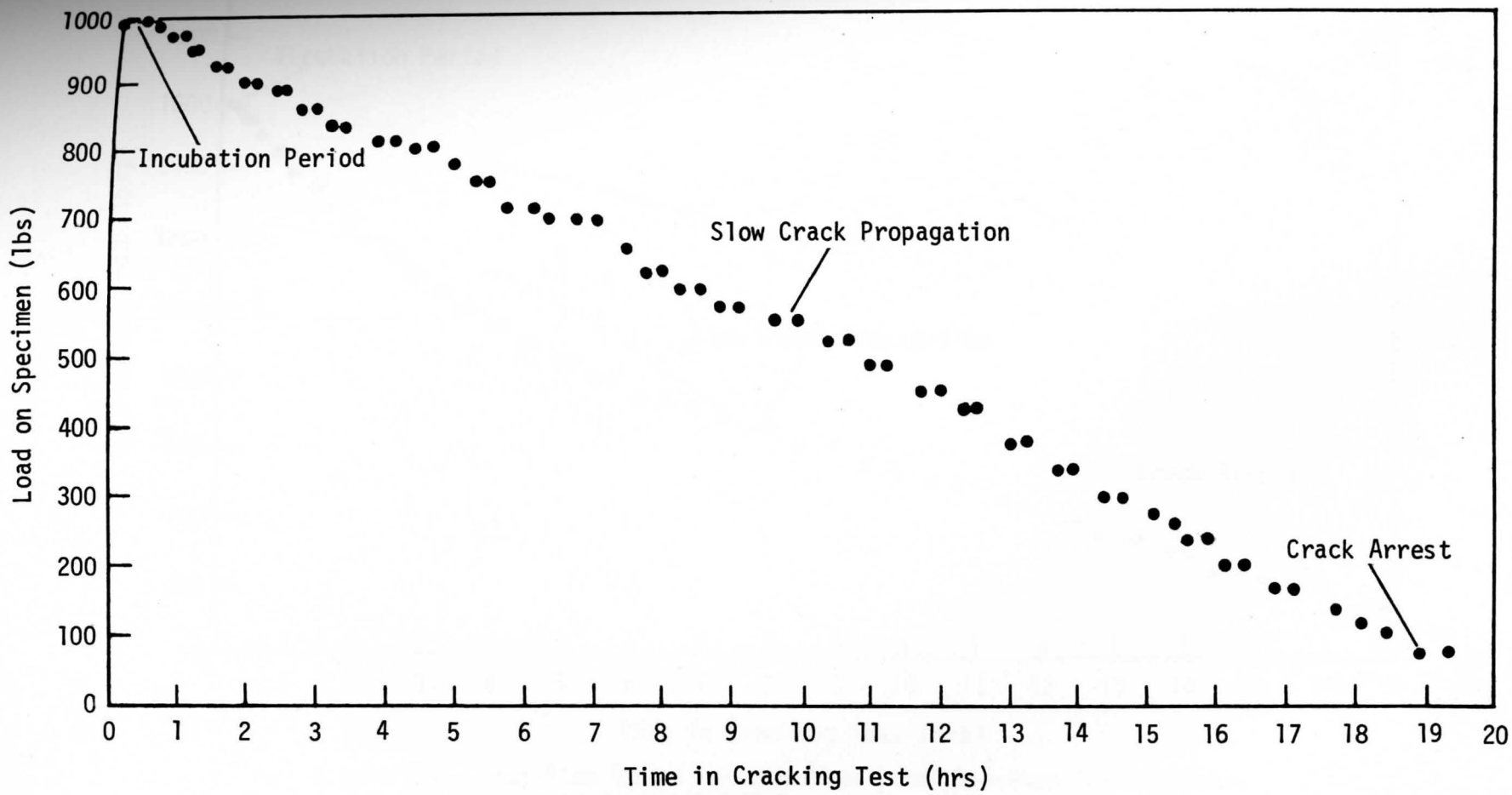

Figure 17. Load-Time Curve for Chromium Steel Specimen Corresponding to Yield Strength 100.0 ksi.

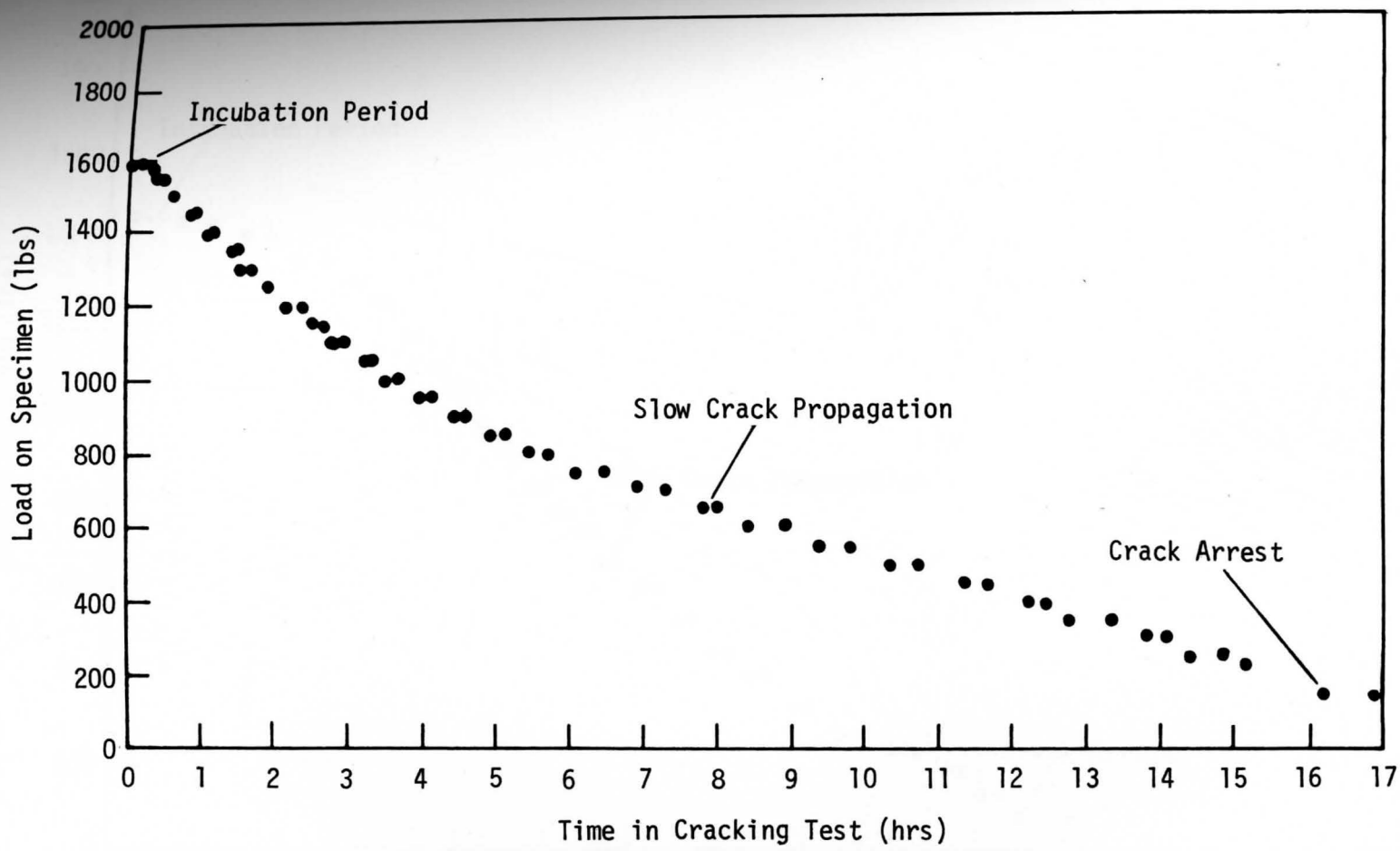

Figure 18. Load-Time Curve for Vanadium Steel Specimen Corresponding to Yield Strength 148.5 ksi.

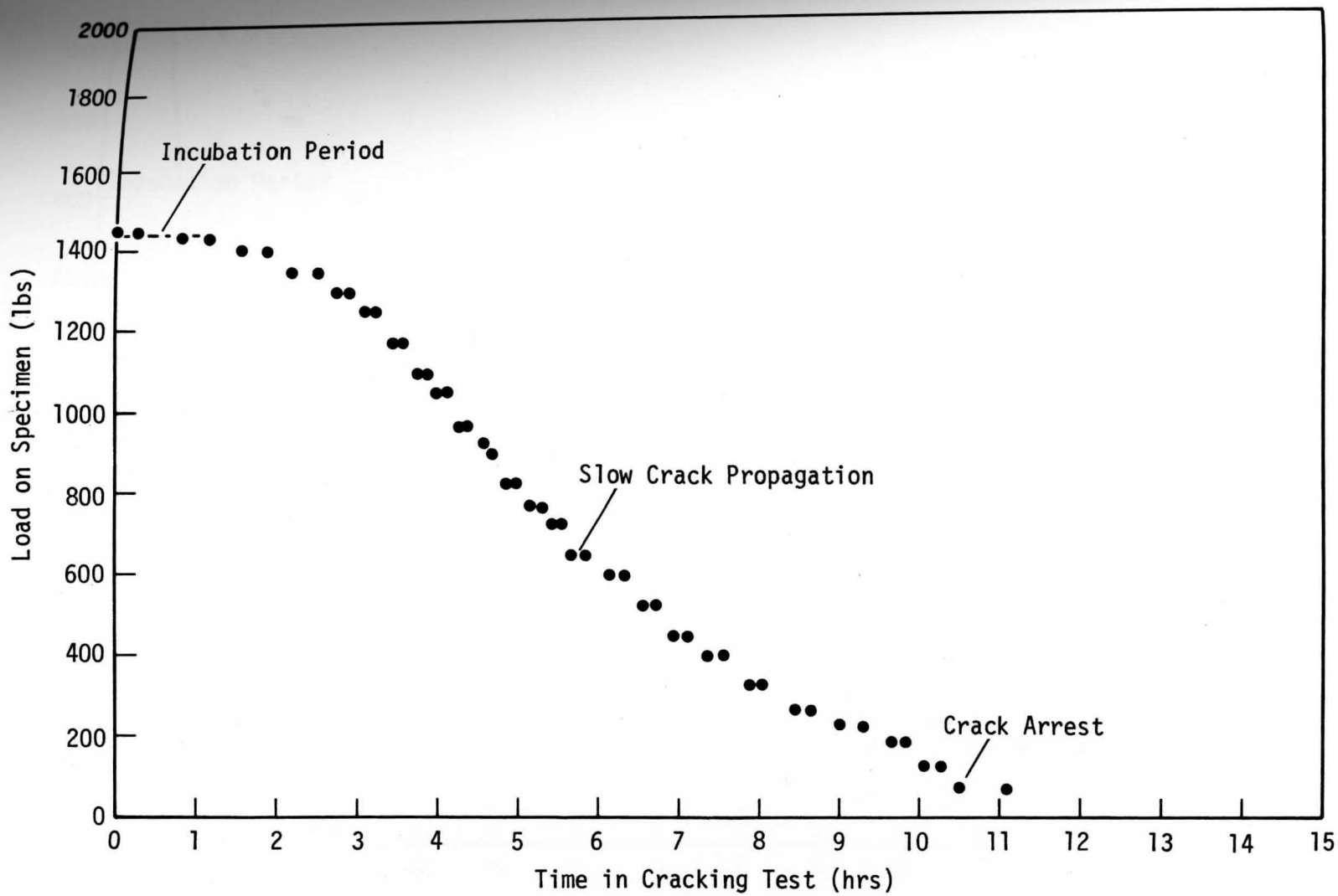

Figure 19. Load-Time Curve for Vanadium Steel Specimen Corresponding to Yield Strength 119.6 ksi.

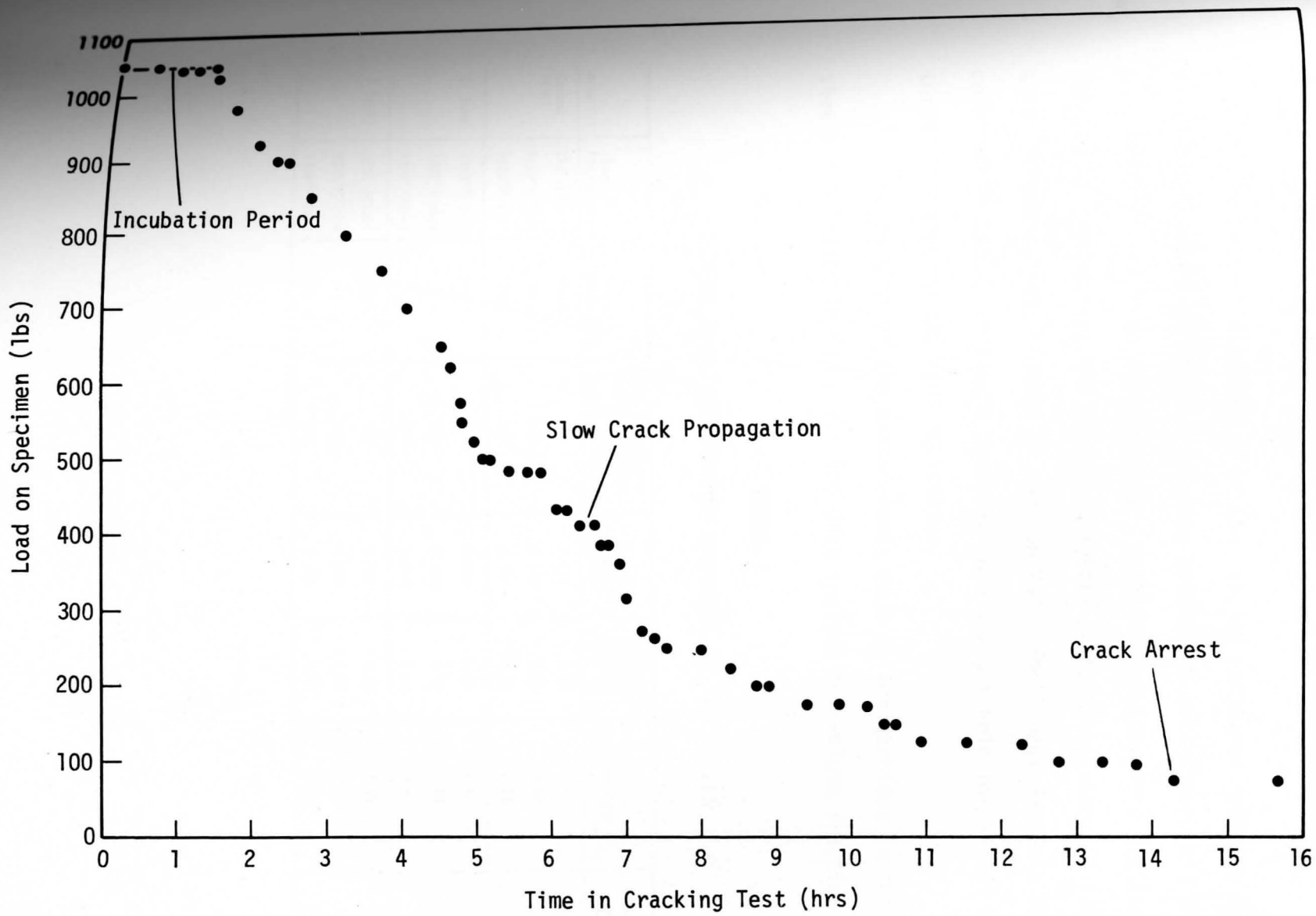

Figure 20. Load-Time Curve for Vanadium Steel Specimen Corresponding to Yield Strength 107.1 ksi.

Correlation of Cracking Resistance With Microstructure

The optical examination of the samples sectioned from the C-ring specimens showed a general correlation between microstructure and cracking resistance for the three steels. When the carbides were distinct throughout the matrix, the steels exhibited a high resistance to sulfide stress cracking (see Figures 21 through 23). The lineal analysis of the carbides in the three steels provided more insight into the effect of these particles on cracking resistance.

The results of the measurements made on the carbides in the three steels are listed in Table 7. The data include the volume fraction of

TABLE 7

LINEAL ANALYSIS DATA OF CARBIDES IN THE STEELS

Material	Temper Treatment	Yield Strength (ksi)	Ratio of Failures in Cracking Tests to Total Specimens Tested	Volume Fraction of Carbides	Average Particle Diameter ($\times 10^{6}$ in.)	Number of Particles per Unit Length of Line ($\times 10^{-4}$ in.$^{-1}$)	Mean Interparticle Spacing ($\times 10^{5}$ in.)
Carbon Steel	110°F/1hr	100.6	3/3	0.137	5.88	3.50	2.47
	1175°F/2hrs	84.0	0/3	0.166	8.53	2.92	2.86
	1250°F/1hr	73.1	0/3	0.189	10.38	2.73	2.97
Cr Steel	1250°F/1hr	100.0	3/3	0.134	4.32	4.63	1.87
	1300°F/2hrs	82.8	1/3	0.172	6.63	3.88	2.13
	1320°F/2hrs	73.0	1/3	0.149	7.14	3.13	2.72
V Steel	1250°F/1hr	148.5	3/3	0.106	3.63	4.36	2.05
	1275°F/2hrs	119.6	3/3	0.103	4.89	3.14	2.86
	1300°F/2hrs	107.1	3/3	0.112	5.69	2.95	3.01

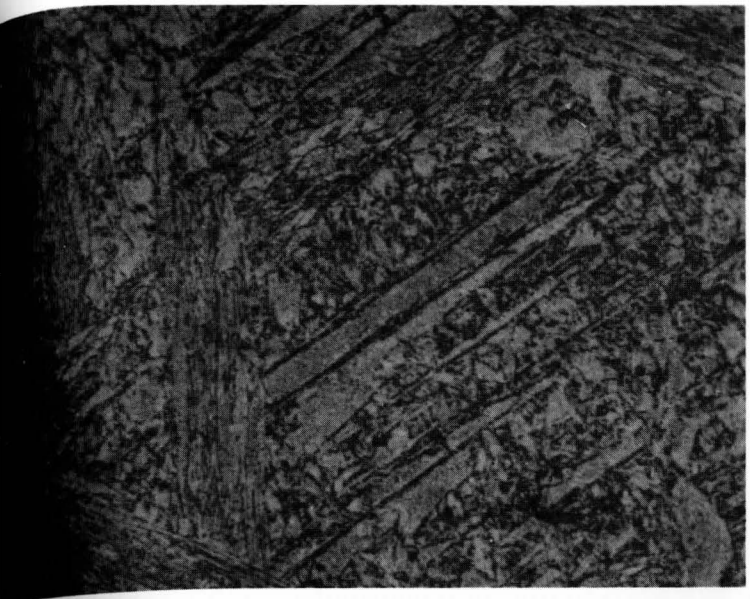

a) Yield Strength 100.6 ksi. Carbides Becoming Visible. All Three Specimens Failed.

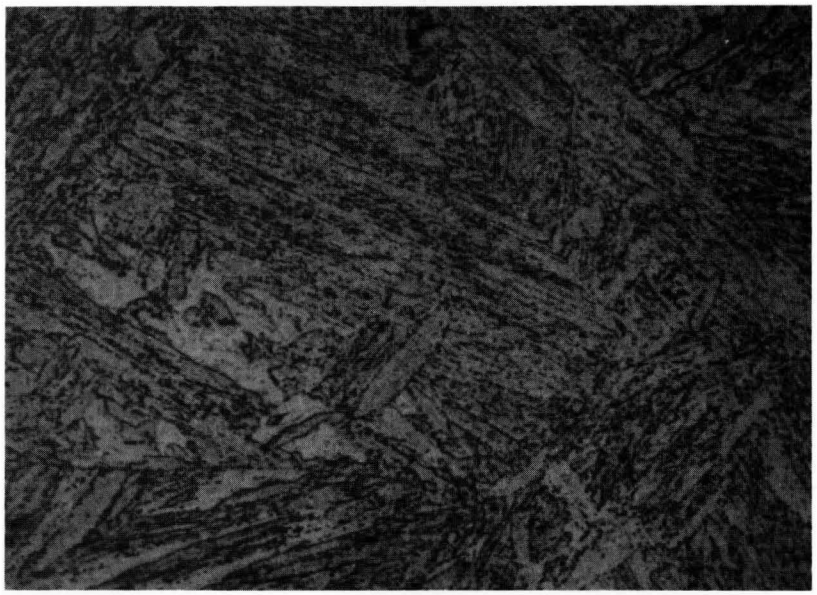

b) Yield Strength 84.0 ksi. Carbides Distinct. None of the Specimens Failed.

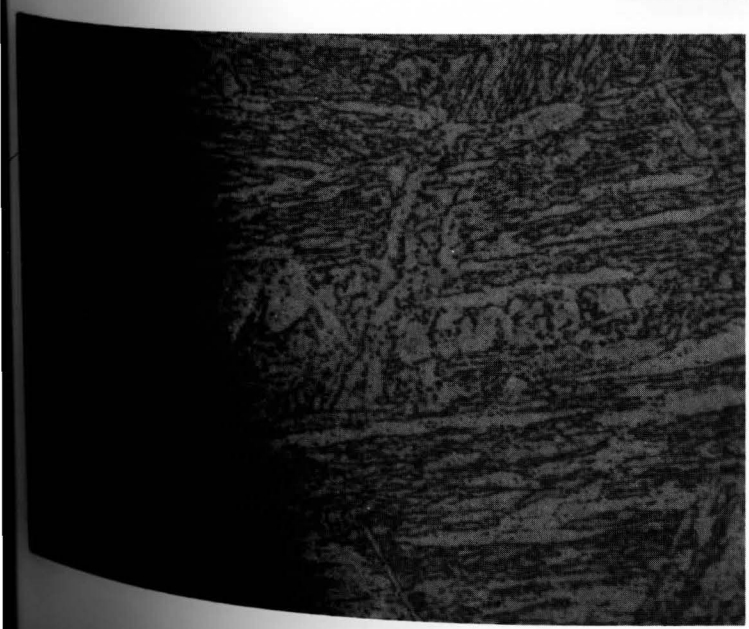

c) Yield strength 73.1 ksi. Carbides Distinct. None of the Specimens Failed.

Figure 21. Microstructures of Carbon Steel C-Ring Specimens. Etchant 2% Nital. 1500X. Oil Immersion.

a) Yield Strength 100.0 ksi. Carbides Becoming Visible. All Three Specimens Failed.

b) Yield Strength 82.8 ksi. Carbides Distinct. One of the Three Specimens Failed.

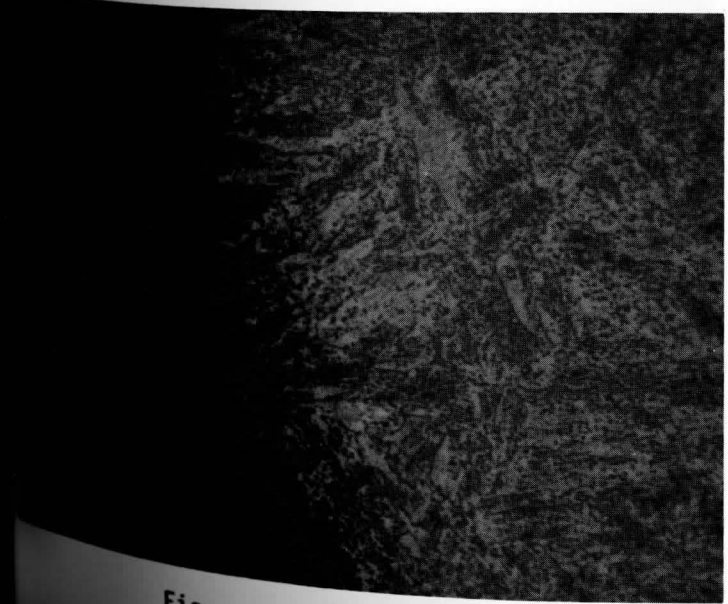

c) Yield Strength 73.8 ksi. Carbides Distinct. One of the Three Specimens Failed.

Figure 22. Microstructures of Chromium Steel C-Ring Specimens. Etchant 2% Nital. 1500X. Oil Immersion.

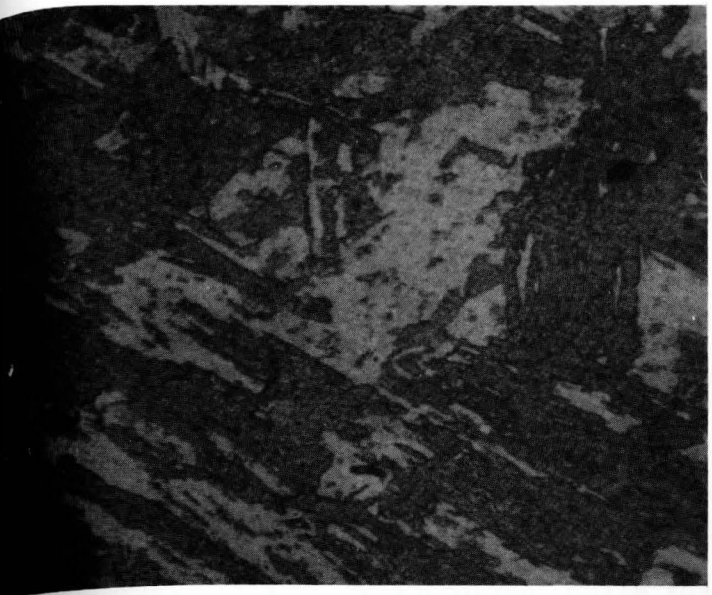

a) Yield Strength 148.5 ksi.
Carbides Not Visible. All
Three Specimens Failed.

b) Yield Strength 119.6 ksi.
Carbides Becoming Visible.
All Three Specimens Failed.

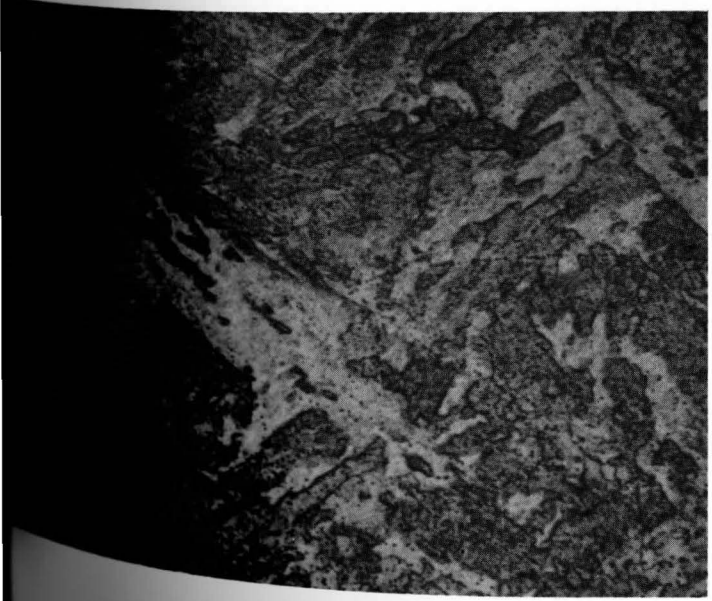

c) Yield Strength 107.1 ksi.
Carbides Still Not Distinct.
All Three Specimens Failed.

Figure 23. Microstructures of Vanadium Steel C-Ring Specimens.
Etchant 2% Nital. 1500X. Oil Immersion.

carbides, the average particle diameter, the number of particles per unit length of line and the mean interparticle spacing. Sample calculations for the carbide parameters are presented in Appendix D along with the raw data. In analyzing the data, one must keep in mind that the measurements made on the particles did not discriminate between the types of carbides present.

In general, the data for the three steels show that as the tempering temperature increased, the carbide size, volume fraction and interparticle spacing increased, while the number of particles decreased. These changes are expected during the tempering of martensitic steels as carbon is rejected from the martensite and the carbides coarsen. It must be noted that the values for the average carbide diameter, the number of particles per unit length of line and the mean interparticle spacing agree favorably with values determined by other researchers in similar low alloy steels[52-56]. On the other hand, the values for volume fraction of carbides are slightly higher than one would expect for steels containing 0.30 wt% carbon. Ashley and Ebeling suggest that errors arise in measuring particle volume fraction from replicas due to variations in the proportion of suitably placed carbides captured on the replica[57].

The data of Table 7 were plotted against the cracking susceptibility factors for the three steels (see Table 6) to determine which of the carbide parameters affected the resistance to sulfide stress cracking. Figures 24 and 25 show that correlations existed between both the volume fraction and size of carbides and the susceptibility to cracking - as these parameters increased the susceptibility decreased. In addition,

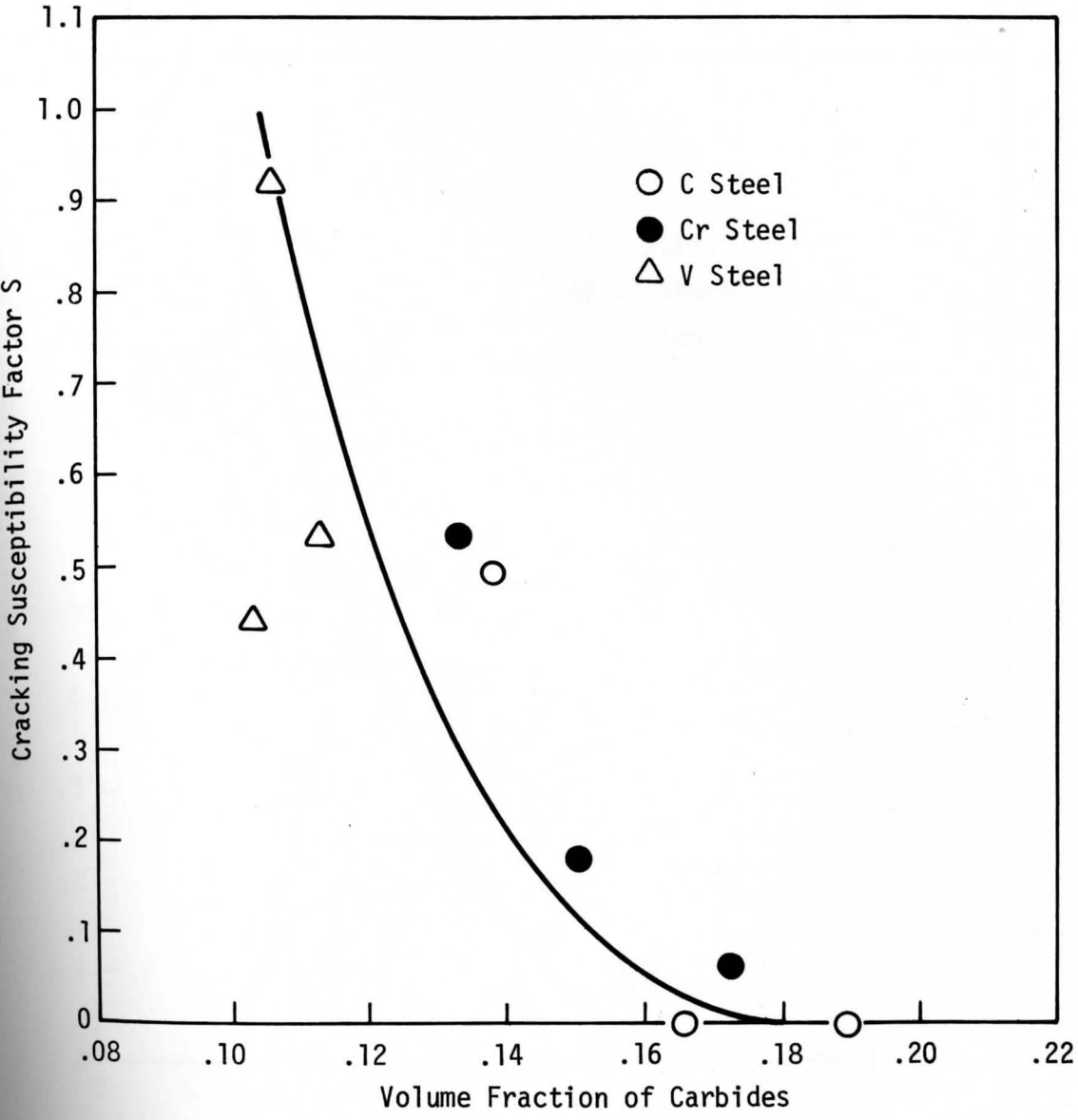

Figure 24. Curve of Cracking Susceptibility Factor Versus Volume Fraction of Carbides.

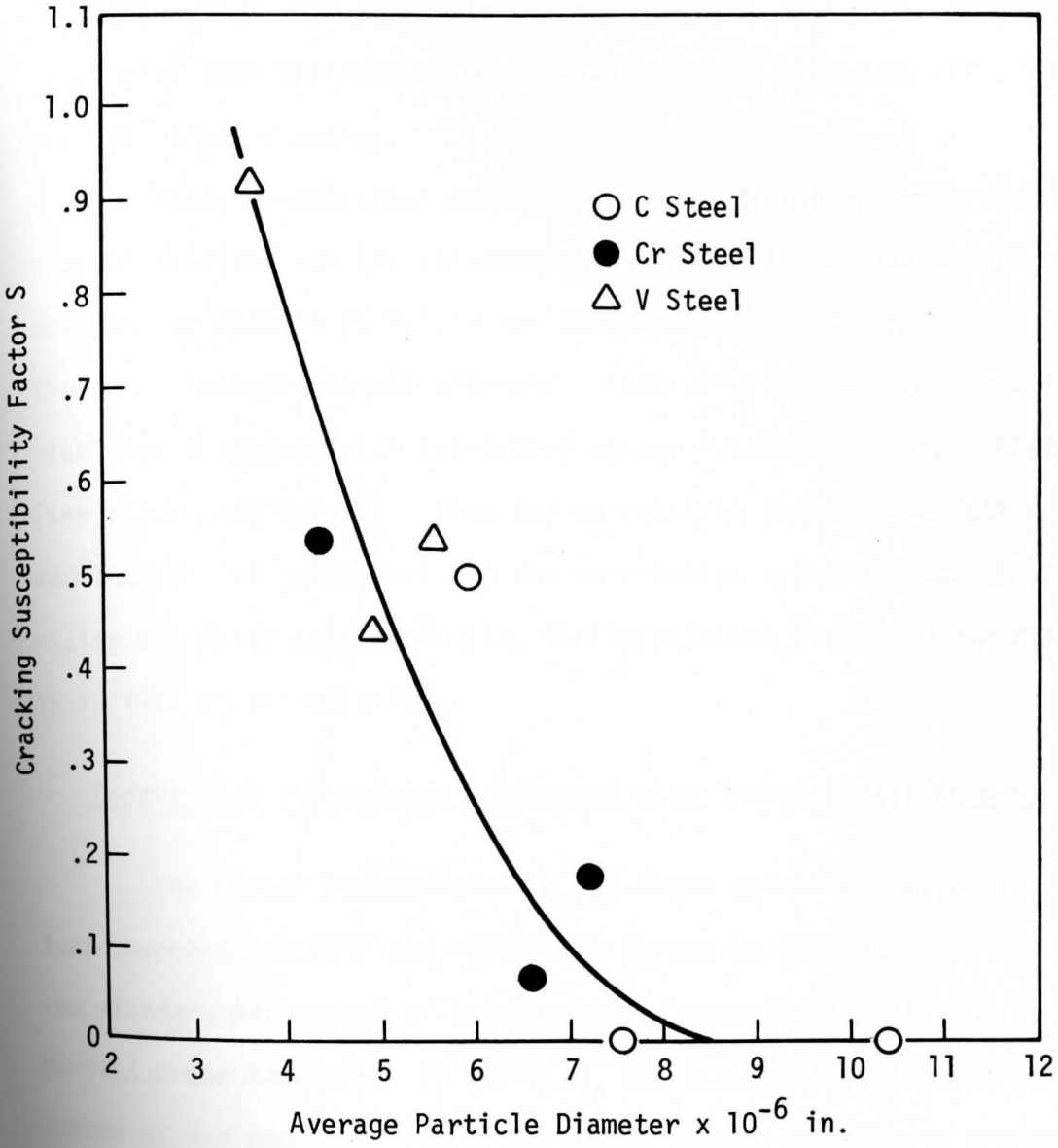

Figure 25. Curve of Cracking Susceptibility Factor Versus Average Particle Diameter.

the nature[+] of the curves suggest that above some critical volume fraction and size of carbides, a steel will resist cracking; since a susceptibility factor of zero is equivalent to no failures in the cracking test. This corresponds to the observations of several researchers that below some critical strength level a steel will completely resist sulfide stress cracking.

Since correlations existed between both the volume fraction and size of carbides and the susceptibility to sulfide stress cracking, an attempt was made to correlate the carbide parameters with the data from the crack propagation measurements. This effort showed that the incubation time increased with increasing volume fraction and size of carbides (see Figures 26 and 27). Thus the correlation between incubation period and the carbide parameters and the correlation between cracking susceptibility and these parameters show that precipitates play an important role in sulfide stress cracking.

Correlation of Cracking Resistance with Charpy Impact Properties

The Charpy impact data for the three steels corresponding to the test temperatures 75°F and -100°F are listed in Table 8. The data include the standard parameters of total energy absorbed, lateral expansion and percent shear fracture. In addition, the data include the energy absorbed at maximum load, i.e., the energy needed to initiate fracture,

---

[+]Based on sulfide stress cracking studies conducted by Greer[58], one would expect an exponential relationship between the cracking susceptibility factor used in the present study and any parameter that affects the yield strength of a steel.

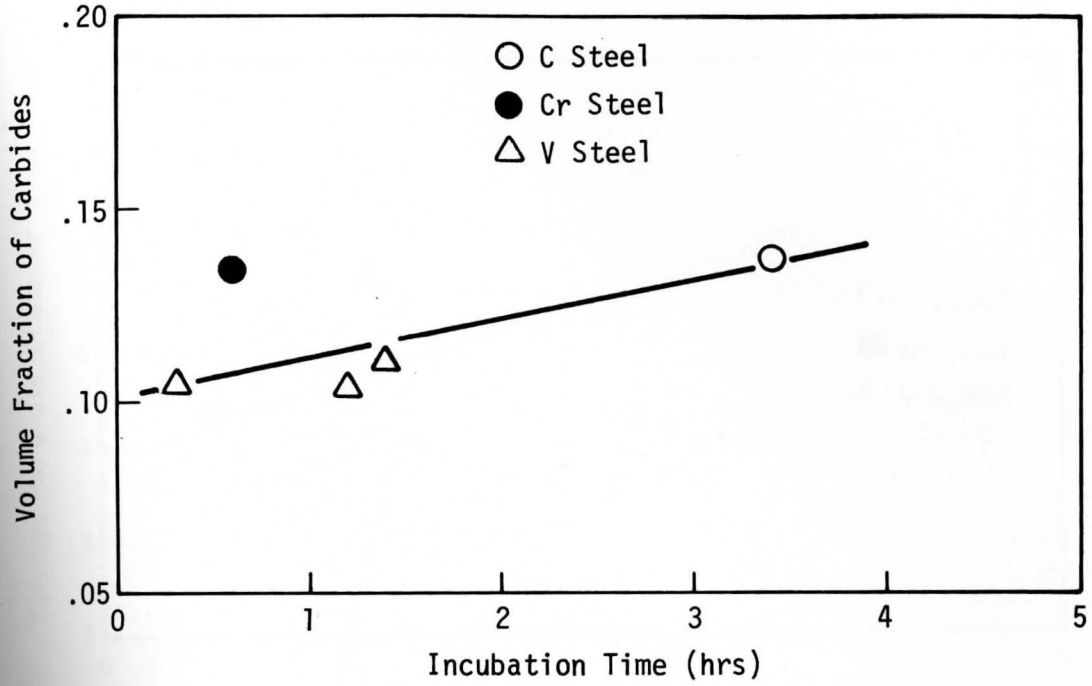

Figure 26. Variation of Incubation Time With Volume Fraction of Carbides.

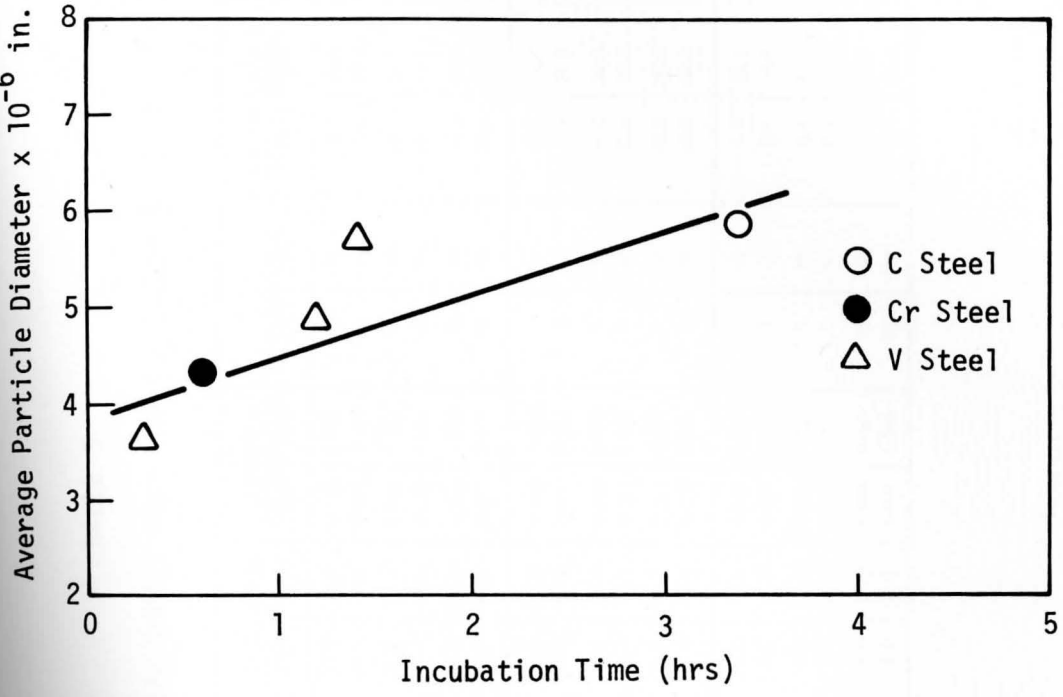

Figure 27. Variation of Incubation Time With Average Particle Diameter.

TABLE 8

CHARPY IMPACT DATA FOR THE STEELS

Material	Temper Treatment	Yield Strength (ksi)	Ratio of Failures in Cracking Tests to Total Specimens Tested	Absorbed Energy (ft-lbs)		Lateral Expansion (in)		Shear Fracture (%)		Absorbed Energy at Max Load (ft-lbs)		Time to Max. Load (sec) x 10^{+3}		Total Time for Impact Test (sec) x 10^{+3}	
				-100°F	75°F	-100°F	75°F	-100°F	75°F	-100°F	75°F	-100°F	75°F	-100°F	75°F
Carbon Steel	1100°F/1 hr	100.6	3/3	33.0	74.0	0.021	0.066	40	99	20.0	30.0	0.295	0.384	1.120	2.600
				36.3	74.2	0.025	0.064	30	99	20.0	32.0	0.297	0.406	0.925	2.450
	1175°F/2 hrs	84.0	0/3	35.4	93.4	0.023	0.071	35	99	27.0	34.0	0.371	0.512	1.000	3.400
				37.9	90.9	0.026	0.060	35	99	27.0	34.0	0.393	0.491	1.000	2.950
	1250°F/1 hr	73.1	0/3	35.9	102.0	0.023	0.083	20	99	31.0	40.0	0.402	0.577	0.800	3.500
				37.7	102.2	0.027	0.078	20	99	30.0	40.0	0.408	0.662	0.740	3.250
Cr Steel	1250°F/1 hr	100.0	3/3	6.0	20.3	0.008	0.023	1	10	4.5	14.0	0.123	0.256	0.150	0.600
				7.2	29.9	0.013	0.028	1	10	3.4	22.0	0.128	0.384	0.180	0.740
	1300°F/2 hrs	82.8	1/3	13.9	43.3	0.010	0.028	1	40	12.0	30.0	0.205	0.491	0.240	1.350
				14.8	43.1	0.011	0.033	1	40	11.5	25.0	0.222	0.410	0.270	1.420
	1320°F/2 hrs	73.0	1/3	15.2	74.6	0.011	0.049	1	80	13.5	30.0	0.231	0.577	0.280	2.500
				16.0	64.5	0.008	0.050	1	90	12.5	30.0	0.239	0.534	0.300	2.350
V Steel	1250°F/1 hr	148.5	3/3	3.2	16.9	0.003	0.003	1	1	1.7	14.0	0.077	0.205	0.120	0.260
				3.3	6.0	0.001	0.002	1	1	2.1	4.5	0.081	0.094	0.120	0.160
	1275°F/2 hrs	119.6	3/3	6.9	46.9	0.001	0.029	1	99	5.0	24.0	0.120	0.363	0.180	1.500
				7.2	46.7	0.005	0.033	1	99	4.6	20.0	0.124	0.290	0.165	1.400
	1300°F/2 hrs	107.1	3/3	15.9	57.9	0.009	0.044	10	99	11.0	24.5	0.206	0.402	0.260	1.700
				9.6	57.9	0.007	0.043	10	99	5.0	25.0	0.128	0.406	0.200	1.900

the time to maximum load, i.e., the time lapsed until fracture initiated and the total time for the impact specimen to fracture. These last three parameters were obtained from energy-time and load-time curves recorded with the added instrumentation on the impact machine. Figure 28 shows an idealized load-time trace with the parameters energy absorbed at maximum load, time to maximum load and total time to fracture identified. Figure 29 shows actual energy-time and load-time traces for the three steels.

In general, the data of Table 8 show that with increasing tempering temperature the standard parameters of total energy absorbed, lateral expansion and percent shear fracture increased for three steels. Similarly the parameters of energy absorbed at maximum load, time to maximum load and total time to fracture increased as the tempering temperature increased. Such changes are expected because martensitic steels generally exhibit an increase in toughness with increasing tempering temperature[59]. The data of Table 8 also show the expected lower toughness values for the three steels corresponding to the -100°F test temperature. This temperature is probably at or near the lower shelf for all three steels.

The data of Table 8 were plotted against the cracking susceptibility factors for the three steels to determine if any correlations existed. Figures 30 thru 37 show that correlations did exist between the susceptibility to sulfide stress cracking and the parameters: total energy absorbed, energy absorbed at maximum load, lateral expansion and time to maximum load. Several important observations can be made from these curves:

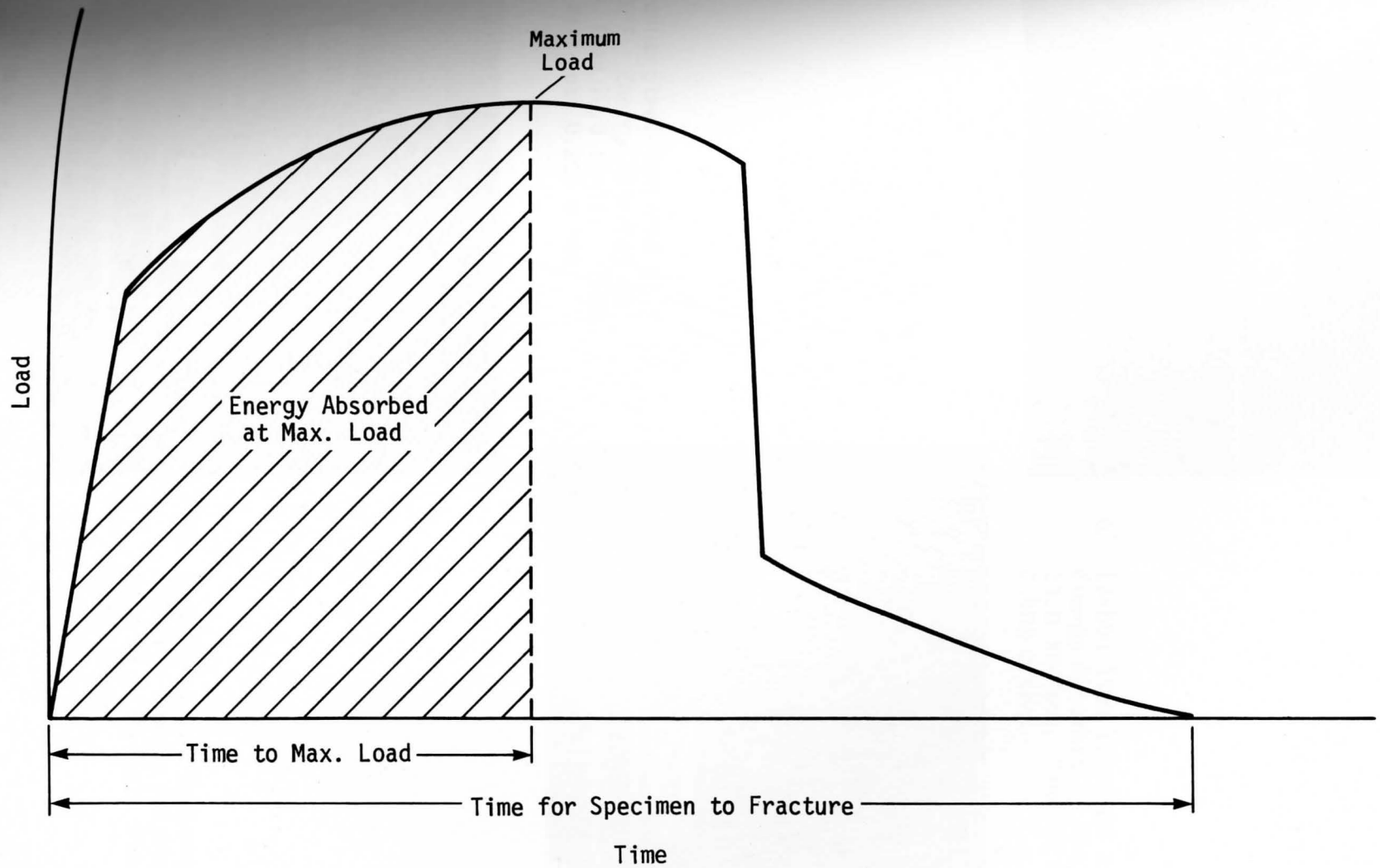

Figure 28. Idealized Load-Time Trace for Charpy Impact Specimen.

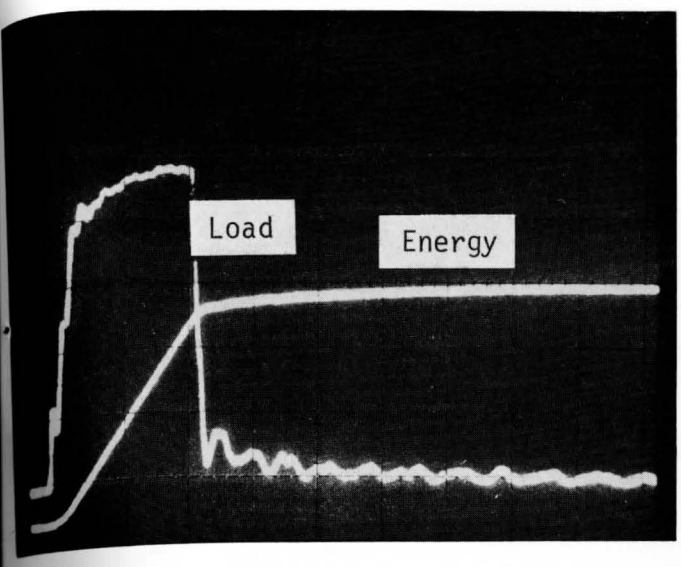

a) Carbon Steel Tempered at 1250°F. Energy Absorbed at Max. Load 31.0 ft-lbs. Time to Max. Load 0.402 m sec.

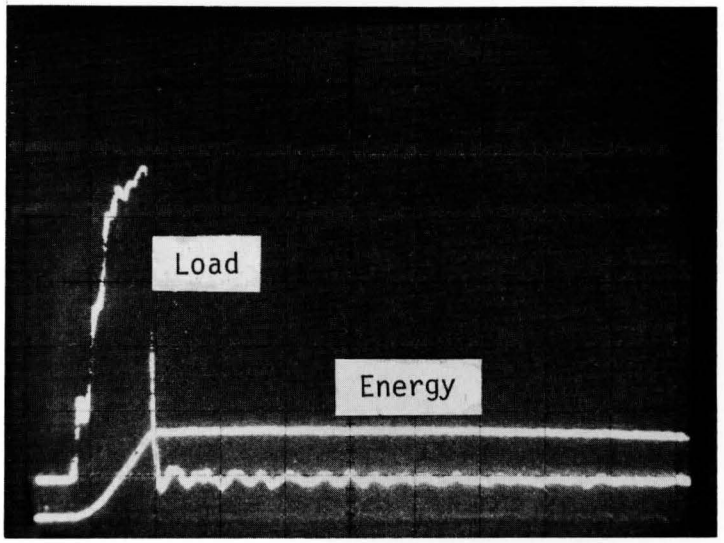

b) Chromium Steel Tempered at 1320°F. Energy Absorbed at Max. Load 12.0 ft-lbs. Time to Max. Load 0.205 m sec.

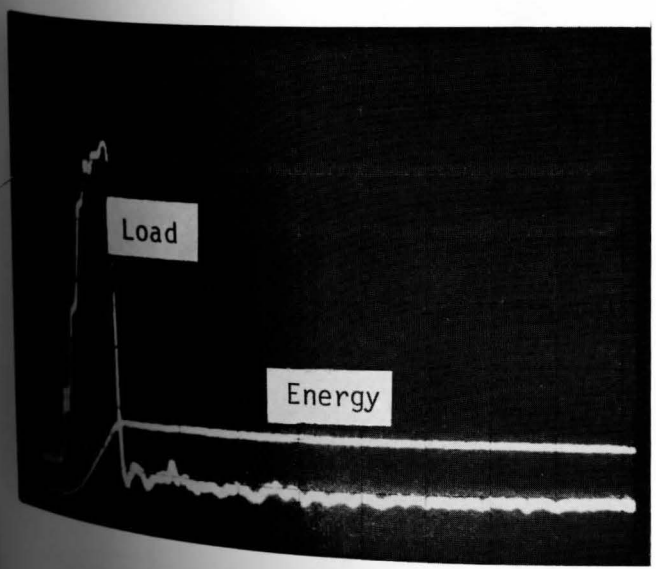

c) Vanadium Steel Tempered at 1300°F. Energy Absorbed at Max. Load 11.0 ft-lbs. Time to Max. 0.206 m sec.

Figure 29. Energy-Time and Load-Time Traces for Instrumented Charpy Impact Tests at -100°F. Vertical Divisions Represent 1000 lbs. for Load and 10 ft-lbs for Energy. Horizontal Divisions Represent 0.2 m sec.

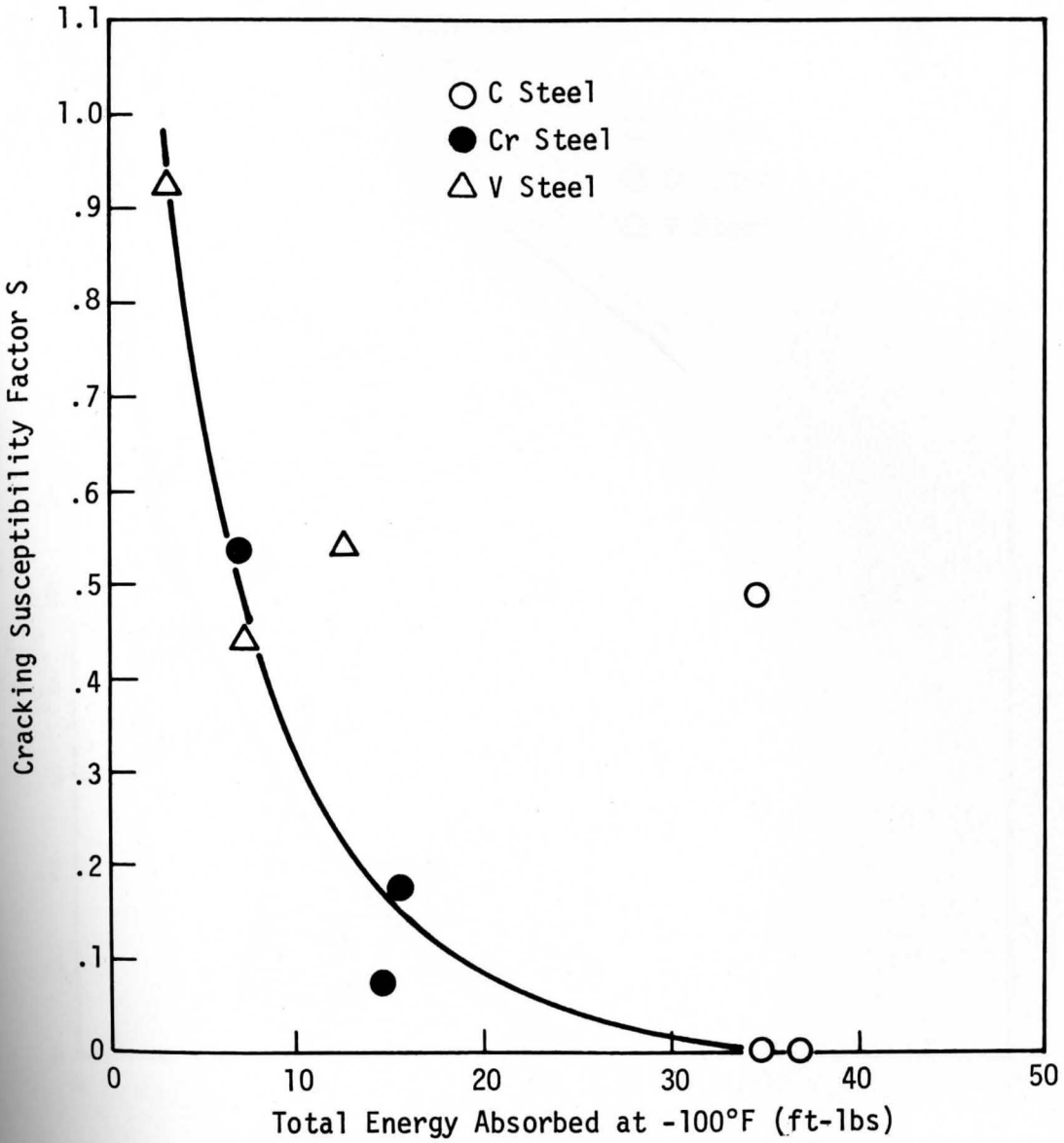

Figure 30. Curve of Cracking Susceptibility Factor Versus Total Energy Absorbed at -100°F.

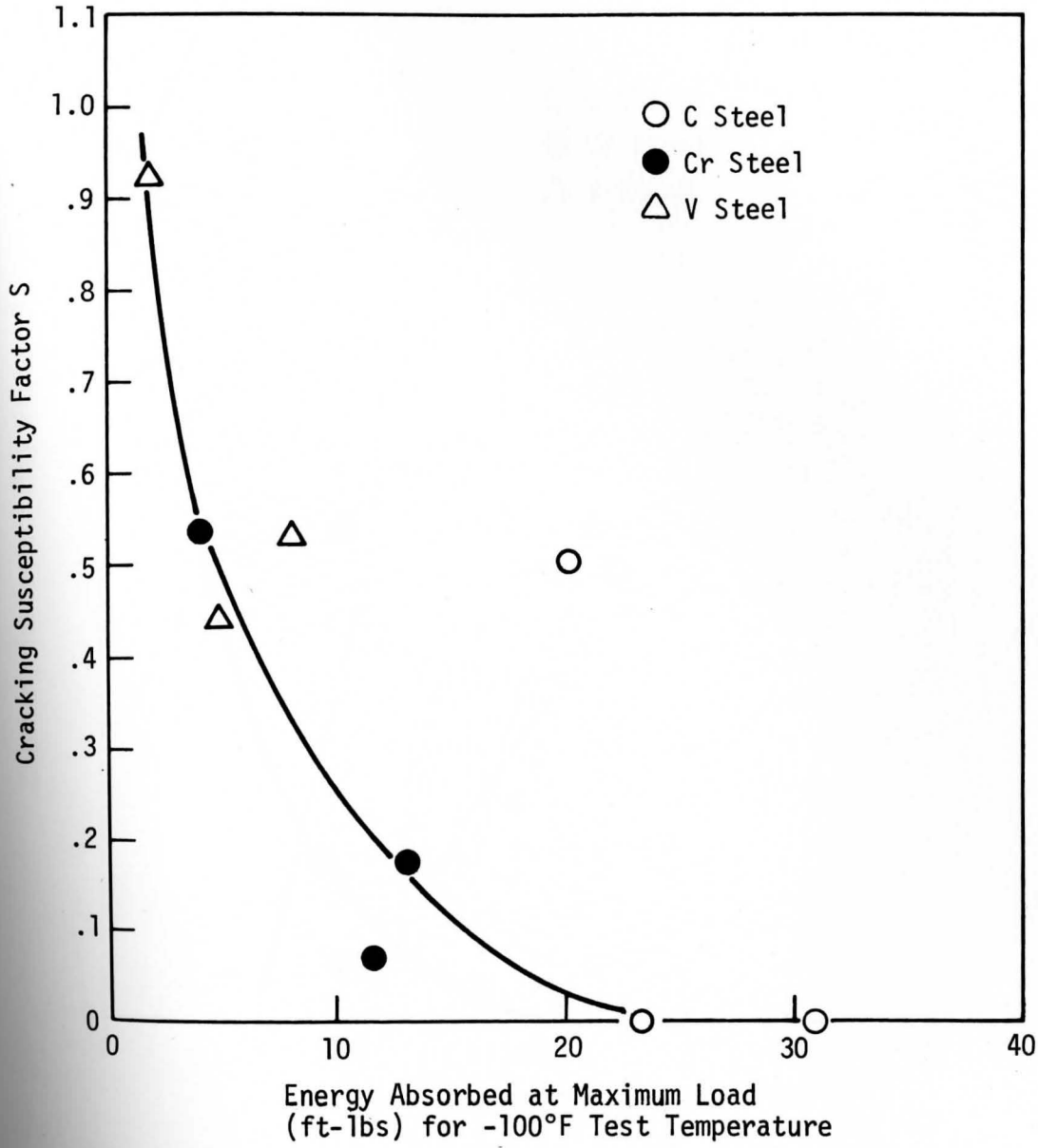

Figure 31. Curve of Cracking Susceptibility Factor Versus Energy Absorbed at Maximum Load at -100°F.

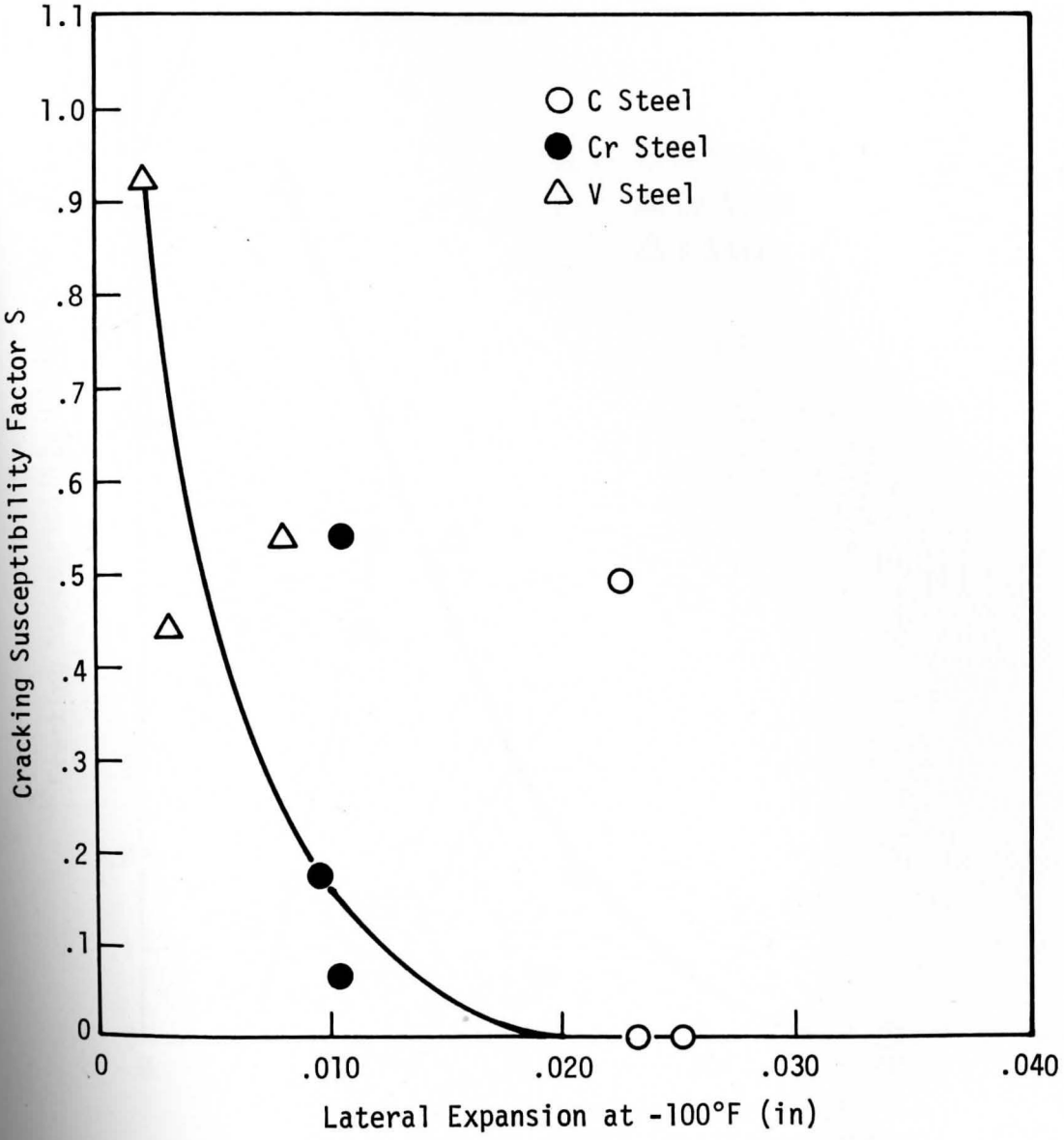

Figure 32. Curve of Cracking Susceptibility Factor Versus Lateral Expansion at -100°F.

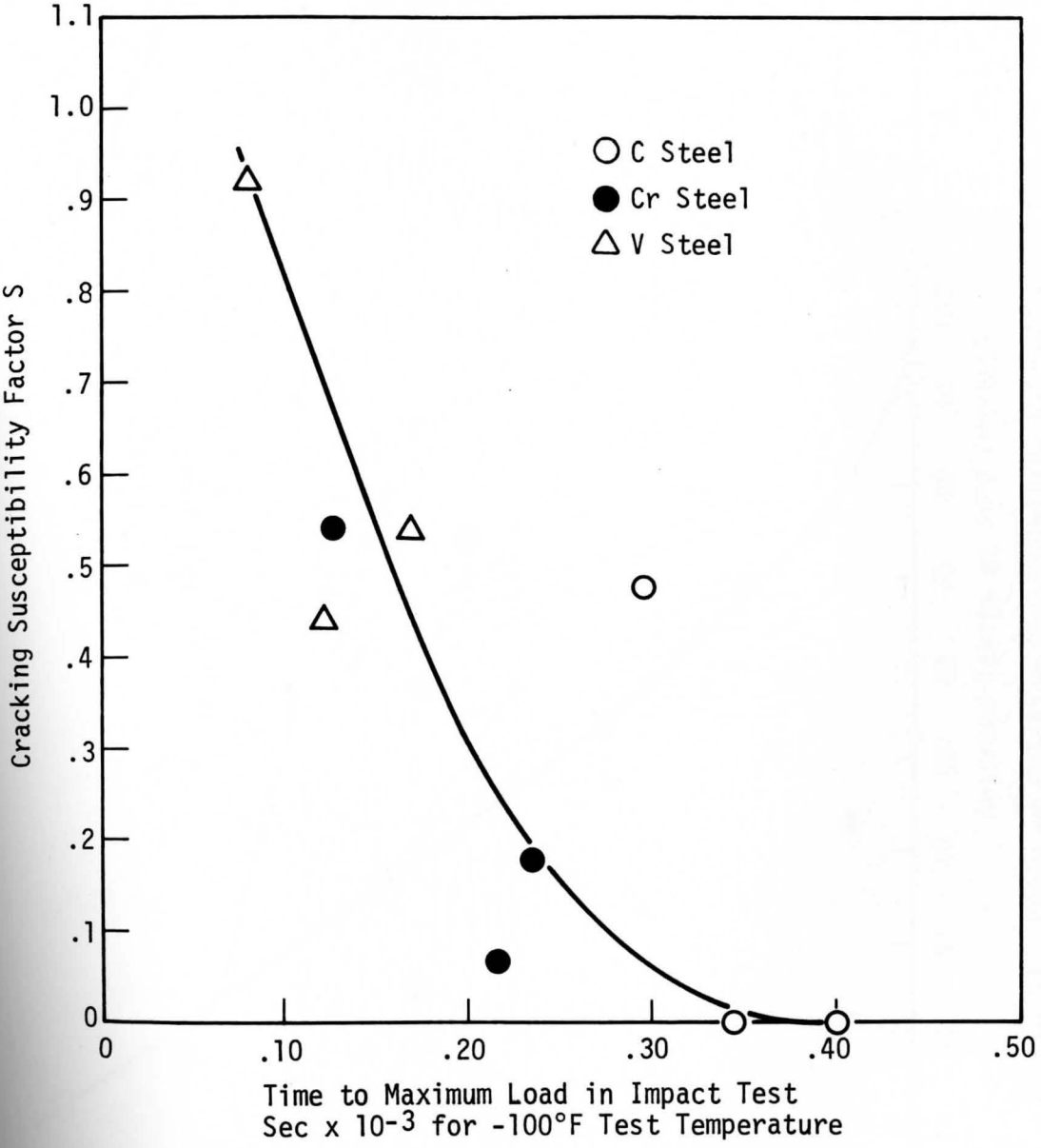

Figure 33. Curve of Cracking Susceptibility Factor Versus Time to Maximum Load at -100°F.

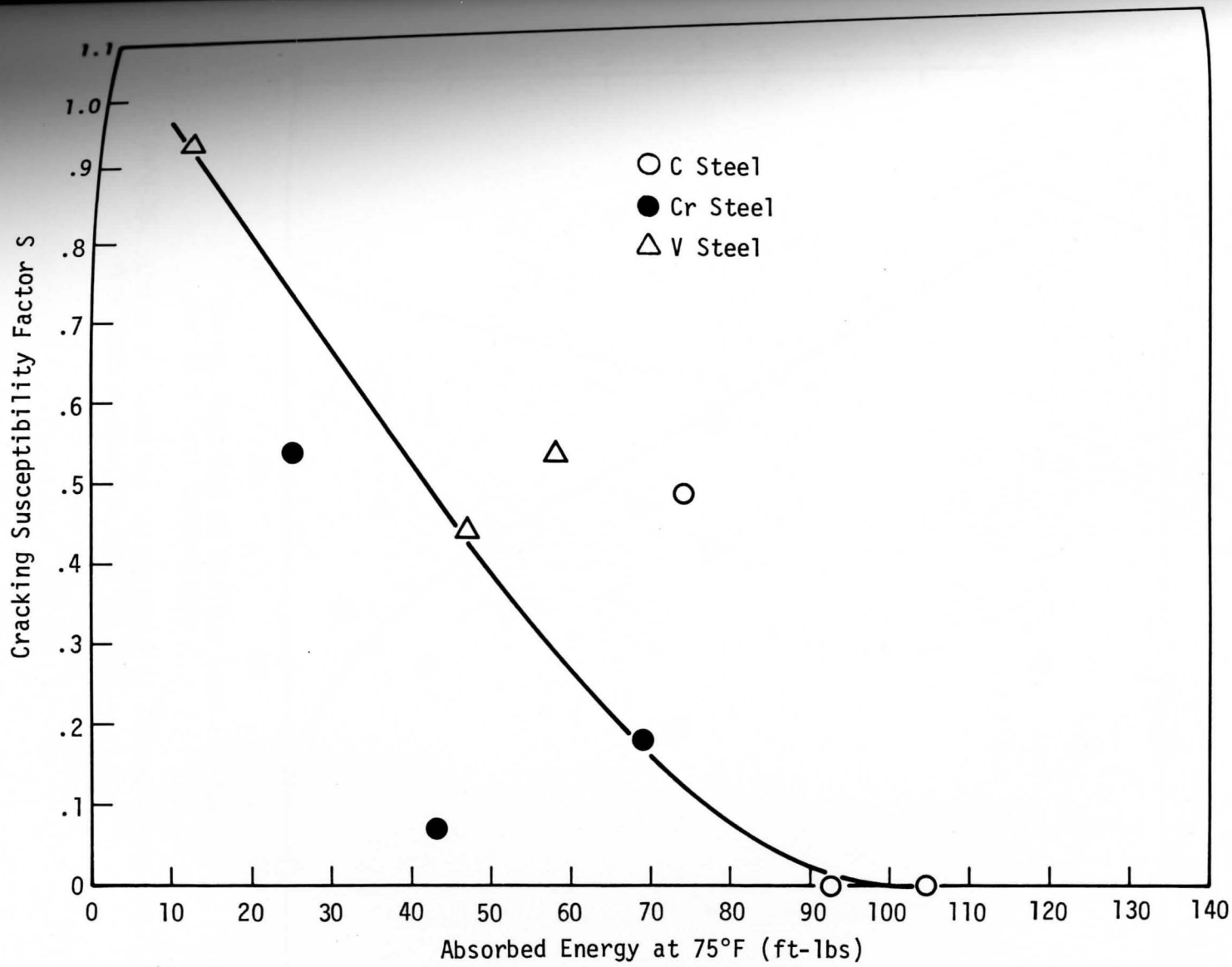

Figure 34. Curve of Cracking Susceptibility Factor Versus Total Energy Absorbed at 75°F.

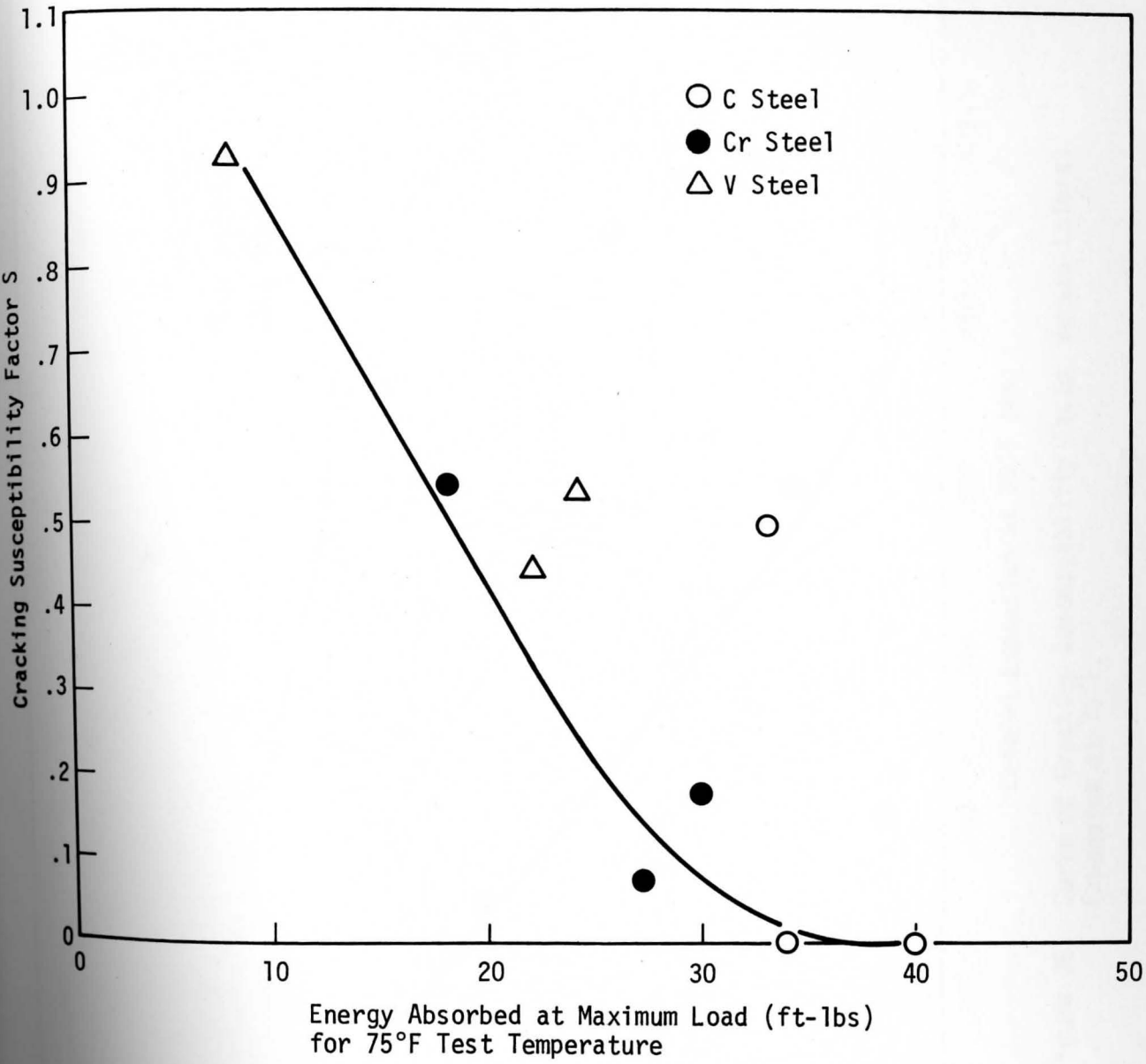

Figure 35. Curve of Cracking Susceptibility Factor Versus Energy Absorbed at Maximum Load at 75°F.

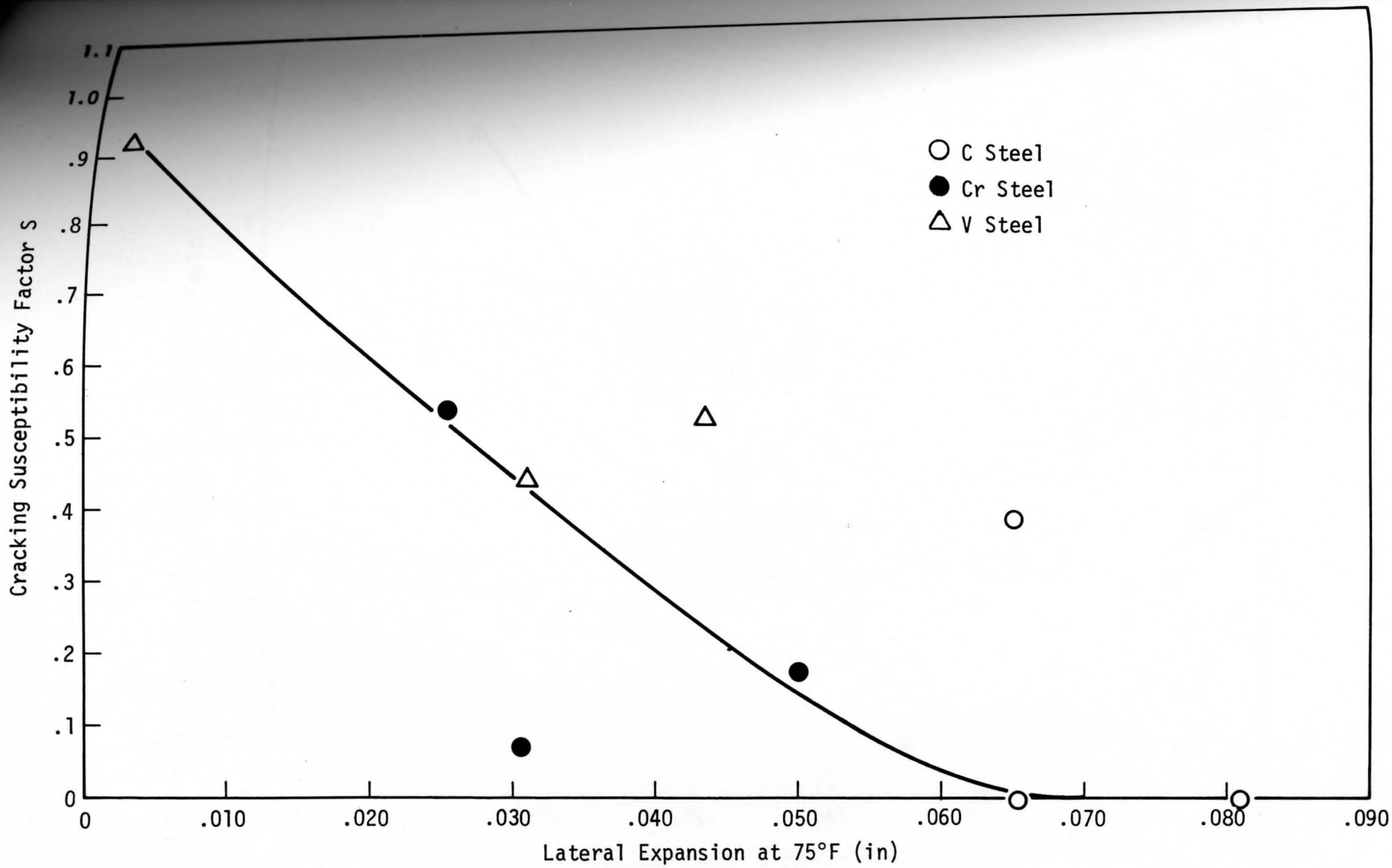

Figure 36. Curve of Cracking Susceptibility Factor Versus Lateral Expansion at 75°F.

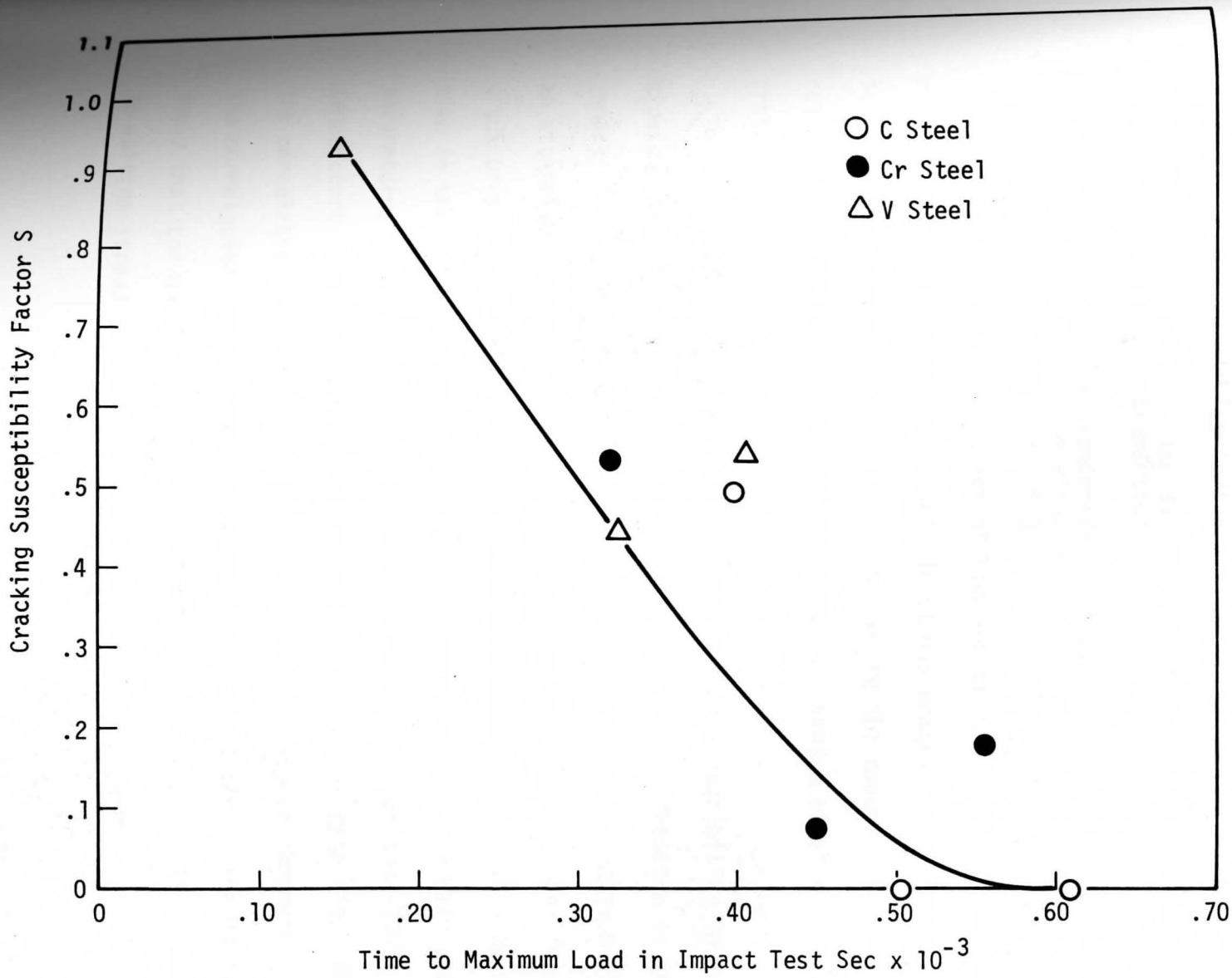

Figure 37. Curve of Cracking Susceptibility Factor Versus Time to Maximum Load at 75°F.

1) The curves are similar in nature to the curves showing correlations between the cracking susceptibility factor and the carbide parameters (see Figures 24 and 25).

2) There was a better data fit, i.e., less scatter, for the -100°F test temperature.

3) For both test temperatures, the parameter that gave the best correlation with susceptibility to sulfide stress cracking was the energy absorbed at maximum load.

The nature of the curves of Figures 30 through 37 suggest that martensitic steels will resist sulfide stress cracking above some critical level of toughness. Again this corresponds to the observations of several researchers that below some critical strength level a steel will resist cracking.

Since a correlation existed between the susceptibility to sulfide stress cracking and two parameters related to crack initiation in the impact test - time to maximum load and energy absorbed at maximum load - an attempt was made to correlate these parameters with the data from the crack propagation measurements. This effort showed that the incubation time in the sulfide stress cracking test increased directly with both parameters. Figures 38 and 39 show the correlations for the -100°F test temperature, the one that consistently gave the better data fit. Thus the correlation between incubation period and the impact parameters and the correlation between cracking susceptibility and these parameters imply that the same microstructural feature that controlled the resistance to sulfide stress cracking in the three steels also governed toughness.

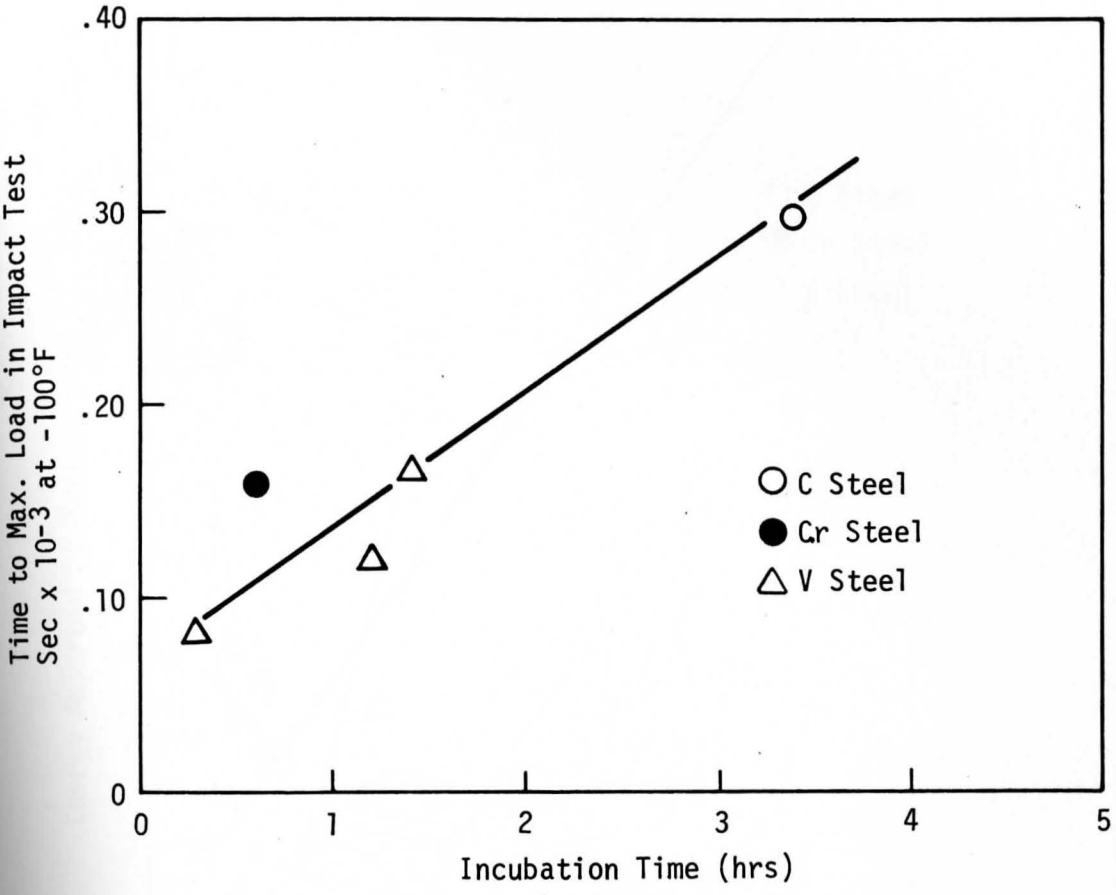

Figure 38. Variation of Incubation Time with Time to Maximum Load at -100°F.

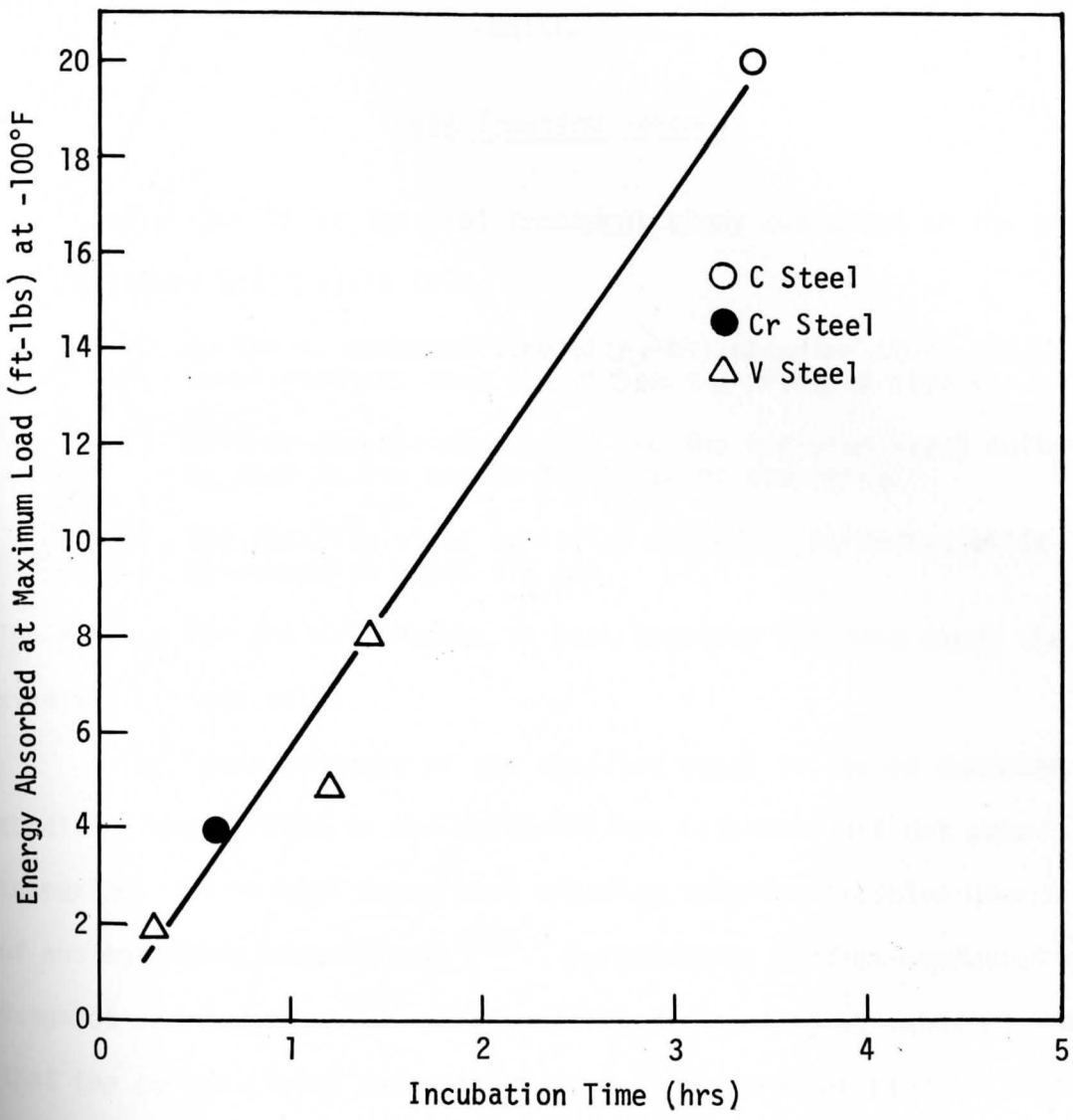

Figure 39. Variation of Incubation Time with Energy Absorbed at Maximum Load at -100°F.

CHAPTER IV

DISCUSSION

Heat Treating Response

The results of the heat treatment study conducted on the three steels showed (see Figure 10):

1) In the as quenched condition, the vanadium steel had a lower hardness than the carbon and chromium steels.

2) Neither the chromium steel nor the vanadium steel softened as much as the carbon steel during tempering.

3) The vanadium steel exhibited secondary hardening while the chromium steel did not.

The reasons for the differences in heat treating response among the three steels are given below.

The lower hardness of the vanadium steel in the as quenched condition was related to the austenitizing treatment and not auto-tempering. It is well known that vanadium carbides dissolve over a range of austenitizing temperatures[60]. Furthermore, studies conducted by Bungardt and coworkers[61] on several steels containing vanadium indicate that the austenitizing temperature used in the present study (1750°F) was not high enough to dissolve all of the existing carbides in the vanadium steel. Since carbon has the primary effect on the hardness of martensite[62], one would expect the vanadium steel to have a lower hardness than the carbon or chromium steels in the as quenched condition.

The fact that the chromium and vanadium steels did not soften as much as the carbon steel during tempering is related to the effects of the alloying elements on the resulting carbide reactions. In the vanadium steel, the reaction $M_3C \rightarrow V_4C_3$ was directly responsible for retarding softening. The V_4C_3 carbide precipitates by separate nucleation and is very fine and coherent with the matrix when it first forms[63]. The coherency of the carbide results in a substantial strengthening of the matrix (secondary hardening). On the other hand, the reaction $M_3C \rightarrow M_7C_3$ was not responsible for retarding softening in the chromium steel. The M_7C_3 carbide forms by an in situ transformation of the iron rich carbide and thus is relatively coarse and not coherent when it first precipitates[64]. In this case, softening is retarded by Cr restricting the growth and spheroidization of the M_3C particles prior to the precipitation of M_7C_3[65]. Thus the chromium and vanadium steels retard softening in different manners.

The reason for the secondary hardening in the vanadium steel is well known. The interatomic distances in the V_4C_3 carbide are considerably greater than those in the ferrite matrix[66]. Thus the coherency strains associated with the precipitation of this carbide are large and this produces the marked hardening effect. On the other hand, the M_7C_3 carbide has interatomic distances similar to those of the matrix and therefore the associated strains should be small[67]. Thus one would not expect an appreciable hardening effect with the precipitation of M_7C_3.

Crack Initiation and Propagation in Sulfide Stress Cracking

The failure process of the three steels in the sulfide stress cracking tests exhibited certain characteristics (see Figures 16 through 20):

1) A finite period before crack initiation ranging from 0.3 to 3.4 hours.

2) A period of slow crack propagation ranging from 9.1 to 18.3 hours.

3) Complete crack arrest when the load on the specimen dropped to a given level.

It must be stressed that the cracking behavior of the three steels was quite similar to that of hydrogenated steels studied by Troiano. As discussed earlier, Troiano used notched tensile specimens under sustained loads in his work and monitored the kinetics of crack initiation and propagation by measuring changes in electrical resistance[68]. Figure 40 shows a typical resistivity-time curve for the hydrogenated specimens. The curve also exhibits an incubation period and a period of relatively slow crack propagation.

There is one difference, however, between the cracking behavior of Troiano's specimens and the specimens used in the present study. In the sustained load tests of Troiano, the stress increases during the period of slow crack propagation and when the stress reaches a certain level, catastrophic failure occurs[69]. Catastrophic failure results in a complete separation of the specimens into two pieces. On the other hand, the load drops off during slow crack propagation in the C-ring specimens used in the present study. Thus relaxation occurs in time and instead of catastrophic failure the crack is arrested.

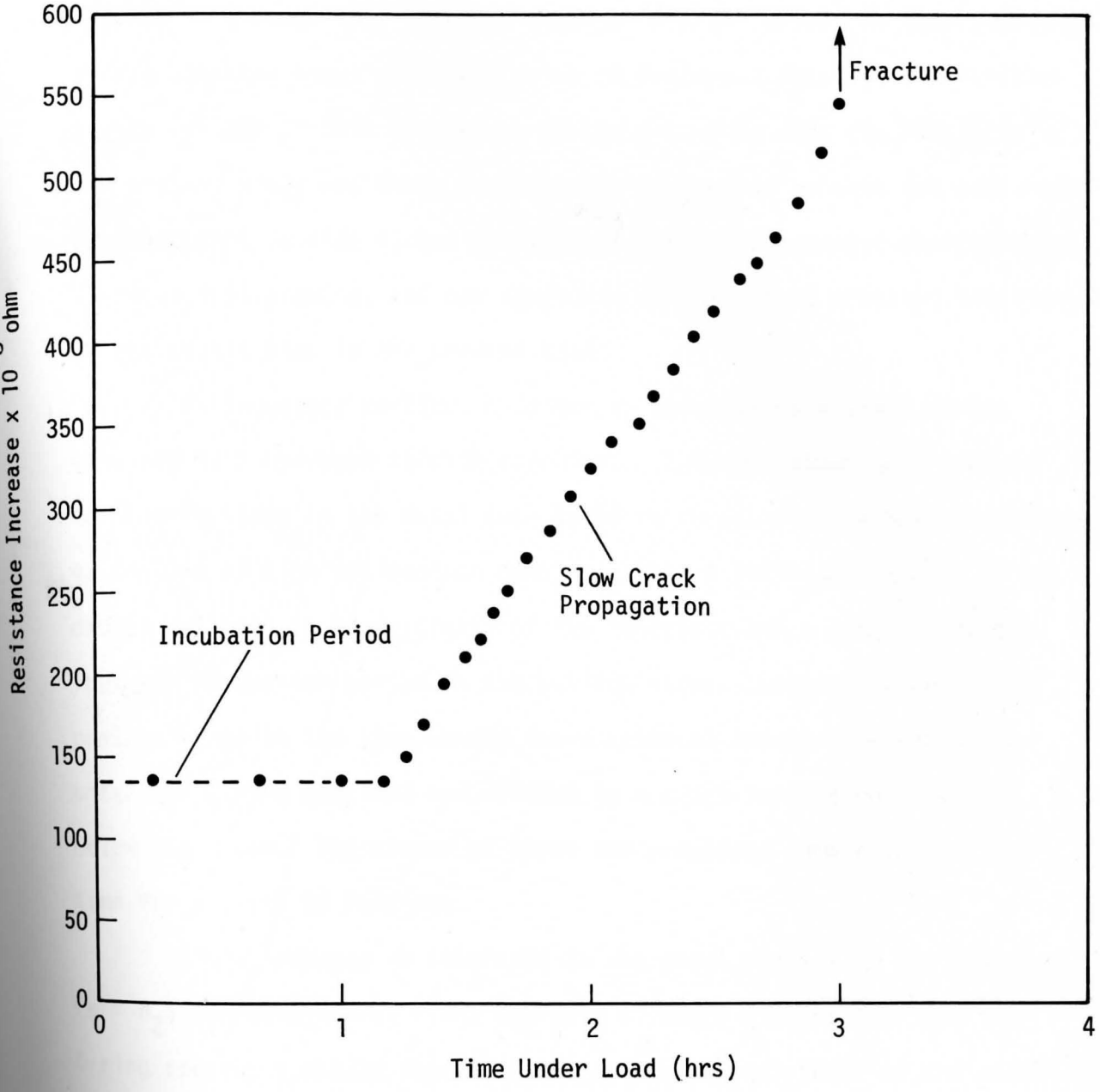

Figure 40. Resistivity-Time Curve for Hydrogenated Specimen of AISI 4340 Steel (after Troiano).

The optical examination of the failed C-ring specimens showed that the cracks were large and non-branched in all three steels (see Figures 11 through 15). Troiano observed similar cracks in the specimens of hydrogenated steel sectioned prior to failure. Thus the similarities in the failure process and nature of the cracks between the steels in the present study and those in the basic studies of Troiano are additional evidence that sulfide stress cracking is a form of hydrogen embrittlement. Based on this premise, one can speculate on the unique cracking behavior of the steels used in the present study.

As suggested earlier, hydrogen is absorbed by a steel during exposure to a hydrogen sulfide corrodent. Hydrogen atoms then diffuse to imperfections in the metal such as microcracks, voids around inclusions or regions of high dislocation density. When a sufficient amount of hydrogen collects in the vicinity of the imperfections a crack initiates. Thus the incubation period in the sulfide stress cracking tests of the present study is the time needed for a critical amount of hydrogen to enter the C-ring specimen and diffuse to a crack initiation site just below the notch. The slower of these two processes should control the time for a crack to initiate.

Since hydrogen is liberated at the steel surface by the reaction, $Fe + H_2S$ (aq soln) $\rightarrow FeS + 2H$, the rate of entry of hydrogen into the C-ring specimens should depend on the corrosion resistance of the steel and hence its composition[71]. There is evidence that Ni, P and S are all promoters of hydrogen absorption[72-73]. On the other hand, Cr should be beneficial because of its general effect on corrosion resistance.

In addition, the rate of hydrogen entry should depend on the active surface area of the specimen. Studies by Snape[74] suggest that this is the surface area of the notch - presumably the oxide on the C-rings hampers the absorption of hydrogen. An effort was made to correlate the measured incubation times for the carbon, chromium and vanadium steels with both composition and notch surface area, but no correlations were found. The lack of correlations suggests that the incubation times in the sulfide stress cracking tests were governed primarily by the diffusion of hydrogen to crack initiation sites. This is in agreement with a very recent study of hydrogen related problems made by Hirth and Johnson[75]. The researchers also concluded that the rate of hydrogen entry from an external source is bulk diffusion controlled.

The driving force for the diffusion of hydrogen in a steel is an activity gradient resulting from a gradient in hydrogen concentration in the lattice or a gradient in the elastic stress field[76]. A concentration gradient may be developed at the surface of a steel exposed to hydrogen environments, while a stress gradient may be produced by notches, sharp defects or bending moments[77]. Both of these types of gradients probably existed in the C-rings used in the sulfide stress cracking tests.

The diffusion of hydrogen is thought to involve the migration of atomic hydrogen through the lattice. Since the rates of hydrogen diffusion are nearly the same in both single crystal and polycrystalline iron, there is no apparent preference for grain boundary diffusion[78]. However, there is evidence that hydrogen diffusion may be hindered by certain non-metallic phases in steel. These phases include some inclusions like

MnS, Ti(C,N) and carbide particles[79]. The observed increase in incubation time with increasing volume fraction and size of carbides for the steels in the present study (see Figures 26 and 27), also suggests that carbides can interfere with the diffusion of hydrogen. Furthermore, these correlations are additional evidence that the incubation time in the sulfide stress cracking test was governed primarily by hydrogen diffusion and not the absorption of hydrogen.

Once a crack initiates, it exhibits a period of relatively slow crack propagation. This period actually involves a series of crack initiations. Presumably, the initial crack propagates until it leaves the region of high hydrogen concentration and then stops[80]. Hydrogen diffuses to the region just ahead of the arrested crack and when a critical concentration is again reached, a new crack initiates. The two cracks connect by tearing and the process repeats until failure occurs[81]. Thus the period of slow crack propagation observed in the sulfide stress cracking tests should also be governed primarily by the diffusion of hydrogen. The crack propagation measurements made on the carbon, chromium and vanadium steels used in the present study did show some evidence of this discontinuous growth (see Figures 16, 17 and 20). However, studies by Troiano and coworkers have shown that only at test temperatures below ambient is the diffusion of hydrogen slow enough to clearly show this effect[82].

The data obtained from the crack propagation measurements of the present study were used to calculate an average slow crack propagation rate for each steel. This quantity was the area of crack propagation in

the C-ring specimen divided by the difference between the time the crack arrested completely and the incubation time. A sample calculation is presented in Appendix E along with the data. As shown in Table 9, the slow crack propagation rates for the three steels ranged from 1.69×10^{-5} to 3.82×10^{-5} cm^2/sec. It is interesting to note that these values are of the same order of magnitude as the generally accepted room temperature value for the diffusivity of hydrogen in iron, 10^{-5} cm^2/sec[83]. Thus the evidence of discontinuous crack growth in the three steels along with the calculated values for slow crack propagation rate imply that hydrogen diffusion did govern crack propagation in the sulfide stress cracking tests.

TABLE 9

AVERAGE SLOW CRACK PROPAGATION RATES FOR THE STEELS

Material	Yield Strength (ksi)	Slow Crack Propagation Rate (cm^2/sec)
Carbon Steel	100.6	1.85×10^{-5}
Cr Steel	100.0	1.96×10^{-5}
V Steel	148.5	2.12×10^{-5}
V Steel	119.6	3.82×10^{-5}
V Steel	107.1	1.69×10^{-5}

Effect of Carbides on Resistance to Sulfide Stress Cracking

The comparison of the sulfide stress cracking data for the three steels with the carbide parameters determined by lineal analysis measurements showed:

1) The incubation time increased with increasing volume fraction and size of carbides (see Figures 26 and 27).

2) The resistance to sulfide stress cracking increased with increasing size and volume fraction of particles (see Figures 24 and 25).

3) Above a critical volume fraction and size of carbides, sulfide stress cracking did not occur.

It must be pointed out again that the lineal analysis data did not discriminate between the various types of carbides present in the three steels.

The correlation between incubation time in the sulfide stress cracking test and the volume fraction and size of carbides in the steels was attributed earlier to the particles interfering with the diffusion of hydrogen to crack initiation sites. The correlation between these carbide parameters and the overall resistance to sulfide stress cracking is additional evidence of interactions between hydrogen and carbides.

In the period 1964-65, Troiano and coworkers suggested that the tolerance of a steel for hydrogen could be increased by trapping hydrogen at precipitate particles and thus not allowing the critical concentration needed for failure to collect its defects[84-85]. Although the exact mechanism for trapping was not known, the researchers felt that hydrogen was bound at the interface between particles and the matrix.

In subsequent years other researchers found evidence of interactions between hydrogen and carbides. Coe and Moreton[86] studied the diffusion of hydrogen from two sets of charged samples of a Cr-Mo-V-W steel with a 0.34C content. One set of samples had been austenitized at ∿2010°F, quenched and had all of the carbon in solution, while the

other set had been austenitized at ∿1740°F, quenched and had undissolved alloy carbides present in the microstructure. Specimens from both sets of samples were subjected to a range of temperatures and the hydrogen that evolved was collected. After evolution had ceased, the specimens were heated to ∿1200°F and the remaining hydrogen was collected. The study revealed that for temperatures above ∿176°F there was little difference between the two sets of samples. However, at 95°F approximately 90% of the hydrogen evolved from the specimens with all carbon in solution, while only 50% of the hydrogen evolved from the specimens with carbides present in the microstructure. Similarly, only 30% of the hydrogen evolved at 32°F from the specimens with carbides present. These findings suggest that carbides do trap hydrogen at ambient temperatures.

In another study, Newman and Shrier determined the effect of carbon content and structure on the solubility and diffusivity of hydrogen in steel[87]. Low alloy steels of different carbon levels were austenitized at 1650°F, water quenched and tempered at various temperatures. Specimens from the steels were charged with hydrogen until saturated and vacuum extraction techniques were used to determine the respective solubilities. Corresponding diffusion coefficients were calculated from hydrogen evolution-time curves. The study yielded two important findings:

1) For a given tempering treatment, an increase in carbon content resulted in an increase in hydrogen solubility and a decrease in diffusivity.

2) The solubility of hydrogen appeared to be related to the interfacial area between the carbides and the ferrite matrix.

These findings not only suggest that carbides act as trapping sites for hydrogen, but also that the hydrogen is bound at the particle-matrix interface.

The fact that the three steels used in the present study exhibited increasing resistance to sulfide stress cracking with increasing volume fraction of carbides is consistent with the theory that hydrogen is trapped at particles in an innocuous state. If hydrogen is bound by carbides as suggested by Troiano, one would expect more of the absorbed hydrogen to be trapped as the volume fraction of carbides increases. This in turn would increase the resistance to sulfide stress cracking. Presumably, a minimum volume fraction of carbides is required to prevent the amount of hydrogen needed for crack initiation from collecting at defects. At or above this critical volume fraction of carbides, hydrogen induced failure will not occur. The correlation of increasing resistance to sulfide stress cracking with increasing carbide size for the steels in the present study is consistent with this, since the volume fraction of carbides varies directly with the average particle diameter[88].

If hydrogen is trapped at the carbide-matrix interface as suggested by Troiano, one would expect a correlation between the total surface area of the carbides and the resistance to sulfide stress cracking for the steels in the present study. In an attempt to verify this, the surface area of the average particle was calculated for the three steels at each strength level and multiplied by the corresponding number of particles per unit length of line (see Appendix F). This new parameter gave an excellent correlation when plotted against the cracking sus-

ceptibility factors for the steels (see Figure 41). Furthermore, the resulting curve showed that above a critical total particle surface area cracking did not occur. Thus the results of the present study also suggest that hydrogen is bound in an innocuous state at the interface between carbides and the matrix.

Although the exact mechanism for trapping hydrogen at carbide particles is not known, it is important to speculate on possible reasons for the phenomenon. Newman and Shreir suggest that hydrogen atoms are attracted to carbides because of the discontinuity that exists at the particle-matrix interface[89]. The atoms at this boundary have a higher free energy than those at a distance from the boundary. Thus hydrogen should diffuse to and collect in these regions because it results in an overall decrease in free energy. Another possible explanation involves the stress fields that exist around carbide particles. Stuart and Ridley measured the thermal expansion coefficients of several types of carbides and found that all had coefficients smaller than that of α iron[90]. Thus on cooling from tempering temperatures where the carbides precipitate, stresses develop due to differences in thermal contraction between the particles and the matrix. The resulting stresses in the matrix are compressive in the radial direction and tensile in the circumferential and axial directions[91]. Hydrogen should migrate to the tensile stress fields around the carbides because this lowers the total strain energy[92]. Since the maximum stresses occur at the particle-matrix interface, one would expect most of the trapped hydrogen to collect there. However, the stress fields around carbides extend a finite

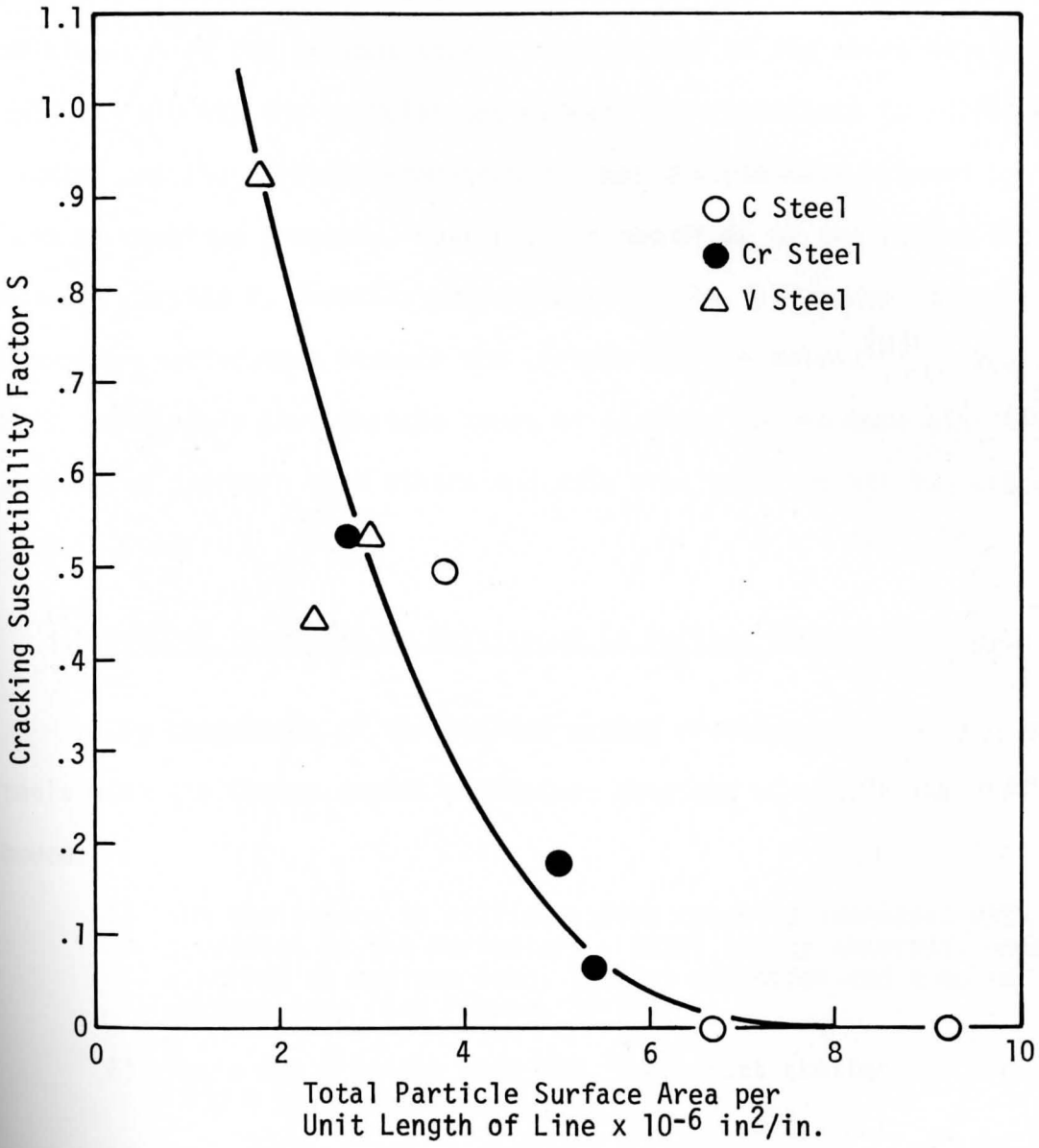

Figure 41. Variation of Cracking Susceptibility Factor With Total Particle Surface Area per Unit Length of Line.

distance and thus some hydrogen may also be bound in the matrix adjacent to the particle.

The work of Stuart and Ridley included the carbides found in the steels from the present study. Thus either of the above possibilities could explain why the correlations between the resistance to sulfide stress cracking and the carbide parameters did not discriminate between the types of carbides present. However, the magnitude of the stress field around a carbide is directly proportional to the difference in thermal expansion coefficients between the carbide and the matrix[93]. Thus, it is conceivable that certain types of carbides may be more effective in trapping hydrogen than others and this area could be the subject of a future study.

Effect of Toughness on Resistance to Sulfide Stress Cracking

The comparison of the sulfide stress cracking data for the three steels with the Charpy impact parameters obtained at -100°F and 75°F showed:

1) The resistance to sulfide stress cracking increased with increases in the parameters - total energy absorbed, energy absorbed at maximum load, lateral expansion and time to maximum load (see Figures 30-37).

2) There was a better data fit, i.e., less scatter for the -100°F test temperature.

3) For both test temperatures, the parameter that gave the best correlation with cracking resistance was the energy absorbed at maximum load.

4) The incubation time in the sulfide stress cracking test increased with increases in the parameters time to maximum load and energy absorbed at maximum load (see Figures 38 and 39).

It has been recognized for some time that the toughness of a steel can be related to its general microstructure . Studies by Chin[94] have shown that if a material contains a high volume fraction of large inclusions, toughness is governed by the inclusions. If this is not the case, some other microstructural feature such as precipitate particles will control the toughness of the material. The three steels used in the present study were laboratory heats and contained low levels of inclusions. This fact and the correlations between the sulfide stress cracking data and the Charpy impact parameters suggest that carbides did govern toughness in the steels.

In dispersed systems, two ideal types of particles can exist; "weak" particles that allow dislocations to pass through them and "strong" particles that are not penetrated by dislocations. Hahn and Rosenfield[95] suggest that for a dispersion of "strong" particles in a polycrystalline matrix, the yield strength of the material is inversely proportional to the average interparticle spacing. Using the data of Table 5, a good correlation was found between the yield strengths of the three steels from the present study and the mean interparticle spacings of the carbides (see Figure 42). This implies that the carbides in the steels act as strong obstacles to dislocation movement.

Hodgson and Tetelman studied the effect of carbide particles on the cleavage strength of several quenched and tempered carbon-manganese steels[96]. The researchers found that the carbides either assisted or inhibited cleavage depending on the particle size and interparticle spacing. For particle diameters and interparticle spacings less than

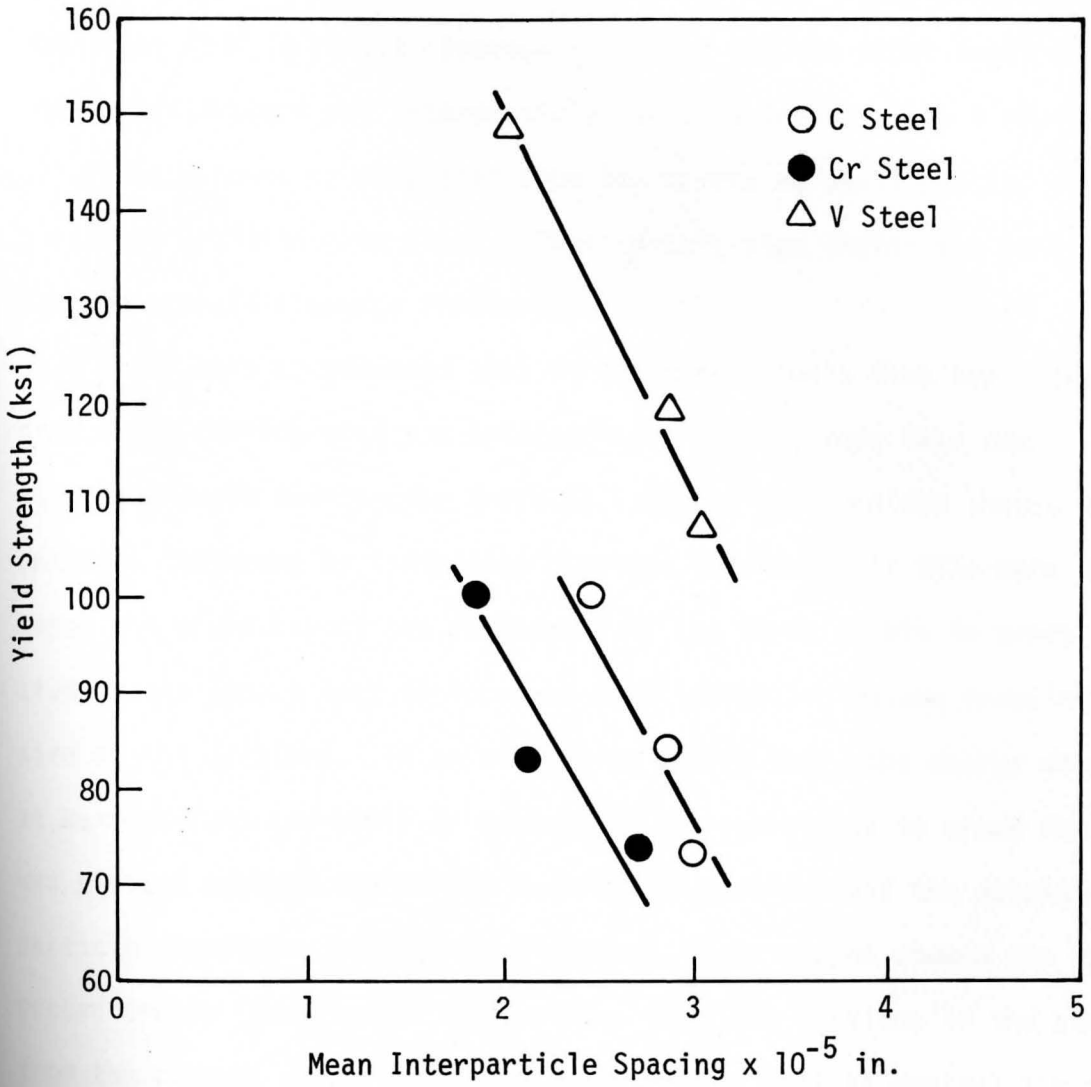

Figure 42. Relation Between Yield Strength of the Steels and Mean Interparticle Spacing.

1 micron (3.94×10^{-5} in.), the particles acted as strong obstacles by blocking slip processes in the matrix and reducing the length of dislocation pile-ups that initiate fracture. Thus, in this size region the particles tend to resist cleavage fracture. On the other hand, for particle diameters and interparticle spacings greater than 1 micron the particles cracked or separated from the matrix at small plastic strains, producing Griffith type flaws. Thus in this size region the particles tend to promote cleavage fracture.

It must be stressed that in the three steels from the present study, the carbide size and interparticle spacing were less than 1 micron at all strength levels (see Table 7). Hence, the carbides should have enhanced toughness by inhibiting cleavage fracture. If this were the case, one would expect the resistance of the three steels to crack initiation in the impact test to increase with increasing volume fraction and size of the carbides. In an attempt to verify this, the energy absorbed at maximum load at -100°F (a measure of the resistance to crack initiation) was plotted against the volume fraction of carbides and the average particle diameter. Despite some scatter, these graphs showed the expected trends (see Figures 43 and 44). Thus the carbides in the steels from the present study did govern toughness as well as control the resistance to sulfide stress cracking.

The correlations between the sulfide stress cracking data of the steels from the present study and the Charpy impact parameters showed a consistently better data fit for the -100°F test temperature. This can be readily understood form the work of Hodgson and Tetelman. The

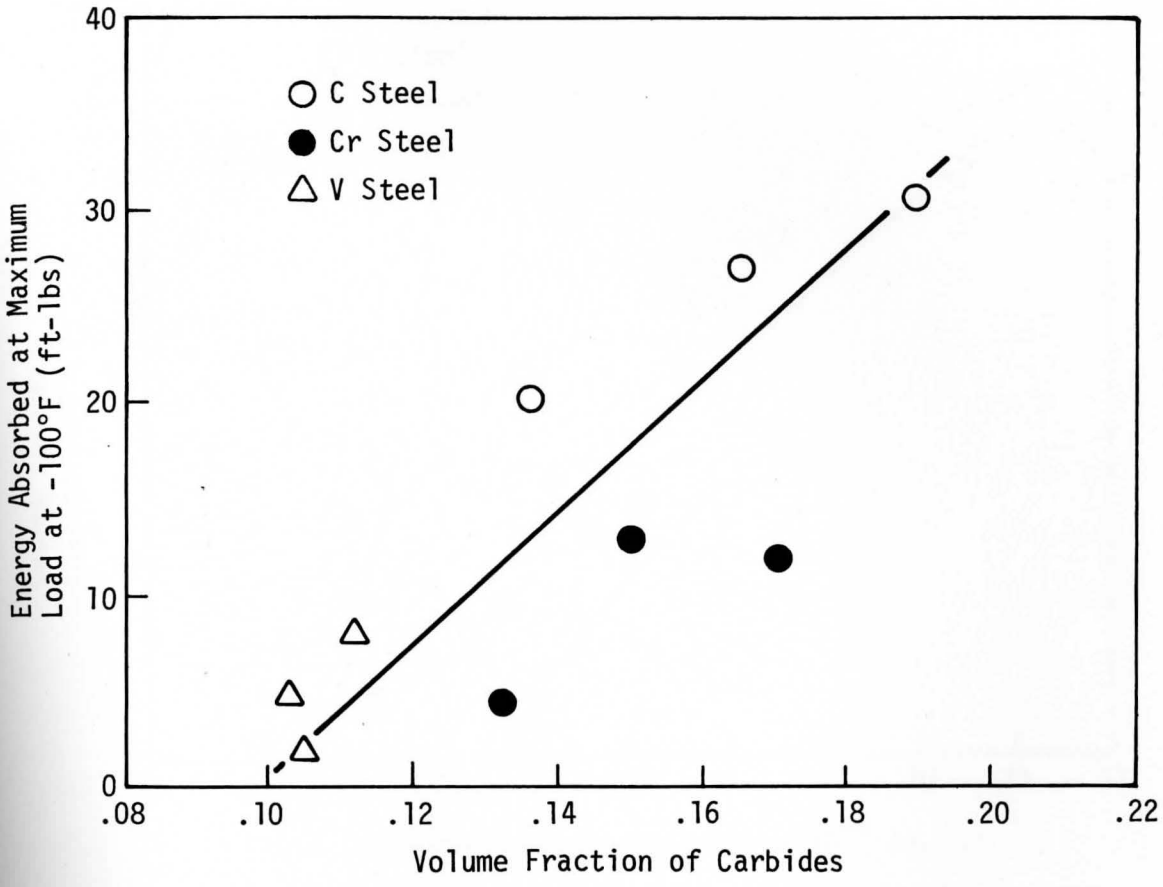

Figure 43. Variation of Energy Absorbed at Maximum Load at -100°F Versus Volume Fraction of Carbides.

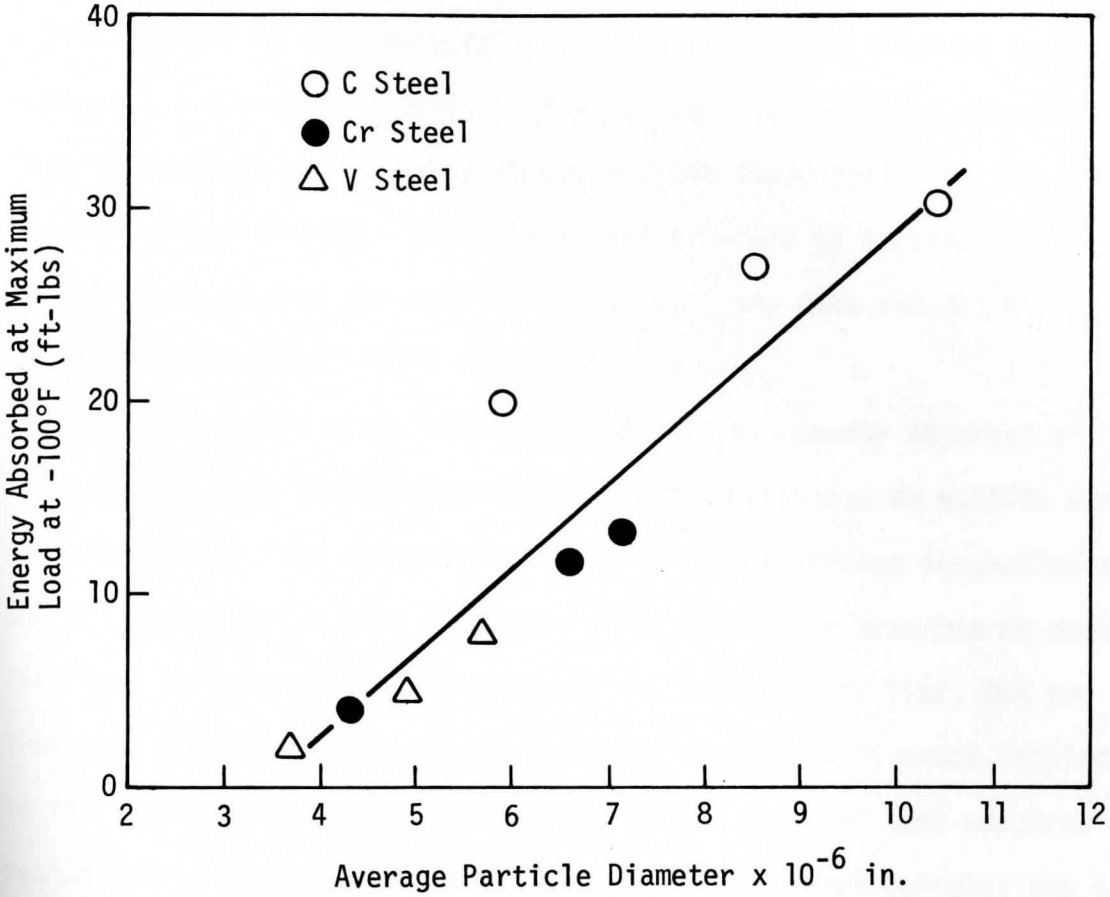

Figure 44. Variation of Energy Absorbed at Maximum Load at -100°F Versus Average Particle Diameter.

resistance of the steels in the present study to sulfide stress cracking was controlled by the carbide particles acting as traps for hydrogen. On the other hand, the toughness of the steels was governed by the ability of the carbides to inhibit cleavage fracture. Hence, one would expect a true measure of this ability at temperatures where cleavage is predominant, i.e., at the lower shelf. As suggested earlier, the -100°F test temperature was probably at or near the lower shelf for the steels from the present study. Thus, less scatter would be expected in the correlations between the sulfide stress cracking data and the Charpy impact parameters at -100°F rather than 75°F.

The present study also revealed that the energy absorbed at maximum load gave the best correlation with resistance to sulfide stress cracking. This fact along with the correlations between incubation time and the parameters - time to maximum load and energy absorbed at maximum load have an interesting implication. As indicated earlier, the two toughness parameters are a measure of the resistance to crack initiation in the impact test. Since the sulfide stress cracking test measures the resistance to hydrogen induced crack initiation, these correlations suggest a similarity between the initiation of cracks in the two tests. This is consistent with the theory of Troiano that hydrogen induced failure is a normal fracture process in which the embrittling effect of hydrogen is superimposed[97]. In effect, the presence of hydrogen lowers the cohesive strength of the lattice.

Two final points must be made. Basic studies have shown that the composition and grain size of a steel affect its Charpy impact properties[98]. Thus an extension of the results of the present study to other martensitic steels should consider the influence of these material factors on toughness. Furthermore, the work by Hodgson and Tetelman suggests that carbides greater than 1 micron in diameter and interparticle spacing assist rather than inhibit cleavage fracture. Since bainitic and pearlitic steels are more likely to have carbides within this range, additional investigations should be conducted to determine if correlations also exist between the resistance to sulfide stress cracking and toughness for these materials.

CHAPTER V

SUMMARY

The present study was conducted to determine the relationship for low alloy martensitic steels between microstructure and resistance to sulfide stress cracking - a type of hydrogen embrittlement. The specific objectives of the study were:

1) to determine if the cracking resistance could be correlated with a measurable carbide parameter such as size, volume fraction or interparticle spacing.

2) to determine if the Charpy impact test, which is sensitive to changes in microstructure, could be used to predict the resistance to sulfide stress cracking.

Sulfide stress cracking tests were conducted at 75°F on three low alloy steels using notched C-ring specimens. The materials, a plain carbon, a chromium and a vanadium steel, were quenched and tempered to various strength levels. In general, the results of the tests showed that the resistance of a steel to sulfide stress cracking increased with decreasing strength level or increasing tempering temperature. In addition, crack propagation rates were measured on select specimens of the three steels. These measurements showed that the failure process consisted of a finite period prior to crack initiation ranging from a few minutes to a few hours and a period of slow, discontinuous crack propagation lasting several hours. Furthermore, these measurements indicated that failure was governed by the diffusion of hydrogen to crack initiation sites in the steel.

The data obtained from the cracking tests were used to calculate sulfide stress cracking susceptibility factors for the three steels at each strength level. The susceptibility factors were correlated with carbide parameters determined from the microstructures of the C-ring specimens. These parameters were obtained using two stage carbon replicas and lineal analysis techniques. The correlations indicated that the resistance to sulfide stress cracking increased with increasing volume fraction of carbides and total particle surface area per unit length of line. In addition, there was a critical volume fraction of carbides and/or total particle surface area above which failure did not occur. These results are consistent with the theory that hydrogen can be trapped in an innocuous state at the interface between precipitates and the matrix.

Instrumented Charpy V-notch impact tests were conducted at -100°F and 75°F for the three steels at the same strength levels as those used in the sulfide stress cracking tests. The impact parameters were correlated with the calculated cracking susceptibility factors. The correlations indicated that the resistance to sulfide stress cracking increased with increases in the parameters - total energy absorbed, energy absorbed at maximum load, lateral expansion and time to maximum load. This implied that the carbides in the steels not only controlled the resistance to sulfide stress cracking but also governed toughness. The size and interparticle spacing of the carbides in each steel were in the range where particles inhibit cleavage fracture by blocking matrix slip processes. In addition, the best correlation between sulfide stress cracking re-

sistance and the impact parameters existed for the -100°F test temperature. This suggests that the inherent resistance of a martensitic steel to hydrogen induced failure is directly related to its inherent toughness, i.e., that at the lower shelf.

The phenomenon of sulfide stress cracking is of great concern to the petroleum industry. Because of the current energy crisis, oil and gas wells are being drilled to depths in excess of 20,000 feet in search of new reserves. Many of these deeper wells have hydrogen sulfide associated with them - the environment needed for sulfide stress cracking. Thus there is a growing demand for high strength tubing materials that will resist cracking. The results of the present study suggest that a critical volume fraction of carbides and/or total particle surface area are needed in the microstructure of these materials to prevent sulfide stress cracking. Furthermore, conventional martensitic steels will have an upper useable strength corresponding to this critical level of precipitates and thus may not be suitable for very deep wells. However, it may be possible to raise the upper useable strength level for tubing materials by controlling the volume fraction of second phase particles with a combination of martensitic strengthening and either precipitation hardening or dispersion strengthening. From this standpoint, additional work is needed to determine the ability of various types of particles (other carbides, nitrides, oxides etc.) for trapping hydrogen. The results of the present study also suggest that the Charpy impact test can be a useful tool in such work, specifically in the areas of screening large numbers of potential materials and in evaluating the effects of different heat treatments on the resistance to sulfide stress cracking.

APPENDIX A

Sample Calculation for Loading of C-Ring Specimen

Carbon Steel Yield Strength 100.6 ksi

C-Ring Measurements: OD = 2.20 in., notch depth = 0.044 in.
wall thickness = 0.206 in.
width = 0.9909 in.

$a = \frac{D-n}{2}$ where a = outside radius
D = specimen OD
n = notch depth

$a = \frac{2.20 \text{ in.} - 0.044 \text{ in.}}{2} = 1.078 \text{ in.}$

$R = a - \frac{h}{2}$ where R = radius of centroid
h = specimen thickness

$R = 1.078 \text{ in.} - \left(\frac{0.206 \text{ in.}}{2}\right) = 0.975 \text{ in.}$

$e = \frac{h^2}{12R}$ where e = distance from neutral axis to centroid

$e = \frac{(0.206 \text{ in.})^2}{12(0.975 \text{ in.})} = 0.0036 \text{ in.}$

$h' = \left(\frac{h}{2} - e\right)$ where h' = distance from neutral axis to outside surface

$h' = \left(\frac{0.206 \text{ in.}}{2} - 0.0036 \text{ in.}\right) = 0.0994 \text{ in.}$

$K = \left[\frac{h'R}{ea} - 1\right]$

$K = \left[\frac{(0.0994 \text{ in.})(0.975 \text{ in.})}{(0.0036 \text{ in.})(1.078 \text{ in.})} - 1\right] = 24.97 - 1 = 23.97$

$P = \frac{\sigma A}{K}$ where P = load on specimen
σ = applied stress = 98% of yield strength
A = cross sectional area below notch

$P = \frac{(0.98)(100{,}600 \text{ lb/in.}^2)(0.206 \text{ in.})(0.9909 \text{ in.})}{23.97} = 839.6 \text{ lb.}$

For load sensitive bolt #5

$$\frac{P}{PL} = \frac{\varepsilon}{\varepsilon L}$$

where PL = load at proof stress of bolt
= 7200 lb
εL = strain at proof stress
= 5564 μin./in.

$$\varepsilon = \left(\frac{839.6 \text{ lb}}{7200 \text{ lb}}\right) (5564 \text{ μin./in.})$$

ε = 648.8 μin./in. = strain on the bolt corresponding to the load on the specimen of 839.6 lb.

APPENDIX B

Sample Calculation of Mean Linear Intercept Grain Size

TABLE B-1

DATA FROM GRAIN SIZE MEASUREMENTS AFTER AUSTENITIZING AT 1750°F

Region of Microstructure	Number of Grain Intercepts		
	C Steel	Cr Steel	V Steel
1	3.5	3.0	3.0
2	3.5	3.0	5.0
3	3.0	2.0	4.5
4	4.0	2.0	2.5
5	2.0	3.0	3.5
6	3.0	2.0	5.0
7	3.0	2.5	3.0
8	4.0	2.0	3.0
9	2.0	3.0	3.0
10	2.0	2.0	3.5
11	3.0	1.0	4.5
12	3.0	2.5	4.0
13	4.0	4.0	2.5
14	4.0	4.0	4.5
15	3.0	4.0	3.0
16	1.0	4.0	4.0
17	5.0	4.0	3.0
18	1.5	3.0	3.0
19	2.0	3.0	3.0
20	4.0	3.0	1.5
Total	60.5	57.0	69.0

Carbon Steel Length of line 3.75 in. at 750x
Actual length = 0.005 in.
Total number of grain intercepts = 60.5

Average number of grain intercepts = $\frac{60.5}{20}$ = 3.025

Average linear intercept grain size = $\frac{0.005 \text{ in.}}{3.025}$ = 0.00165 in.

APPENDIX C

Sample Calculation of Cracking Susceptibility Factor

Carbon Steel Yield Strength 100.6 ksi

Cracking Data from Table 5:

Specimen	Test Results
1	F. between 1.7-17.1 hrs.
2	F. between 1.7-17.1 hrs.
3	F. between 3.7-16.2 hrs.

$$S = \frac{1}{n} \sum_{i=1}^{n} \left(\frac{r}{t}\right)_i$$

where S = susceptibility factor
t = earliest possible time* of failure in hrs.
r = ratio of measured yield stress to applied stress

For all of the C-ring tests the applied stress was 98% of the yield strength

$$S = \frac{1}{3}\left[\left\{\frac{100{,}600 \text{ lb/in.}^2}{(0.98)(100{,}600 \text{ lb/in.}^2)}\right\}\left\{\frac{1}{1.7} + \frac{1}{1.7} + \frac{1}{3.7}\right\}\right] = 0.492$$

*If failure does not occur in 500 hours, the failure time is taken as ∞.

APPENDIX D

Sample Calculations of Carbide Parameters

Carbon Steel Yield Strength 100.6 ksi

From Table D-1:

Total number of carbides intersecting random lines = 312.5

Sum of lengths of carbides that intersected random lines = 20.58 in.

Total length of line = 150 in.

Magnification = 16,800x

The equations used below in calculating the carbide parameters were taken from the works of Ashby and Ebeling[57] and Corti and coworkers[88].

Number of Particles per Unit Length of Line N_L

$$N_L = \frac{NM}{L_T}$$

where N = total number of carbides intersecting lines
L_T = total line length
M = magnification

$$N_L = \frac{(312.5 \text{ particles})(16{,}800x)}{150 \text{ in.}} = 3.50 \times 10^4 \text{ particles/in.}$$

Volume Fraction of Carbides V_F

$$V_F = \frac{L_P}{L_T}$$

where L_P = sum of lengths of carbides intersecting the random lines

$$V_F = \frac{20.58 \text{ in.}}{150 \text{ in.}} = 0.137$$

Average Particle Diameter D

$$D = \frac{3V_F}{2NL}$$

$$D = \frac{3(0.137)}{2(3.50 \times 10^4 \text{ particles/in.})} = 5.88 \times 10^{-6} \text{ in.}$$

Mean Interparticle Spacing λ

$$\lambda = \frac{1-V_F}{N_L}$$

$$\lambda = \frac{1 - (0.137)}{(3.50 \times 10^4 \text{ particles/in.})} = 2.47 \times 10^{-5} \text{ in.}$$

TABLE D-1

LINEAL ANALYSIS MEASUREMENTS OF CARBIDE PARTICLES

Material	Yield Strength (ksi)	Carbide Parameter	Microstructural Field 1	2	3	4	5	Total
Carbon Steel	100.6	N	58.5	72.0	64.0	61.5	56.5	312.5
		L_p	4.30	4.43	4.08	4.17	3.60	20.58
	84.0	N	50.5	48.5	60.0	55.5	46.0	260.5
		L_p	4.21	4.23	5.56	4.88	5.99	24.87
	73.1	N	40.0	40.5	47.0	60.0	56.0	243.5
		L_p	5.71	5.90	6.28	6.00	4.46	28.35
Cr Steel	100.0	N	73.5	86.0	89.0	91.5	73.5	413.5
		L_p	3.66	3.90	3.75	5.47	3.34	20.12
		N	61.5	74.5	52.0	75.0	83.0	346.0
		L_p	5.72	5.39	4.10	4.79	5.83	25.83
		N	59.0	44.0	66.5	58.0	52.0	279.5
		L_p	4.08	3.42	5.91	4.65	4.30	22.36
V Steel	148.1	N	58.5	84.5	92.0	78.5	75.5	389.0
		L_p	2.59	3.25	3.91	3.23	2.87	15.85
	119.6	N	47.5	67.0	49.5	59.0	57.0	280
		L_p	2.52	3.22	2.55	3.36	3.73	15.38
	107.1	N	49.0	59.5	45.0	50.0	60.0	263.5
		L_p	2.92	3.37	2.52	3.77	4.20	16.78

N = total number of carbides intersecting random lines
L_p = sum of lengths of carbides intersecting random lines (inches)
Total length of line per field = 30 inches

APPENDIX E

Sample Calculation of Average Slow Crack Propagation Rate

TABLE E-1

DATA FROM CRACK PROPAGATION MEASUREMENTS

Material	Yield Strength (ksi)	Incubation Time (hrs)	Propagation Time (hrs)	Crack Depth (in)	Specimen Width (in)
C Steel	100.6	3.4	17.3	.144	0.9985
Cr Steel	100.0	0.6	18.9	.186	1.085
V Steel	148.5	0.3	16.3	.188	1.005
V Steel	119.6	1.2	10.5	.195	1.090
V Steel	107.0	1.4	14.3	.155	1.055

Carbon Steel Yield Strength 100.6 ksi

Data from Table: incubation time = 3.4 hrs.
time until crack arrest = 17.3 hrs.
average crack depth = 0.144 in.
specimen width = 0.9985 in.

Area of Crack Propagation = (0.144 in.)(0.9985 in.)
$= 0.1437 \text{ in.}^2$

Time of Slow Crack Propagation = 17.3 hrs. - 3.4 hrs.
= 13.9 hrs.

$$\text{Propagation Rate} = \frac{0.1437 \text{ in.}^2}{13.9 \text{ hrs.}} = 1.033 \times 10^{-2} \text{ in.}^2/\text{hr.}$$

Changing to $\text{cm}^2/\text{sec.}$

$$\text{Propagation Rate} = 1.033 \times 10^{-2} \text{ in.}^2/\text{hr.} \times \frac{(2.54 \text{ cm/in.})^2}{(3600 \text{ sec/hr.})}$$

$$= 1.033 \times 10^{-2} \text{ in.}^2/\text{hr.} \left(1.795 \times 10^{-3} \frac{\text{cm}^2/\text{in.}^2}{\text{sec/hr.}}\right)$$

$$\text{Propagation Rate} = 1.85 \times 10^{-5} \text{ cm}^2/\text{sec.}$$

APPENDIX F

Sample Calculation of Total Surface Area of Carbides Per Unit Length of Line

Carbon Steel Yield Strength 100.6 ksi

Average particle diameter = 5.88×10^{-6} in.
Number of particles per unit length of line = 3.50×10^{4} particles/in.

Total Surface Area of Carbides per Unit Length of Line A_T

$A = \pi D^2$ where A = surface area of average particle
D = diameter of average particle

$A = \pi(5.88 \times 10^{-6} \text{ in.})^2 = 1.09 \times 10^{-10} \text{ in.}^2/\text{particle}$

$A_T = AN_L$ where N_L = number of particles per unit length of line

$A_T = (1.09 \times 10^{-10} \text{ in.}^2/\text{particle})(3.50 \times 10^{4} \text{ particles/in.})$

$A_T = 3.78 \times 10^{-6} \text{ in.}^2/\text{in.}$

TABLE F-1

CALCULATED VALUES OF TOTAL SURFACE AREA OF CARBIDES PER UNIT LENGTH OF LINE

Material	Yield Strength (ksi)	Average Particle Diameter ($\times 10^6$ in.)	Number of Particles per Unit Length of Line ($\times 10^{-4}$ in.$^{-1}$)	Total Surface Area per Unit Length of Line ($\times 10^6$ in.^{2}/in.)
Carbon Steel	100.6	5.88	3.50	3.78
	84.0	8.53	2.92	6.68
	73.1	10.38	2.73	9.27
Cr Steel	100.0	4.32	4.63	2.77
	82.8	6.63	3.88	5.38
	73.0	7.14	3.13	5.08
V Steel	148.5	3.63	4.36	1.81
	119.6	4.89	3.14	2.37
	107.1	5.69	2.95	2.99

REFERENCES

1. A. E. Schuetz and W. D. Robertson, Hydrogen Absorption, Embrittlement and Fracture of Steel, Corrosion Vol. 13, July 1957, pp. 33-54.

2. C. G. Interrante, Basic and Research Aspects, WRC Bulletin 145: Interpretive Report on Effect of Hydrogen in Pressure Vessel Steels, October 1969, p. 8.

3. G. E. Dieter, Mechanical Metallurgy, New York, McGraw-Hill Book Company, Inc., 1961, p. 389.

4. A. R. Troiano, Delayed Failure of High Strength Steels, Corrosion Vol. 15, 1959, pp. 57-62.

5. A. R. Troiano, The Role of Hydrogen and Other Interstitials in the Mechanical Behavior of Metals, Transactions of the ASM, Vol. 52, 1960, pp. 54-80.

6. Troiano, pp. 64-65.

7. Troiano, p. 75.

8. Dieter, pp. 194-5.

9. A. S. Tetelman, The Mechanism of Hydrogen Embrittlement in Steel, Department of Materials Science Report, Stanford Univeristy, July 1967, p. 4.

10. Tetelman, p. 3.

11. Tetelman, p. 4.

12. Troiano, p. 75.

13. Tetelman, p. 5.

14. A. S. Tetelman, Recent Developments in Classical (Internal) Hydrogen Embrittlement, Paper from International Conference on Hydrogen in Metals, Champion, Pennsylvania, September 23-27, 1973.

15. J. B. Greer, Factors Affecting the Sulfide Stress Cracking Performance of High Strength Steel, Paper No. 55, International Corrosion Forum, March 1973, pp. 55/1-55/22.

16. R. S. Treseder and T. M. Swanson, Factors in Sulfide Corrosion Cracking of High Strength Steels, Corrosion, Vol. 24, February 1968, pp. 31-37.

17. J. B. Greer et al., Effect of Temperature and State of Stress on Hydrogen Embrittlement of High Strength Steel, Corrosion Vol. 28, 1972, pp. 378-384.

18. E. E. Hofmann et al., Embrittlement of Various Steels Through Absorption of Hydrogen from Wet Hydrogen Sulfide, Brutcher Translation.

19. C. St. John and W. W. Gerberich, The Effect of Loading Mode on Hydrogen Embrittlement, Metallurgical Transactions, Vol. 4, February 1973, pp. 589-594.

20. J. D. Gottschling and P. S. Ayres, Sulfide Stress Cracking - A Literature Review, Internal Report of the Babcock & Wilcox Company, September 1971.

21. J. P. Fraser and G. G. Eldredge, Influence of Metallurgical Variables on Resistance of Steels to Sulfide Corrosion Cracking, Corrosion Vol. 14, November 1958, pp. 524t-530t.

22. E. Snape, Sulfide Stress Corrosion of Some Medium and Low Alloy Steels, Corrosion, Vol. 23, June 1967, pp. 154-172.

23. E. Herzog, Conditions for Stress Corrosion in Hydrogen Sulfide - Durability of Unalloy and Low Alloy Steels Under Stress in Hydrogen Sulfide, Revue de Metallurgie, Vol. 55, 1958.

24. L. W. Vollmer, Hydrogen Sulfide Corrosion Cracking of Steel, Corrosion, Vol. 8, 1952, pp. 326-60.

25. Fraser and Eldredge, pp. 524t-530t.

26. M. Kowaka and S. Nagata, Effects of Strength and Composition on Sulfide Corrosion Cracking of Low Alloy Steels, Twelfth Japan Congress on Materials Research, March 1969, pp. 141-145.

27. Herzog.

28. Interrante, p. 9.

29. Snape, pp. 154-172.

30. E. Snape, Roles of Composition and Microstructure in Sulfide Cracking of Steel, Corrosion, Vol. 24, No. 9, September 1968, pp. 261-293.

31. G. L. Kehl, The Principles of Metallographic Laboratory Practice, New York, McGraw-Hill Book Company, Inc., 1949, pp. 292-293.

32. The 1975 Annual Book of ASTM Standards, Vol. 11, Metallography, Nondestructive Tests, American Society for Testing and Materials, Philadelphia, Pennsylvania, p. 220.

33. J. B. Greer, Results of Interlaboratory Sulfide Stress Cracking Using the NACE T-1F-9 Proposed Test Method, Paper No. 97, International Corrosion Forum, Toronto, Canada, April 1975, pp. 97/1-97/12.

34. J. P. Fraser et al., Laboratory and Field Methods for Quantitative Study of Sulfide Corrosion Cracking, Corrosion, Vol. 14, November 1958, pp. 517t-523t.

35. S. O. Fernandez and G. F. Tisinai, Stress Analysis of Unnotched C-Rings Used for Stress Cracking Studies, Paper No. 67-Pet.-2, Petroleum Mechanical Engineering Conference, Philadelphia Pa., September 1967.

36. Snape, Sulfide Stress Corrosion of Some Medium and Low Alloy Steels, Corrosion, Vol. 23, June 1967, p. 157.

37. R. A. Wullaert, Applications of the Instrumented Charpy Impact Test, Impact Testing of Metals, ASTM Special Technical Publication 466, American Society for Testing and Materials, Philadelphia, Pa., March 1970, pp. 148-164.

38. K. Narita et al., The Isolation and Determination of Carbides in Steel, Transactions of the Iron and Steel Institute of Japan, Vol. 16, 1976, pp. 168-179.

39. J. H. Woodhead and A. G. Quarrel, The Role of Carbides in Low-Alloy Creep-Resisting Steels, Booklet Published by Climax Molybdenum Company Limited, London, England, p. 6.

40. J. Nutting, The Physical Metallurgy of Alloy Steels, Journal of the Iron and Steel Institute, June 1969, pp. 872-893.

41. Woodhead and Quarrel, p. 6.

42. T. Sato et al., On the Carbide Reactions, Secondary Hardening and Volume Change Occurring in the Fourth Stage of Tempering of Alloy Steels, The Journal of the Australian Institute of Metals, Vol. 5, No. 2, August 1960, pp. 123-130.

43. K. Bungardt et al., Die Loslichkeit des Vanadinkarbids in Austenit, Archiv fur das Eisenhuttenwesen, January 1956, pp. 61-66.

44. Narita, p. 172.

45. Nutting, pp. 885-887.

46. Woodhead and Quarrel, p. 7.

47. Sato, p. 125.

48. N. E. Hannerz and F. De Kazinczy, Kinetics of Austenite Grain Growth in Steel, Journal of the Iron and Steel Institute, May 1970, pp. 475-481.

49. Schuetz and Robertson, p. 445t.

50. M. Watkins et al., Fractography of Sulfide Stress Cracking, Paper No. 98, International Corrosion Forum, April 1975, Toronto, Canada, pp. 98/1-98/14.

51. J. D. Gottschling and P. S. Ayres, Sulfide Stress Cracking Studies of C-95 Normalized and Tempered Oil Well Tubing Material, Formal Report 8036 of the Babcock & Wilcox Company, May 1972.

52. M. W. Lui and I. LeMay, Relations Between Tensile Strength and Carbide Size in AISI 4140 Steel, Metallurgical Transactions, Vol. 6A, March 1975, pp. 583-4.

53. T. Mukherjee et al., Kinetics of Coarsening of Carbides in Chromium Steels at 700°C, Journal of the Iron and Steel Institute, May 1969, pp. 621-631.

54. A. D. Batte and R. W. K. Honeycombe, Precipitation of Vanadium Carbide in Ferrite, Journal of the Iron and Steel Institute, April 1973, pp. 284-289.

55. F. B. Pickering, Some Aspects of the Relationship Between Microstructure and Mechanical Properties, Iron and Steel, April 1965, pp. 178-182.

56. K. F. Hale, An Electron Microscope Study of Changes in a 2-1/4% Cr, 1 % Mo Super-heater Tube Steel During Tempering and Creep, Metal Treatment, Vol. 29, 1959, pp. 145-153.

57. M. F. Ashby and R. Ebeling, On the Determination of the Number, Size, Spacing and Volume Fraction of Spherical Second-Phase Particles from Extraction Replicas, Transactions of the Metallurgical Society of AIME, Vol. 236, October 1966, pp. 1396-1404.

58. J. B. Greer, Results of Interlaboratory Sulfide Stress Cracking Using the NACE T-1F-9 Proposed Test Method, Paper No. 97, International Corrosion Forum, Toronto, Canada, April 1975, pp. 97/1-97/12.

59. Dieter, p. 386.

60. K. J. Irvine et al., Grain Refined C-Mn Steels, Journal of the Iron and Steel Institute, February 1967, pp. 161-182.

61. Bungardt, pp. 61-66.

62. K. J. Irvine et al., The Effect of Composition on the Structure and Properties of Martensite, Journal of the Iron and Steel Institute, September 1960, pp. 66-81.

63. R. W. K. Honeycombe, Some Strengthening Mechanisms in Alloy Steels, Reprint from Metallurgical Developments in High-Alloy Steels, ISI Special Report 86, June, 1964, pp. 1-14.

64. Honeycombe, p. 4.

65. R. W. Balluffi et al., The Tempering of Chromium Steels, Transactions of the ASM, Vol. 43, 1951, pp. 497-525.

66. Sato, pp. 127-130.

67. Sato, p. 130.

68. Troiano, Delayed Failure of High Strength Steels, Corrosion Vol. 15, 1959, pp. 58-59.

69. Troiano, The Role of Hydrogen and Other Interstitials in the Mechanical Behavior of Metals, Transactions of the ASM, Vol. 52, 1960, p. 62.

70. Troiano, Delayed Failure of High Strength Steels, Corrosion Vol. 15, 1959, p. 59.

71. Shuetz and Robertson, p. 457t.

72. Snape, Roles of Composition and Microstructure in Sulfide Cracking of Steel, Corrosion, Vol. 24, No. 9, September 1968, p. 261.

73. Interrante, p. 9.

74. E. Snape, Stress Induced Failure of High-Strength Steels in Environments Containing Hydrogen Sulfide, British Corrosion Journal, Vol. 4, September 1969, pp. 253-259.

75. J. P. Hirth and H. H. Johnson, Hydrogen Problems in Energy Related Technology, Corrosion, Vol. 32, No. 1, January 1976, pp. 3-25.

76. Interrante, p. 4.

77. Interrante, p. 5.

78. Interrante, p. 4.

79. Interrante, p. 3.

80. Troiano, The Role of Hydrogen and Other Interstitials in the Mechanical Behavior of Metals, Transactions of the ASM, Vol. 52, 1960, pp. 62-63.

81. Troiano, p. 63.

82. Troiano, pp. 63-64.

83. Interrante, p. 5.

84. H. R. Gray and A. R. Troiano, How Hydrogen Affects Maraging Steel, Metals Progress, April 1964, pp. 75-78.

85. W. M. Cain and A. R. Troiano, Steel Structure and Hydrogen Embrittlement, Petroleum Engineer, May 1965, pp. 78-82.

86. F. R. Coe and J. Moreton, Diffusion of Hydrogen in Low-Alloy Steel, Journal of the Iron and Steel Institute, April 1966, pp. 366-370.

87. J. F. Newman and L. L. Shreir, Effect of Carbon Content and Structure of Steels on Solubility and Diffusion Coefficient of Hydrogen, Journal of the Iron and Steel Institute, October 1969, pp. 1369-1372.

88. C. W. Corti et al., The Evaluation of the Interparticle Spacing in Dispersion Alloys, International Metallurgical Reviews, Vol. 19, 1974, pp. 77-88.

89. Newman, p. 1371.

90. H. Stuart and N. Ridley, Thermal Expansion of Some Carbides and Tessellated Stresses in Steels, Journal of the Iron and Steel Institute, December 1970, pp. 1087-1092.

91. Stuart and Ridley, p. 1092.

92. H. W. Hayden et al., The Structure and Properties of Materials, Vol. III, Mechanical Behavior, New York, John Wiley and Sons, Inc., 1965, p. 74.

93. Stuart, p. 1090.

94. L. L-J. Chin, A Model for Toughness Studies of Welds, Welding Journal, July 1964, pp. 290s-294s.

95. G. T. Hahn and A. R. Rosenfield, A Modified Double Pile-Up Treatment of the Influence of Grain Size and Dispersed Particles on Brittle Fracture, Acta Metallurigica, Vol. 14, December 1966, pp. 1815-1825.

96. D. E. Hodgson and A. S. Tetelman, The Effect of Microstructure on the Cleavage Strength of Quenched and Tempered Steels, Fracture 1969 - Proceedings of the Second Conference on Fracture, Chapman and Hall Ltd., London, April 1969.

97. Troiano, The Role of Hydrogen and Other Interstitials in the Mechanical Behavior of Metals, Transactions of the ASM, Vol. 52, 1960, pp. 64-65.

98. Dieter, pp. 381-383.